LANDESSTERNWARTE HEIDELBERG-KÖNIGSTUHL

Final Design Report

for the

Fiber-fed Extended Range Optical Spectrograph

FEROS

Document:

A. Kaufer

June 13, 1997

Identification:

FEROS Contract: ESO-SPE-TRS-094-0328-GW

FEROS Consortium
Principal Investigator: Prof. Dr. Bernhard Wolf
Address: Landessternwarte Heidelberg, Königstuhl 12, D-69 117 Heidelberg
Telephone: +49 6221 509 0
Telefax: +49 6221 509 202
e-mail: B.Wolf@lsw.uni-heidelberg.de

Members of Consortium:

Landessternwarte Heidelberg – Königstuhl (Prof. Dr. B. Wolf)
Astronomical Observatory, Copenhagen University (Prof. Dr. J. Andersen)
Institut d'Astrophysique de Paris (Prof. Dr. M. Dennefeld)
Observatoire de Paris/Meudon (Prof. Dr. R. Cayrel)

Contents

1 Overview **13**

2 Instrument Description and Capabilities **15**

2.1 General Description 15

2.2 Spectral Format 16

2.3 Overall Efficiency 17

3 Optical Design **21**

3.1 Micro Lenses and Fibers 22

3.1.1 Micro Lenses 22

3.1.2 Fibers 23

3.2 F/N Adaption Lens System 23

3.3 Image Slicer 25

3.4 Collimators 26

3.5 Flat Folding Mirror 27

3.6 Echelle Grating 28

3.7 Crossdisperser 28

3.8 Camera 29

3.8.1 General 29

3.8.2 Optical Characteristics 29

3.8.3 Image Quality 31

3.8.4 Transmission 31

3.8.5 Environmental Sensitivity 32

3.8.6 Focussing, Centering 32

3.8.7 Ghost Image and Sky Concentration Analysis 33

3.9 Coatings . . . 35
3.9.1 Mirrors . . . 35
3.9.2 Lenses . . . 36
3.10 Straylight . . . 36
3.10.1 Mirrors . . . 37
3.10.2 Lenses . . . 37
3.10.3 Echelle Grating . . . 38
3.11 Optical Tolerances for the Alignment of the CCD . . . 38
3.12 Overall Efficiency of the FEROS Instrument . . . 38
3.13 Spot diagrams of the complete FEROS system . . . 39
3.14 Image analysis of the complete FEROS system . . . 40

4 Mechanical Design 41
4.1 General description . . . 41
4.1.1 Movable parts . . . 41
4.1.2 Materials and Painting . . . 42
4.1.3 Kinematic mounts . . . 42
4.1.4 Miscellaneous . . . 42
4.2 Optical Table . . . 45
4.3 Fiber entrance with fiber connectors . . . 45
4.4 Fiber link . . . 46
4.5 Fiber-exit unit with F/N System and Image Slicer . . . 47
4.5.1 Fiber exits . . . 48
4.5.2 F/N System . . . 48
4.5.3 Image Slicer . . . 48
4.6 Collimators . . . 53
4.7 Folding Mirror . . . 55
4.8 Echelle . . . 57
4.9 Crossdisperser Prism . . . 59

4.10 Camera, Shutter, and CCD Continuous-flow Dewar 61
4.10.1 Camera 61
4.10.2 Shutter 61
4.10.3 CCD 62
4.11 Removable Enclosure 64
4.12 Spectrograph Room 65

5 CCD detector **67**
5.1 CCD Detector 67
5.2 CCD Mounting and Alignment 68
5.3 Detector Head and Cryostat 69
5.4 Interface to Spectrograph 69
5.5 Controller 69

6 Calibration Unit **71**
6.1 General Description 71
6.2 Conceptional Design of the FCU 71
6.2.1 Components 71
6.2.2 Operational Modes 75
6.3 Opto-mechanical layout of the FCU 75
6.4 Mechanical and Optical Interfaces between FCU and B&C 76
6.5 Electronic Interface 76

7 Instrument Control: DAISY **83**

8 Instrument Simulation **85**
8.1 Raw-Data Simulator 85
8.2 Physical Model 86
8.3 Exposure-Time Calculator 87

9 Data Reduction Software **89**

10 Alignment Concept **93**

10.1 General 93

10.2 Alignment tools 93

10.3 Centering of the Microlens on the Fiber 94

10.4 Internal alignment of the Fiber-exit heads 94

10.5 Pre-alignment of the basement of the Fiber-exit unit 96

10.6 Position and focus of Collimator 1 96

10.7 Position of Folding Mirror 97

10.8 Focus of Collimator 2 97

10.9 Mounting and alignment of Fiber-exit unit 97

10.10 Position and tilt of Echelle grating 97

10.11 Position of crossdisperser prism 98

10.12 Alignment of the unit Camera – Fieldlens – CCD 98

10.13 Position of Camera–CCD unit 99

11 Concept for Verification Tests **101**

12 Maintenance Concept **103**

13 Safety Aspects **105**

14 Planning and Management **107**

14.1 Strategy 107

14.2 Responsibilities 107

14.3 Key Personnel 107

14.4 Description of Work Components 112

14.5 Time Schedule 117

14.6 Manpower Estimate 119

14.7 Procurement Plan 120

15 Critical Items **123**

15.1 Image Slicer 123

15.2 Camera 124

15.3 Fiber-Flatfield stability 124

16 User/Operational Manual (Draft) **127**

16.1 Introduction 127

16.2 Instrument Configurations / Observing Modes 128

16.2.1 The Object + Sky Configuration 129

16.2.2 The Object + Calibration Configuration 129

16.3 FEROS Spectral Characteristics 130

16.3.1 Spectral Coverage 130

16.3.2 Spectral Resolution 130

16.3.3 Efficiency and Limiting Magnitudes 130

16.3.4 Instrument Simulation and Exposure-Time Calculator . . 130

16.4 Observations 130

16.4.1 The DAISY Instrument Control 130

16.4.2 Selection of the Observing Mode 130

16.4.3 Object+Sky Exposures 130

16.4.4 Object+Calibration Exposures 131

16.4.5 Flatfield Exposures 131

16.4.6 Wavelength-Calibration Exposures 131

16.4.7 Dark Exposures 131

16.5 Observing run: Example and Advice 132

16.5.1 Preparation of the Observations 132

16.5.2 Preparation of the Instrument 132

16.5.3 Object+Sky Exposures 132

16.5.4 Object+Calibration Exposures 132

16.5.5 High-accuracy Radial-Velocity Observations 132

16.6 The CCD detector . . . 132
16.7 (On-line) Data Reduction Software . . . 133
16.7.1 Purposes . . . 133
16.7.2 Requirements . . . 133
16.7.3 Capabilites . . . 133
16.8 Data Archiving . . . 133

A Optical System Data **135**
A.1 ZEMAX system data for the FEROS complete optical system . . . 135

B Mechanical drawings **143**
B.1 Optical Table . . . 144
B.2 Microlens . . . 145
B.3 Fiber-exit unit . . . 146
B.4 Image Slicer . . . 147
B.4.1 Slicer Prism . . . 148
B.4.2 Entrance Prism . . . 149
B.4.3 Slicer Plate . . . 150
B.4.4 Image Slicer Housing . . . 151
B.5 Main Collimator . . . 152
B.6 Transfer Collimator . . . 153
B.7 Folding Mirror . . . 154
B.8 Echelle . . . 155
B.9 Crossdisperser Prism . . . 156
B.10 Camera – CCD Unit . . . 157
B.11 Axial Supports . . . 158
B.12 Clamps . . . 159
B.13 Stops . . . 160
B.14 Removable Enclosure . . . 162
B.15 Calibration Unit . . . 163

B.15.1 Boller&Chivens interface 164
B.15.2 Wavelength-Calibration Unit 1 (WCU1) 165
B.15.3 Wavelength-Calibration Unit 2 (WCU2) 166
B.15.4 Flatfield Unit (FFU) 167

List of Tables

2.1 *Main parameters of FEROS.* 16
2.2 *Efficiency of FEROS* 18
14.1 *FEROS Procurement Plan.* 121
16.1 *Main parameters of FEROS.* 127

List of Figures

2.1 Simulated Flatfield and Thorium-Argon frames. 17

2.2 Expected S/N ratio in V band 19

3.1 FEROS optical system 21

3.2 Entrance micro lens layout 22

3.3 F/N Adaption Lens System 23

3.4 Spot diagrams of the F/N System 24

3.5 Layout of the Image Slicer (side view). 25

3.6 Layout of the Image Slicer (front view). 26

3.7 Layout of the off-axis paraboloid collimators 27

3.8 Layout of the flat folding mirror. 28

3.9 Measured Echelle Efficiency 29

3.10 Layout of the LF5 prism crossdisperser. 30

3.11 Layout of the FEROS camera. 31

3.12 Diameter of 80% encircled energy of the FEROS Camera 32

3.13 Polychromatic encircled energy of the FEROS Camera 33

3.14 Spot diagrams of the FEROS Camera 34

3.15 Total transmission of the FEROS Camera 35

3.16 Reflectivity of mirror coating 36

3.17 Transmission curves of the multi-layer lens coatings 37

4.1 FEROS complete system 44

4.2 Optical table 46

4.3 Layout of the fiber-entrance connectors 47

4.4 Layout of the fiber-exit unit 50

4.5 Layout of the housing of the image slicer. 51
4.6 Mounting of the Main Collimator. 53
4.7 Mounting of the Transfer Collimator. 54
4.8 Mounting of the Flat Folding Mirror. 56
4.9 Mounting of the Echelle grating. 58
4.10 Mounting of the Crossdisperser Prism. 60
4.11 The Camera–CCD Unit. 63
4.12 Design of the spectrograph's enclosure. 64

5.1 Quantum efficiency curve of EEV 2kx4k chip 70

6.1 Output intensity distribution of the Flatfield Unit 72
6.2 Output intensity distribution of the Wavelength Calibration Unit . 74
6.3 78
6.4 Electronical layout of the RSM control. 79
6.5 Electronical layout of the WCU1, WCU2, FFU control. 80
6.6 Electronical layout of the NDFW control. 81
6.7 Electronical layout for the wiring of the FCU components on the telescope's side. 82

8.1 Physical model: distortion of echellogram 88

10.1 The Fiber-Exit Unit 95
10.2 Image-slicer model 96
10.3 Alignment steps for the FEROS system. 100

14.1 Organigram 111

15.1 Flatfield Stability 125

16.1 FEROS optical system 128
16.2 Expected S/N ratio in V band 131

Chapter 1: Overview

FEROS, the **F**iber fed **E**xtended **R**ange **O**ptical **S**pectrograph is a fiber-fed bench-mounted prism-crossdispersed echelle spectrograph for the ESO 1.52-m telescope at La Silla. It works in quasi Littrow mode and in white pupil configuration. For the object and the nearby sky, the complete optical spectrum from $370 - 860$ nm is recorded in one exposure with a resolving power of $R = 48\,000$ by the use of a two-beam, two-slice image slicer.

A first concept of FEROS which is supposed to replace ECHELEC at the 1.52-m telescope was presented by [Pasquini et al., 1992, "FEROS for the ESO 1.52-m Telescope", 32nd Scientific Technical Committee Meeting, Garching]. Designed as a fiber-linked spectrograph connected to the permanently mounted Boller & Chivens spectrograph it has the advantage of being always available. Because FEROS provides high-dispersion spectroscopy with a wide, simultaneous wavelength coverage, this instrument mounted on an intermediate size telescope fills a gap in the present and future ESO instrumentation park. It will allow to realize many important scientific programs of objects down to about $16^{\rm th}$ magnitude with high efficiency, little constraints on operations and relief of pressure on larger telescopes.

FEROS is built for ESO by a consortium of four astronomical institutes under the leadership of the Landessternwarte Heidelberg (LSW). Principal Investigator (PI) of the FEROS project is Prof. Dr. Bernhard Wolf at the LSW. Further members of the consortium are the the Astronomical Observatory Copenhagen (AOC), the Institut d'Astrophysique de Paris (IAP), and the Observatoire de Paris/Meudon (OPM). The contract between ESO and the FEROS Consortium was signed in September 1996 (Contract: ESO-SPE-TRS-094-0328-GW). It is planned that the instrument will be fully available to the community in early 1999.

The purpose of this document is to present a report on the final opto-mechanical design of the instrument and a detailed management plan that defines the work packages, the time schedule, and the responsibilities within the project. This Final Design Report (FDR in the following) is based on the FEROS Conceptual Design (FCD) by Pasquini et al., 1992, and the FEROS Proposal (FP) submitted to ESO in April 1995.

The Final Optical Design (FOD) was already presented in October 1996 and approved by ESO. This was necessary to allow the start of the procurement of the major optical parts of FEROS already at the end of 1996.

This FDR will be the reference document for the complete FEROS project.

Chapter 2: Instrument Description and Capabilities

2.1 General Description

The **F**iber fed **E**xtended **R**ange **O**ptical **S**pectrograph FEROS and its capabilities will be described in this chapter.

The following capabilities for the FEROS instrument are foreseen:

- **Prism crossdispersed Echelle spectrograph**, working in quasi-Littrow mode with a **two-beam, two-slice image slicer**.
- **White pupil** configuration.
- **Bench mounted** in the thermally stabilized and humidity controlled coudé room of the ESO 1.52-m telescope.
- **Fiber fed**, two fibers will simultaneously feed the spectrograph. One fiber will record the object spectrum. Simultaneously, the second fiber will be fed either by the sky background or by a calibration lamp to monitor the instrument stability during the exposure.
- **Resolving power** 48 000 (2 pixel resolution).
- **Entrance aperture** of 2.7 arcsec; this keeps slit losses below 12 % for a seeing of 1.5 arcsec and keeps the effect of differential atmospheric refraction up to $z = 60^\circ$ ($\mathrm{airmass} = 2$) negligible.
- **Wavelength range** $3\,700 - 8\,600$ Å.
- **Large-size CCD detector**, a thinned, back-illuminated, LN_2 cooled, monolithic 2k$\times$4k chip is foreseen.
- **High efficiency** 27% peak efficiency, 7 (1.7)% in the extreme blue at 3 700 (3 500) Å and 8% in the extreme red at 9 000 Å.
- **Fixed configurations**, the bench-mounted part of the spectrograph contains *no* movable or remotely controlled components besides the CCD shutter. This ensures easy maintenance and reproducible and stable output formats. With this an accuracy in radial velocities of better than 50 m/s is expected (including software techniques like cross correlation).
- Full **on-line data reduction** in the MIDAS environment and tools for subsequent archiving and analyses e.g. radial-velocity and time-series analyses.

The main parameters and the expected performance for FEROS are already summarized in Tab. 2.1.

Table 2.1: *Main parameters of FEROS.*

Wavelength range	
in one exposure (object+sky)	$3700 - 8600$ Å (40 orders, 2 fibers)
Resolving Power (with 2-slice image slicer)	$\lambda/\Delta\lambda = 48\,000$
Entrance Aperture	2.7 arcsec
Fiber Input/Output Focal Ratio	F/4.6
Spectrograph Beam Size	136 mm diameter
Off-axis Collimators	F/11, cut from one parent paraboloid
Echelle	R2, 79 lines/mm, 154 mm by 306 mm
Crossdisperser Prism	LF5 glass, 55° apex angle
Dioptric Camera	
Wavelength Range	$350 - 900$ nm
F/#	F/3.0
Focal Length	410 mm
Field Diameter	69 mm
Image Quality (E_{80})	< 25 μm
Efficiency	$> 85\%$
CCD	2048×4096, 15 μm, thinned
Expected Detection Efficiency (without telescope)	7% (3700 Å), 27% (5000 Å), 8% (9000 Å)
Expected Limiting Magnitudes at the ESO 1.52	16 mag in V ($S/N = 15$, 2 h)
	12.5 mag in V ($S/N = 100$, 2 h)
Expected Radial-Velocity Accuracy	< 25 m/s, < 5 m/s with iodine cell
	(contract: < 50 m/s)

2.2 Spectral Format

The image slicer output equals two slits (object + sky/external calibration) in 0.9 mm distance with a 120×600 μm aperture. For each order this leads to slit images on the detector with a size of 2.2×10.9 pixels and 16.4 pixels separation in crossdispersion direction leaving a sufficient fixed interorder space of 5.5 pixels for the background definition. The distance between two orders is smallest in the red with about 30 pixels and increases to about 100 pixels in the blue.

The spectral range from 3 680 to 8 550 Å is available in one exposure for the object and sky/calibration spectra. The wavelength range above 8 550 Å up to 9 200 Å is in principle also available on the detector, but with small gaps in the spectral coverage. By a simple turn of the crossdisperser prism by 0.5 degrees, the wavelength region from 3 500 to 6 800 Å is in principle accessible without refocussing of the spectrograph camera.

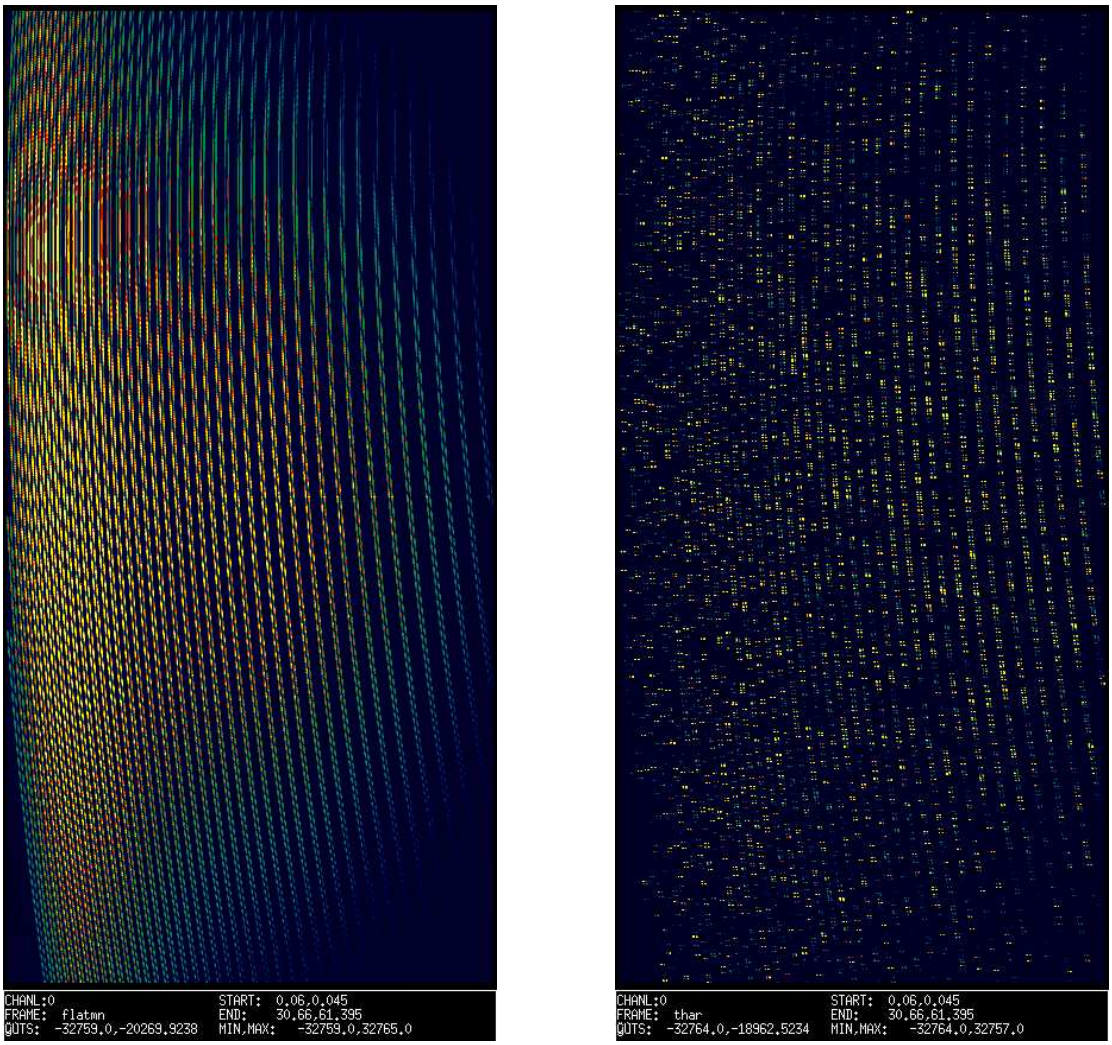

Figure 2.1: Simulated Flatfield and Thorium-Argon frames.

Figure 2.1 shows the simulated raw-data frames of a flatfield- and a wavelength-calibration through object and sky fiber. The simulation includes the efficiency of the instrument (cf. Sect. 2.3), the blaze function, the image slicer, the pixel sampling, and the wavelength dependent flux of the light sources.

2.3 Overall Efficiency

The efficiencies of the subcomponents of the instrument as well as the overall efficiency including the fibers and the CCD are given in Table 2.2. The column "Fibers" includes the micro lens, the fiber, the F/N lens and the image slicer. For these four components transmission values are taken from the glas, fiber, and coating data sheets; for the coupling efficiency of the fiber a value of 75% and for the efficiency of the image slicer a value of 90% is assumed. The values in

the column "Echelle" were measured in early 1996 by ESO. For the CCD the guaranteed minimum quantum efficiencies of the thinned and back-illuminated EEV chip are given.

Table 2.2: *Efficiency of FEROS. For details see text.*

λ	Fibers	Mirrors	Echelle	Crossd.	Camera	CCD	Total
(350)	0.50	0.24	0.73	0.55	0.70	0.50	0.017
370	0.52	0.52	0.73	0.79	0.80	0.58	0.07
400	0.56	0.92	0.73	0.90	0.85	0.72	0.21
450	0.57	0.94	0.73	0.91	0.85	0.85	0.26
500	0.58	0.96	0.73	0.91	0.85	0.85	0.27
600	0.59	0.94	0.73	0.89	0.85	0.85	0.26
700	0.60	0.94	0.73	0.88	0.85	0.78	0.24
800	0.60	0.92	0.73	0.87	0.85	0.55	0.16
900	0.60	0.92	0.73	0.86	0.85	0.28	0.08

Assuming these efficiencies and an efficiency of 60 % for the 1.52-m telescope, a spectrum of a $10^{\rm th}$ magnitude star can be taken in 15 minutes with a $S/N \approx 100$ per wavelength bin in V (Fig. 2.2). Within one hour for a star of $16^{\rm th}$ magnitude star still a S/N of 10 is reached. These numbers were derived assuming a slit length of 10 pixels, each pixel contributing with a read-out noise of $3\,{\rm e}^-$ and a dark current of $4\,{\rm e}^-$/h as given by the CCD characteristics.

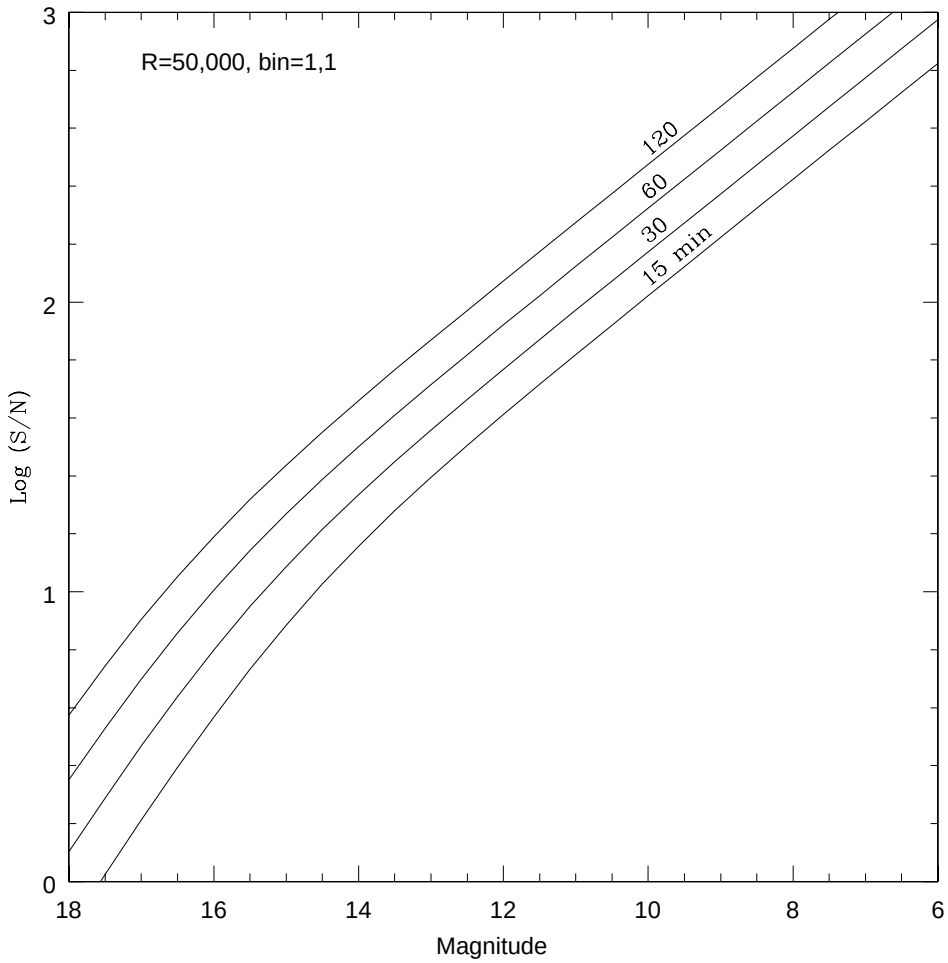

Figure 2.2: Reachable S/N ratio per wavelength bin for different exposure times.

Chapter 3: Optical Design

The schematic layout of the FEROS instrument is shown in Fig. 3.1. The system data for the complete optical system can be found in Appendix A.

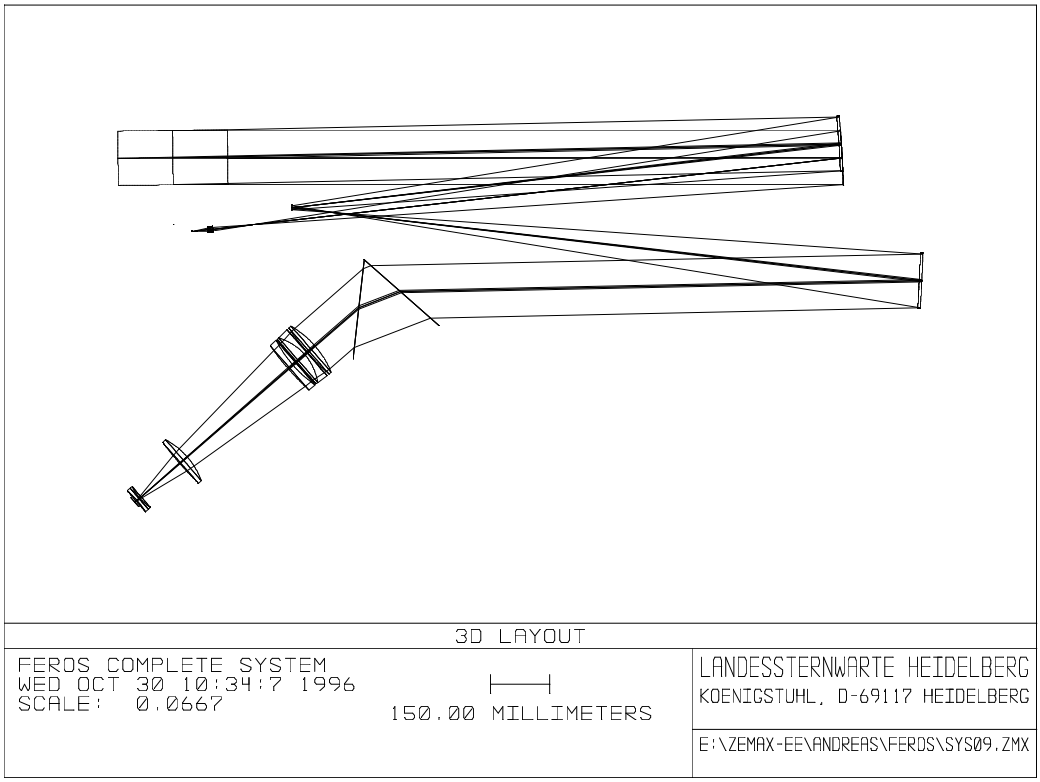

Figure 3.1: FEROS optical system from fiber exits to detector.

Two fibers are coupled to the Cassegrain focus of the telescope by micro lenses. In the coudé room, the fiber exit is converted to the F/11 focal ratio accepted by the spectrograph via a F/N lens system. A two beam, two-slice image slicer in the F/11 focal plane halves the width of the image of the fiber in the direction of dispersion. The fibers are re-imaged on the Echelle grating through the first collimator, the Main Collimator. Then, the light goes back to the Main Collimator and is reflected by the Folding Mirror to the second collimator, the Transfer Collimator. The entrance surface of the prism crossdisperser is located near the pupil image and the light is finally imaged by the dioptric camera on the detector.

The detector foreseen is a monolithic 4096×2048 15 μm pixel CCD aligned with the long side in direction of dispersion.

The beam of the spectrograph is 136 mm. The fiber input/output focal ratio is F/4.6, the collimators focal ratio is F/11 and that of the camera is F/3.

3.1 Micro Lenses and Fibers

The spectrograph is fed by two fibers simultaneously. At the Cassegrain focus (F/15) of the ESO 1.52-m telescope 1 arcsec corresponds to 109 μm. A micro lens in front of the fibers is needed to preserve an efficient coupling of the spectrograph to the telescope. The micro lens converts the F/15 beam from the telescope to a F/4.6 beam for the coupling into the fibers and acts as a focal reducer. With a fiber of 100 μm diameter, only 90 μm of the fiber core is used due to the micro lens. This gives an effective aperture projected on the sky of 2.7 arcsec.

At the fiber exit, the fibers will be mounted on a plate with 0.38 mm separation. This results in a separation of 16 pixel on the detector.

3.1.1 Micro Lenses

The micro lens dimensions are shown in Fig. 3.2.

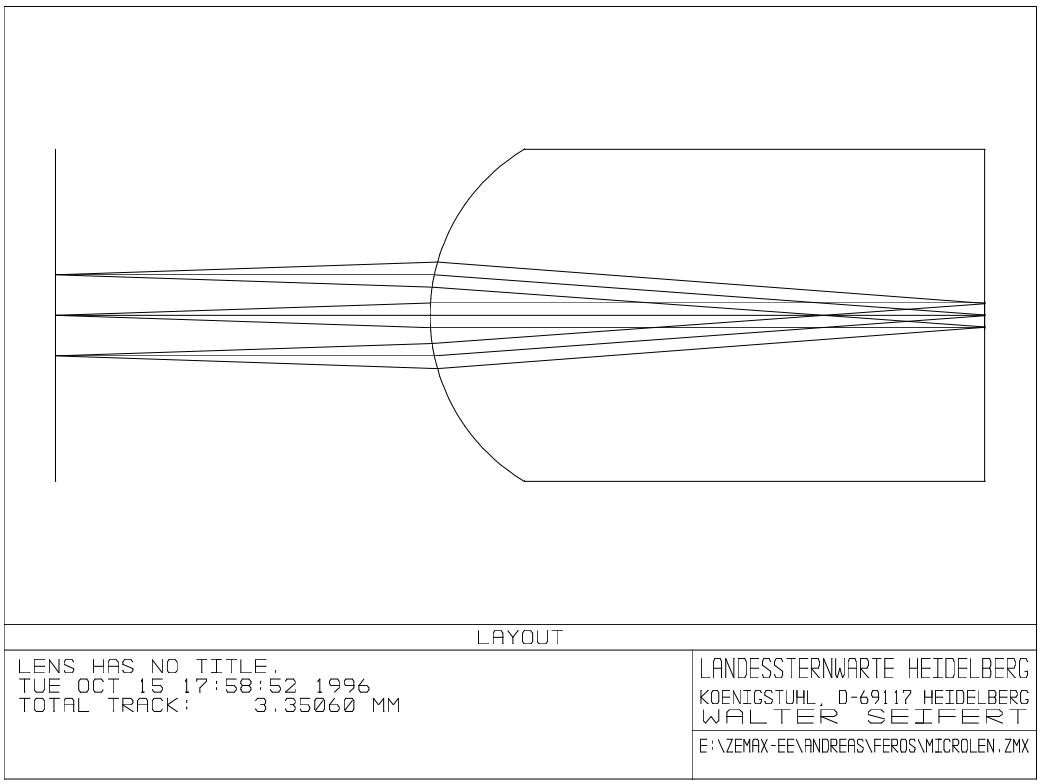

Figure 3.2: Entrance micro lens layout. The lens is made of BK7, the curvature radius of the entrance surface is 0.7 mm, thickness is 2 mm, diameter is 1.1 mm.

The design is optimized for having a 90 μm pupil on its exit surface. The lens will be made of BK7. The internal transmission losses are negligible; for the entrance surfaces of the microlenses, a multilayer anti-reflection coating (Balzers SuperTriolin) is used (cf. the transmission curve in Fig. 3.17, Sect. 3.9.2).

3.1.2 Fibers

As fibers, the CeramOptec OPTRAN WF 100/110 P fiber with 100 μm core diameter will be used. The length of the fibers will be about 12 m. The transmission as a function of wavelength was measured for a 200 μm fiber by ESO [G. Avila et al., 1996, FUEGOS status report, Fig. 1].

According to Fig. 6 from [Guerin and Felenbock, 1988, in 'Very Large Telescopes and their Instrumentation', p. 1131], the efficiency (due to the focal ratio degradation) should be about 75% for an input/output F/4.6.

3.2 F/N Adaption Lens System

The lens system which converts the F/4.6 output beam of the fibers to the F/11 beam required by the spectrograph is shown if Fig. 3.3.

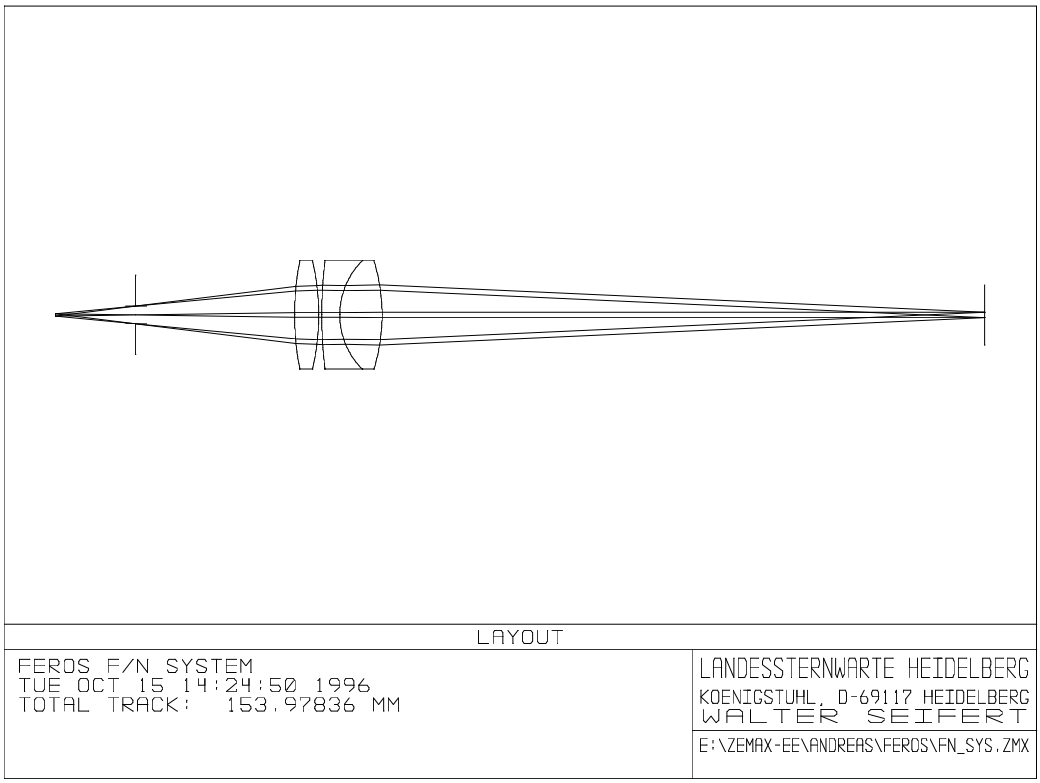

Figure 3.3: F/N Adaption Lens System: The lens system has 3 lenses in two groups made of FK54 and LLF6. The total length of this preslit system is 154 mm.

The lens system has 3 lenses in two groups made of FK54 and LLF6. The surface data are as follows:

Surf	Type	Radius	Thickness	Glass	Diameter
OBJ	STANDARD	Infinity	13.3		0.376
STO	STANDARD	Infinity	26.3		2.9
2	STANDARD	46	4	FK54	18
3	STANDARD	−39.6	0.5		18
4	STANDARD	73.1	3	LLF6	18
5	STANDARD	12.7	7	FK54	18
6	STANDARD	−31	99.87836		18
IMA	STANDARD	Infinity	0		10

The total length of this preslit system is 154 mm. The polychromatic image degradation is small compared to the projected diameter of the fiber ($240\,\mu$m). The lenses will be coated with the multilayer coating from Fa. Tafelmaier, which is described in Section 3.9.2. With this, the efficiency should be better than 95%. The spot diagrams of this optics is shown in Fig. 3.4.

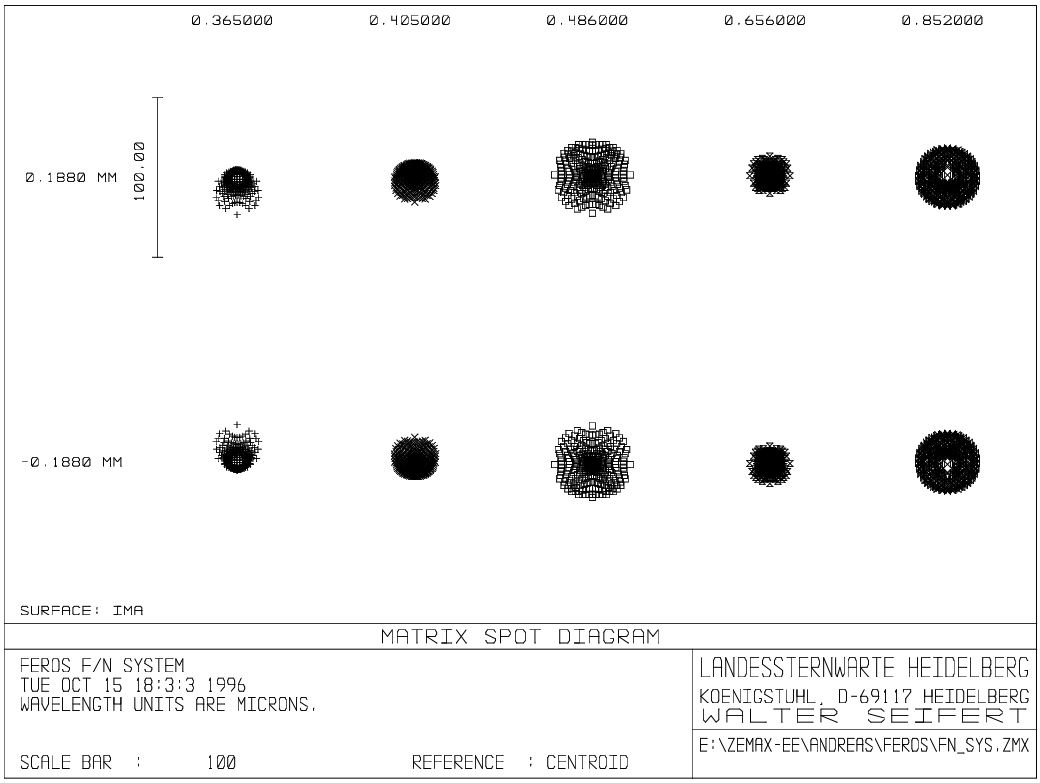

Figure 3.4: Spot diagrams of the F/N Adaption Lens System.

The axes of the two fibers are concentric to a stop placed 13.3 mm ahead. With a fiber output of F/4.6, the diameter of the stop is 2.9 mm. It will be re-imaged on the echelle grating. The separation of the slits on the F/11 side is 0.9 mm.

3.3 Image Slicer

A Bowen-Walraven two-beam, two-slice image slicer is placed at the position of the F/11 focus of the F/N lens system. It produces two slices (half moons) of the projected fiber images with half the width of the original image in the direction of dispersion and 2.25 times the original height in the crossdispersion direction. The design of the image slicer is shown in Figs. 3.5 and 3.6.

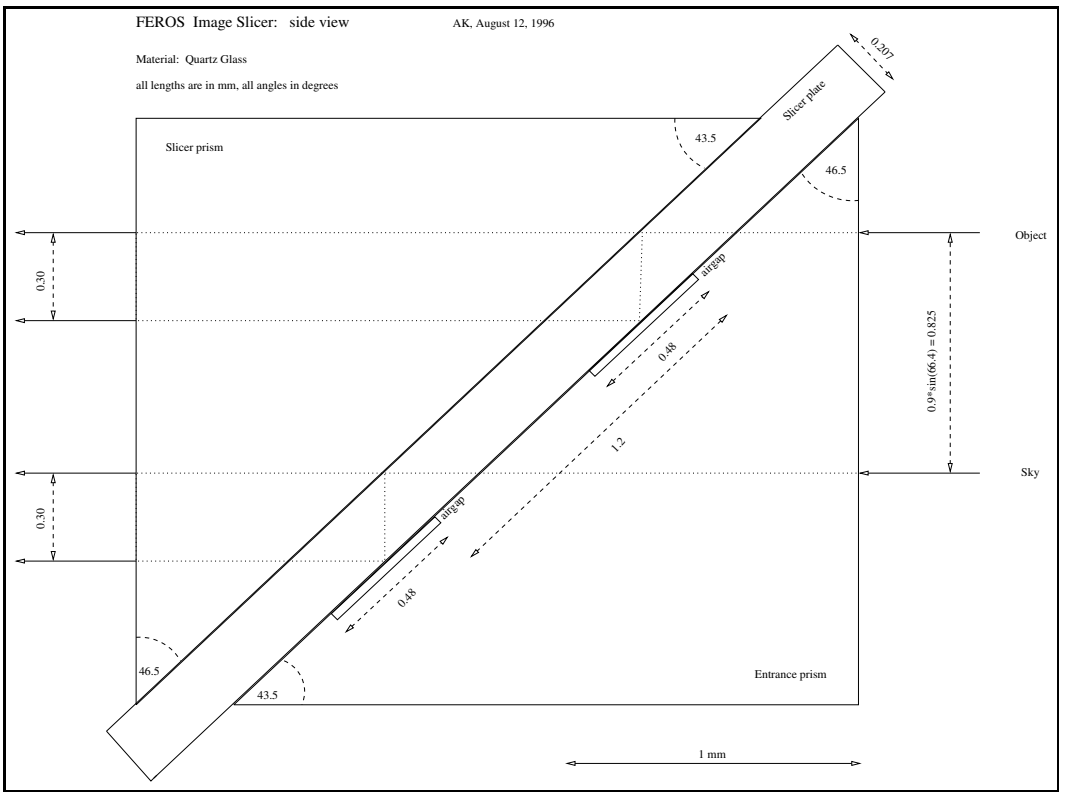

Figure 3.5: Layout of the Image Slicer (side view).

The geometry and principal function of this image slicer has been tested with a 15:1 scaled model made from Acrylic. Figure 10.2 shows the outputs of the sliced and unsliced object and sky beams.

All parts of the image slicer are made of Homosil having a low thermal expansion coefficient and high transmission. To fulfil the conditions for total reflection for Homosil – air in the complete wavelength range of the instrument, a prism angle of 46.5° was chosen. The base prism and the slicer plate are connected by optical contact; the slicer prism is cemented to the slicer plate. The entrance prism has two air gaps to preserve the total internal reflection necessary for the second slice of both fiber images.

The different optical path length of the two slices causes a defocussing. This will result in a blur on the detector of about 0.3 pixel, which is not critical concerning

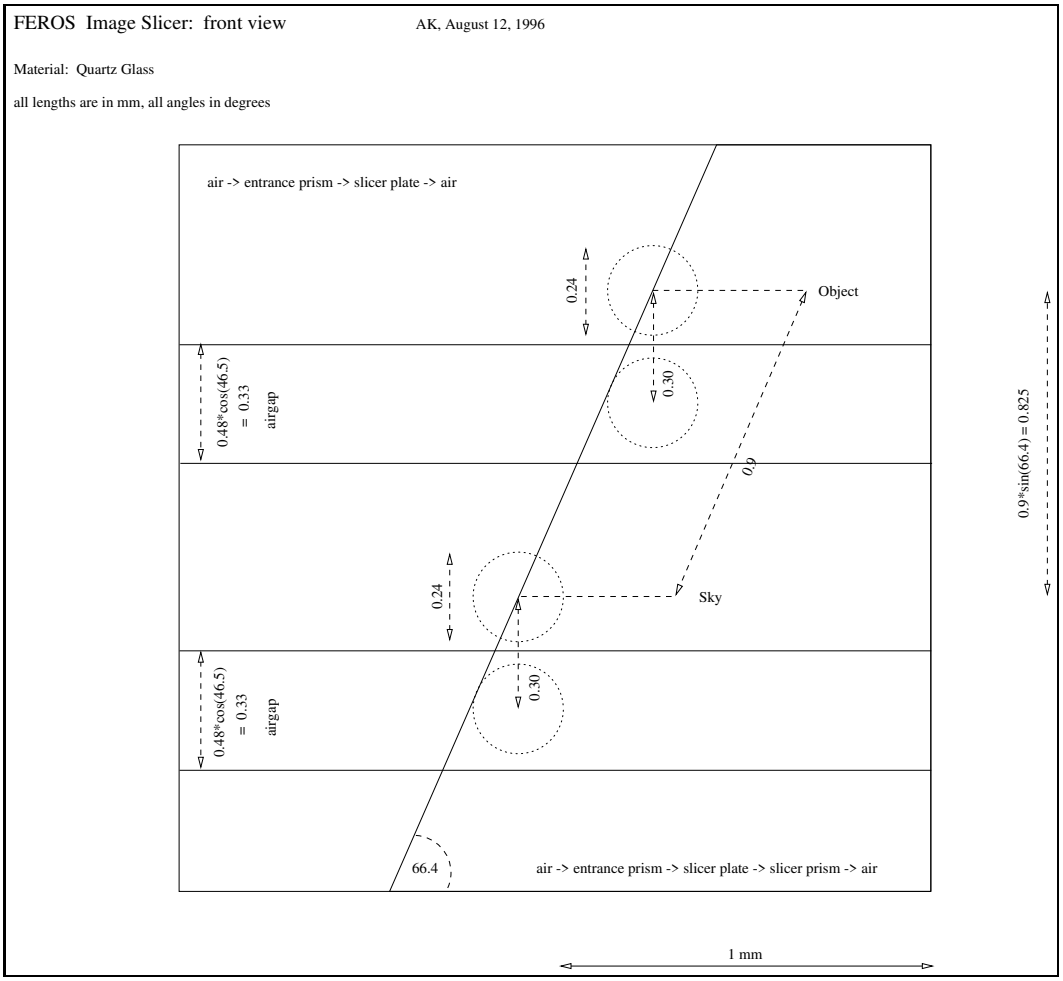

Figure 3.6: Layout of the Image Slicer (front view).

the spectral resolution. The width of the resulting slit corresponds to 2 pixels on the detector, its height will be about 10 pixels. Thus the separation between the object and the sky spectra will be 6 pixels.

AR coated Homosil plates will be glued on the entrance and exit surfaces of the image slicer to form a dust and humidity tight unit (cf. Fig. 4.5). The coating used is the Tafelmaier multi-layer broad-band coating (cf. Fig. 3.17, Sect. 3.9.2). The over-all performance and efficiency of the image slicer will be investigated in detail on a prototype, but the efficiency is expected to be higher than about 80%.

3.4 Collimators

The collimators are two off-axis paraboloids in symmetrical mountings. They are segments of the same paraboloid with a focal length of 1500 mm and a diameter of 660 mm, i.e., an effective focal ratio of F/2.2. The dimensions of the mirrors are given in Fig. 3.7.

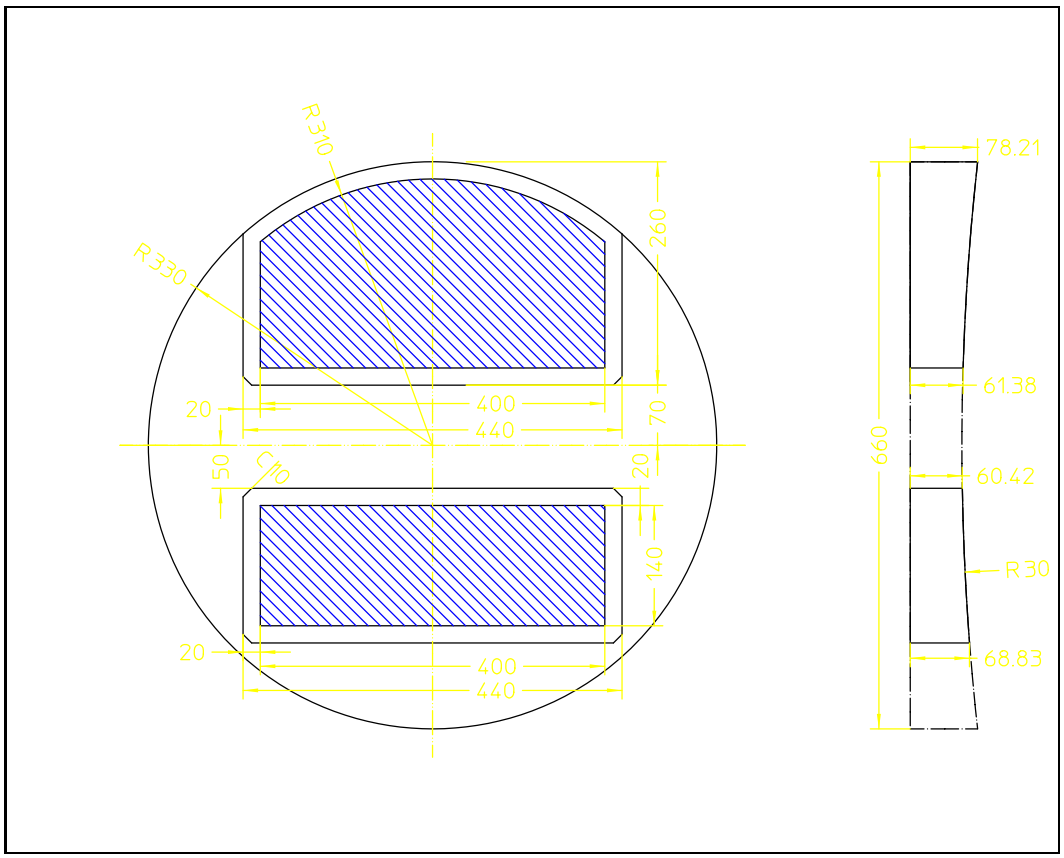

Figure 3.7: Layout of the off-axis paraboloid collimators (top: Main Collimator, bottom: Transfer Collimator).

The mirrors will be made of Zerodur. The wavefront distortion should be less than $\lambda/15$ (at 633 nm) over the diameter of the collimated beam. The micro roughness should be less than 25 Å rms (corresponding to '3 Rauten' polishing, DIN 3140). The coating foreseen for the mirrors is described in Section 3.9.1.

3.5 Flat Folding Mirror

The flat Folding Mirror will be located at a distance of about 100 mm from the intermediate focus. This gives a diameter of an individual beam on its surface of about 9 mm. The dimensions of the mirror are given in Fig. 3.8.

This mirror will also be made of Zerodur. The wavefront distortion should be less than $\lambda/15$ (at 633 nm) over 15 mm. The flatness should be better than $\lambda/8$. The micro roughness should be less than 25 Å rms (corresponding to '3 Rauten' polishing, DIN 3140). The coating foreseen is described in Section 3.9.1.

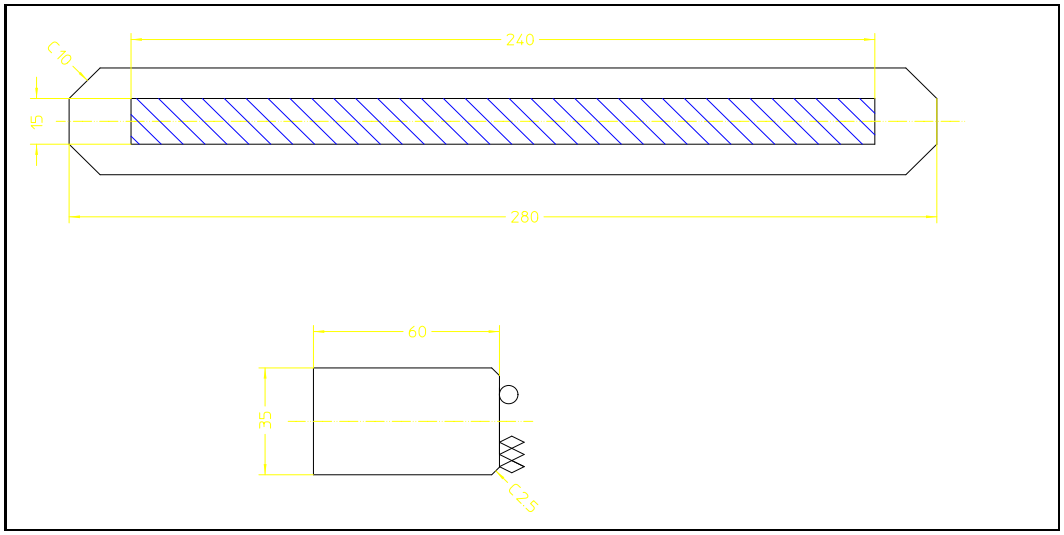

Figure 3.8: Layout of the flat folding mirror.

3.6 Echelle Grating

The R2 echelle grating with 79 lines/mm is contributed by ESO. According to ESO document VLT-VTE-96/2152 (Echelle #1, catalogue no. Bausch & Lomb: 35.13.44.401) the measured blaze angle is $63°24'$. It is used at this angle in Littrow mode. The beam is reflected with an angle of 1.2° in the direction perpendicular to the dispersion. The useful area is 154 mm by 306 mm. The reflectivity measured in early 1996 is almost constant with 73% over the wavelength range $300 - 1000$ nm (cf. Fig. 3.9). Two blemishes on two corners and one scratch of 4 cm length are visible, the latter partially affecting the optically active surface (which is an ellipse with 136×303 mm).

3.7 Crossdisperser

A prism as crossdisperser allows the full coverage of the free spectral range with high efficiency and without any second-order contamination. On the other hand, the prism dimensions get very large for the required order separation of 30 pixels between the reddest orders. Thus a high homogeneity of the glass, low stress birefringence, and a good surface quality are required. The entrance surface of the prism will be located at the instrument pupil to minimize the size of the prism.

The crossdisperser consists of a large prism made of LF5 in PH3 quality with an apex angle of 55° working at minimum deviation. The layout is shown in Fig. 3.10.

The transmitted wavefront error will be $\lambda/4$ at 633 nm. The efficiency of the crossdisperser is given in Section 3.12. The entrance and exit surfaces of the prism will be coated with the SuperTriolin multi-layer broad-band coating by

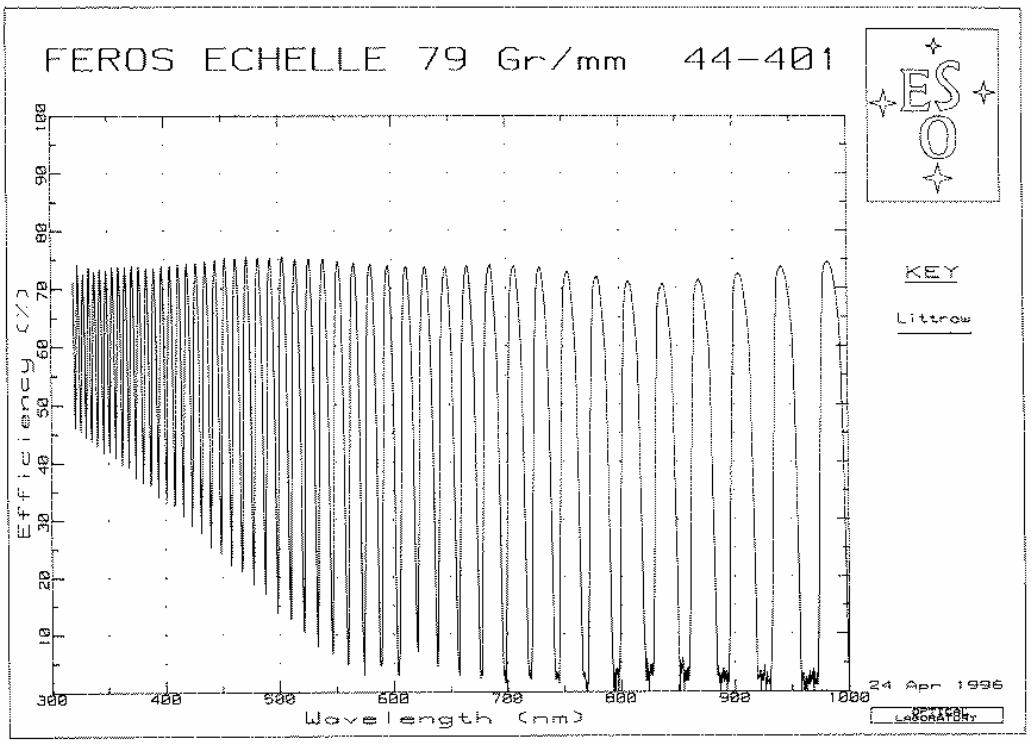

Figure 3.9: Measured efficiency of the FEROS echelle grating 35.13.44.401.

Balzers (cf. Fig. 3.17) optimized for the used wavelength range and 45° angle of incidence.

3.8 Camera

3.8.1 General

The design of the camera given in our 'FEROS Proposal' was derived from the design given in the 'FEROS Conceptual Design' by doubling the focal length while preserving the entrance aperture. The FEROS camera presented here was designed by B. Delabre at ESO and was reduced to 7 lenses in 5 groups. The camera field lens will act as entrance window of the dewar, and the front part of the camera will be moved relatively to this to provide focussing. The clearance between the back surface of the camera field lens and the detector is 4.5 mm.

3.8.2 Optical Characteristics

The optical layout is shown in Fig. 3.11.

The fabrication data for the optics are given here:

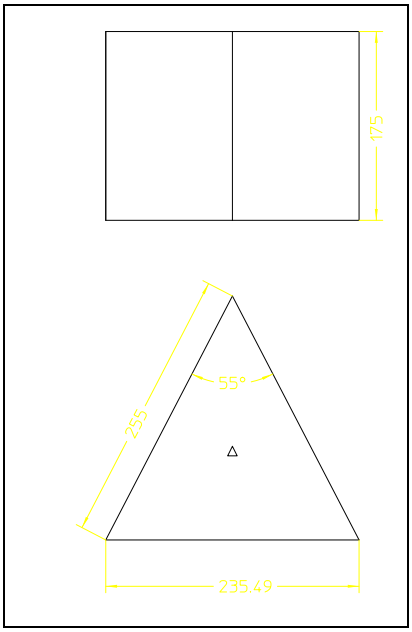

Figure 3.10: Layout of the LF5 prism crossdisperser.

Surf	Type	Radius	Thickness	Glass	Diameter	Cyl.Rad.
OBJ	STANDARD	Infinity	Infinity		0	
STO	STANDARD	Infinity	-100		136	
2	STANDARD	-240.7799	-25	CAF2	158	
3	STANDARD	622.6922	-1		158	
4	STANDARD	-4761.222	-8	PSK3	158	
5	STANDARD	-139.2893	-30	FK54	153	
6	STANDARD	1003.717	-10		153	
7	STANDARD	313.5372	-15	BK7	153	
8	STANDARD	711.9877	-340.4111		153	
9	STANDARD	-195.9967	-25	FK5	141	
10	STANDARD	1020.826	-134.3647		141	
11	STANDARD	135.6392	-2	LAK16A	74	
12	STANDARD	Infinity	-10	SILICA	74	
13	TOROIDAL	Infinity	-4.5		74	230.7881
IMA	STANDARD	Infinity	0		69.95755	

The camera field lens includes a cylindrical surface on its back side (surface 13) with a radius of 230.79 mm. The main optical characteristics of the FEROS camera are summarized in the following table:

Focal length:	410 mm
Entrance aperture:	155 mm
Effective focal ratio:	3.0
Field diameter:	68.7 mm, 9.6°
Axial colour correction:	$350 - 900$ nm
Lateral colour correction:	none

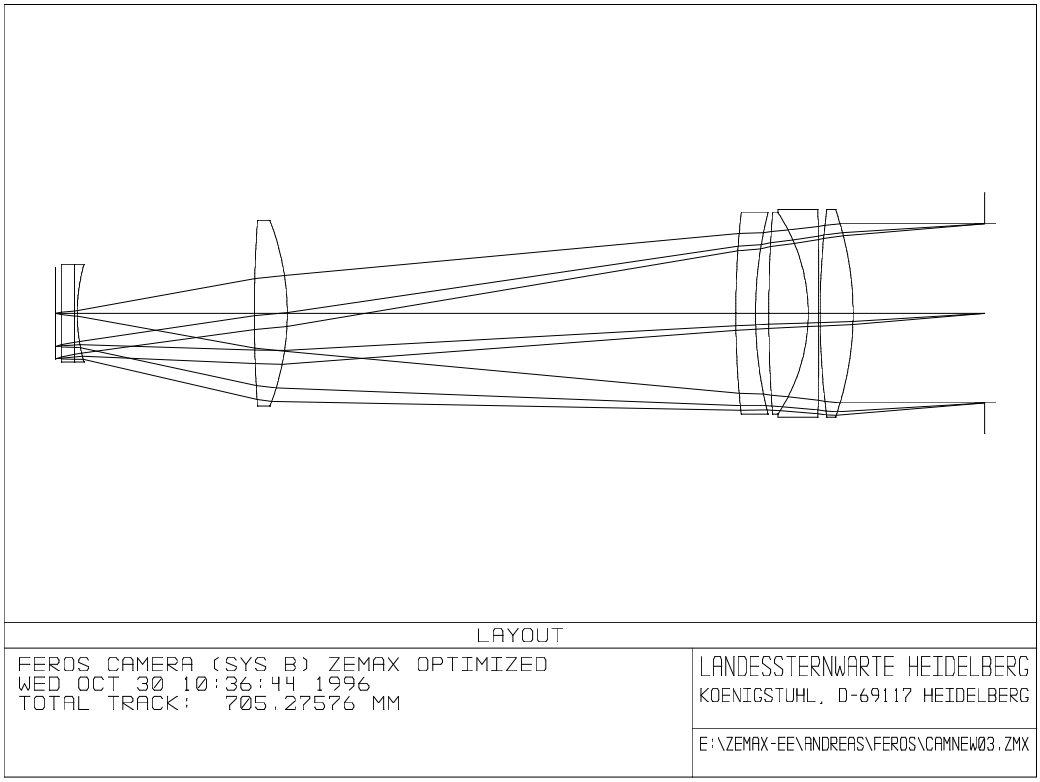

Figure 3.11: Layout of the FEROS camera.

3.8.3 Image Quality

The computed image quality is given in the following figures:

Fig. 3.12 80% energy concentration without the cylindrical field lens
Fig. 3.13 Polychromatic encircled energy without the cylindrical field lens
Fig. 3.14 Spot diagrams without the cylindrical field lens

3.8.4 Transmission

The camera uses CaF_2, FK54 and Silica to optimize the blue transmission. The coating proposed (see Section 3.9.2) will be applied to all glass – air surfaces and is efficient all over the free spectral range ($R \leq 1.5\%$). The theoretical transmission was computed with this coating and the values given in the glass catalog and is shown in Fig. 3.15. In the transmission table in Section 3.12, lower limit values are given.

A slight vignetting will occur for the extreme orders and wavelengths due to the decentering of the beam leaving the crossdisperser prism. According to our image analysis, vignetting should be less than 10% in the worst case. The exact amount depends on the necessary separation of the camera from the prism exit surface.

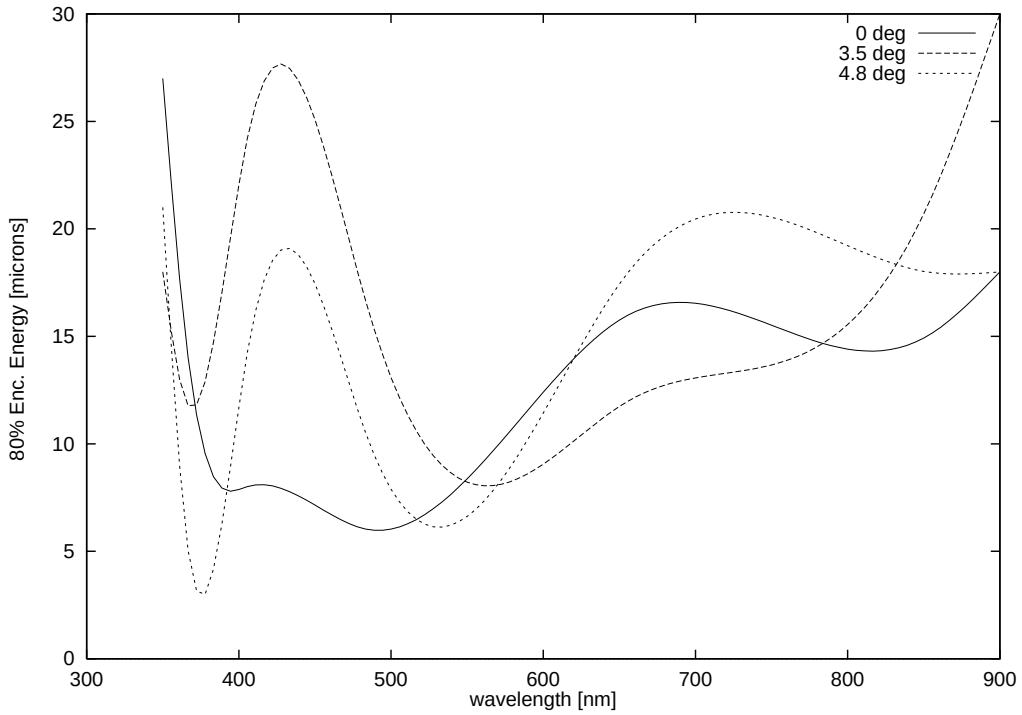

Figure 3.12: Diameter of 80% encircled energy of the FEROS Camera (without the cylindrical field lens). Two pixels are $30\ \mu$m.

3.8.5 Environmental Sensitivity

The operating range of the camera will be 10 to 20°C. It will be used in a thermally controlled environment (16 $\pm$ 0.5°C). The camera has to be refocussed by 20 μm per 1°C variation of the temperature. The effective degradation of the resolution for $\pm$ 1°C temperature variation without refocussing will be less than 15% for 2 pixel resolution. The maximum resolution degradation after applying a temperature step of 1°C without refocussing should be less than 20%. This is a worst case estimate, as an infinite thermal time constant was assumed for this investigation.

The thermal stability of the camera will be enhanced by introducing a self compensation. Based on the computed values above, a 20 cm Delrin rod (TCE= $100 \cdot 10^{-6}$) will be necessary.

The designing was done for sea level conditions. For a reduction of the ambient pressure to La Silla level (0.75 atm) a refocussing by $80\ \mu$m is required.

3.8.6 Focussing, Centering

The camera will be refocussed manually by changing the separation of the camera with respect to the camera field lens. The relative centering of these two components has to be better than 50 μm for decentering and 1 arcmin for tilt. For the

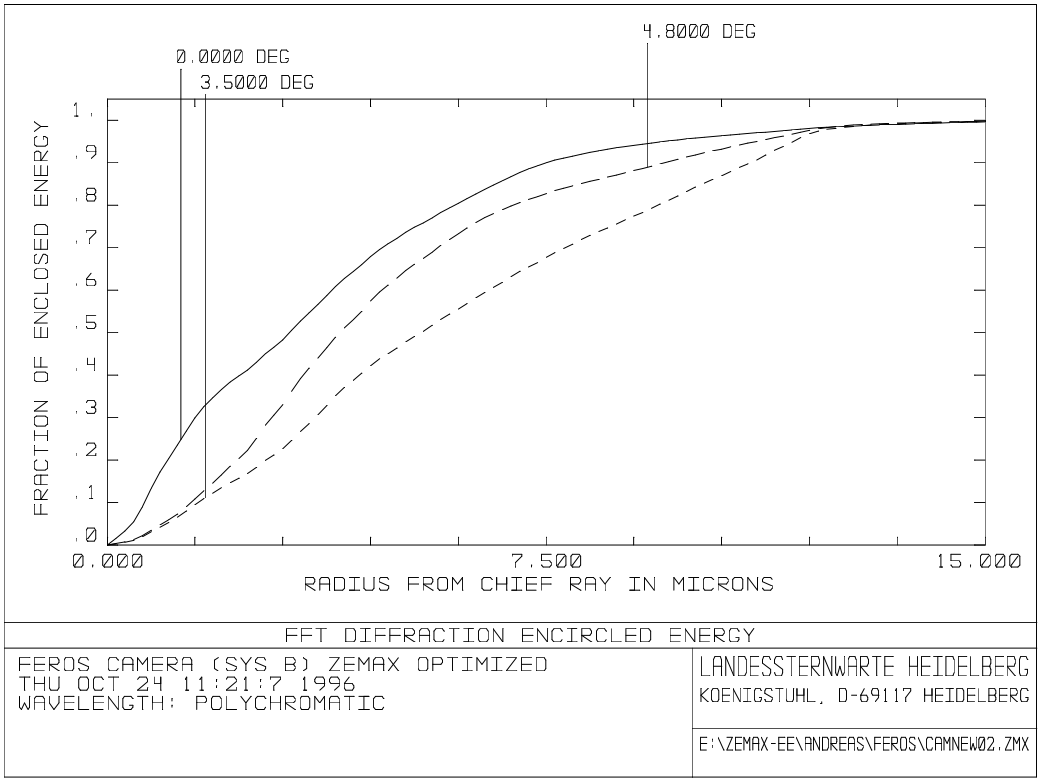

Figure 3.13: Polychromatic encircled energy of the FEROS Camera (without the cylindrical field lens) for 3650, 4860, and 8520 Å as function of the distance from the chief ray. The maximum radius is the size of one pixel ($15\,\mu$m). Therefore, $> 80\%$ of the energy are within 2×2 pixels.

centering precedure, a removable auxiliary tube between focussing unit and field lens is used.

3.8.7 Ghost Image and Sky Concentration Analysis

The computation for this investigation was made with paraxial rays and does not include vignetting. The size of ghost images for an on-axis star are given in the following upper table. This shows no evidence for bright ghosts, the relative intensity of the superposition of all ghosts will be about 10^{-5}. In the lower table, the position of the ghost image of an off-axis star located in the corner of the detector (34.5 mm from the center) is given. If this value is small, an image of the pupil is formed close to the CCD and if the corresponding value in the upper table is also small, then the reflected light will be concentrated on the detector. No evidence for a significant sky concentration arises from the computed values.

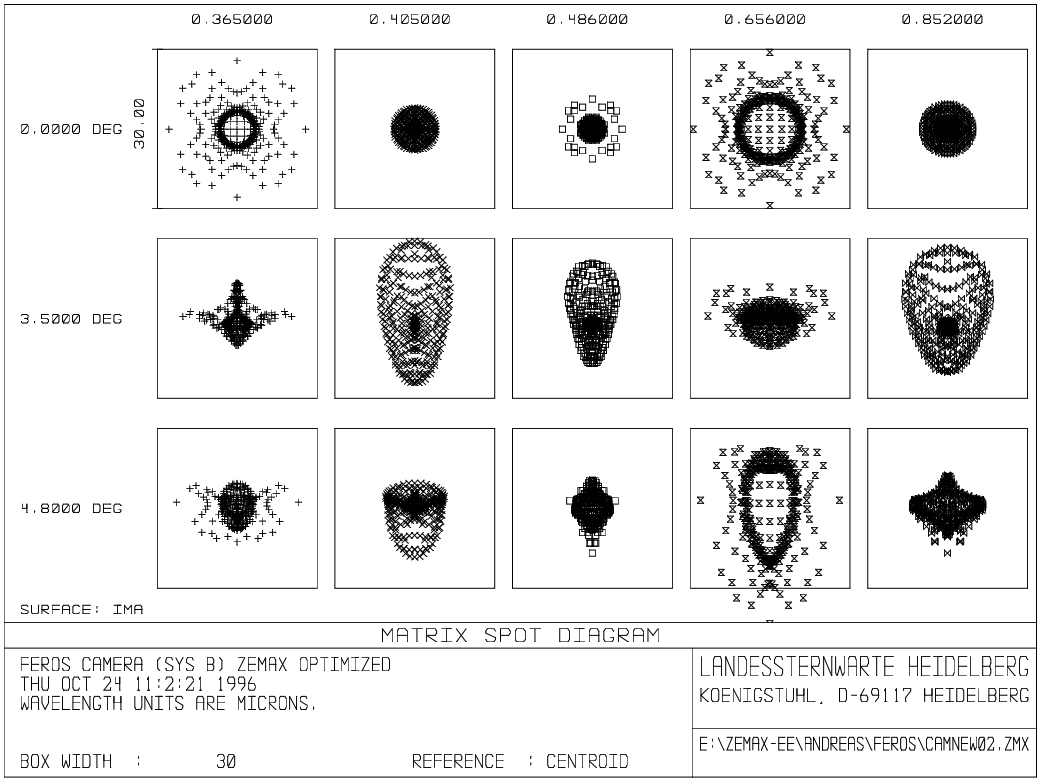

Figure 3.14: Spot diagrams of the FEROS Camera (without the cylindrical field lens). The box size is 2×2 pixels.

Size of ghost images:

	2	3	4	5	6	7	8	9	10	11	12	13
3	414											
4	329	98										
5	106	660	29									
6	321	23	169	27								
7	350	118	74	26	111							
8	269	29	223	32	8	101						
9	381	393	91	19	283	441	228					
10	270	359	85	26	263	381	214	74				
11	269	260	145	27	187	297	150	**16**	64			
12	203	197	191	35	141	224	113	12	48	0.2		
13	220	208	185	33	149	239	120	17	55	2.8	2.2	
CCD	231	216	180	32	154	248	124	21	60	4.8	3.7	1.5

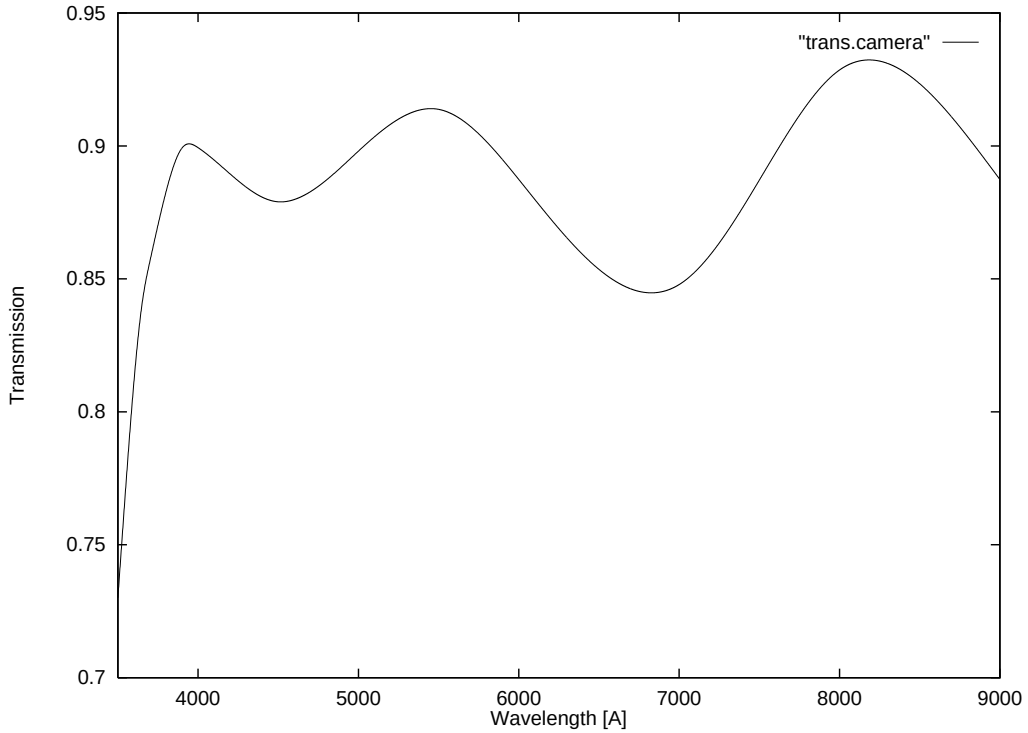

Figure 3.15: Total transmission of the FEROS Camera (with the cylindrical field lens).

Position of ghost images:

	2	3	4	5	6	7	8	9	10	11	12	13
3	31											
4	19	50										
5	44	139	121									
6	40	48	29	75								
7	54	23	5	92	15							
8	51	59	35	96	43	64						
9	781	843	485	1460	609	936	492					
10	124	219	144	254	163	221	133	83				
11	693	724	411	1290	522	810	421	**7.6**	130			
12	425	341	170	765	240	410	191	90	147	46		
13	439	350	174	789	247	422	197	95	153	48	37	
CCD	448	356	177	805	251	430	200	97	156	50	38	36

3.9 Coatings

3.9.1 Mirrors

Due to the large number of reflections (4) in the spectrograph the mirrors will be coated with a high-reflectivity coating in the spectral range from 350 nm to 900 nm.

For all reflecting surfaces (2 collimators and flat folding mirror) the Balzers Silflex VIS single-layer coating will be used. For this type of coating we do not expect any problems with the high angles of incidence on the off-axis paraboloids. The reflectivity of this coating is shown in Fig. 3.16.

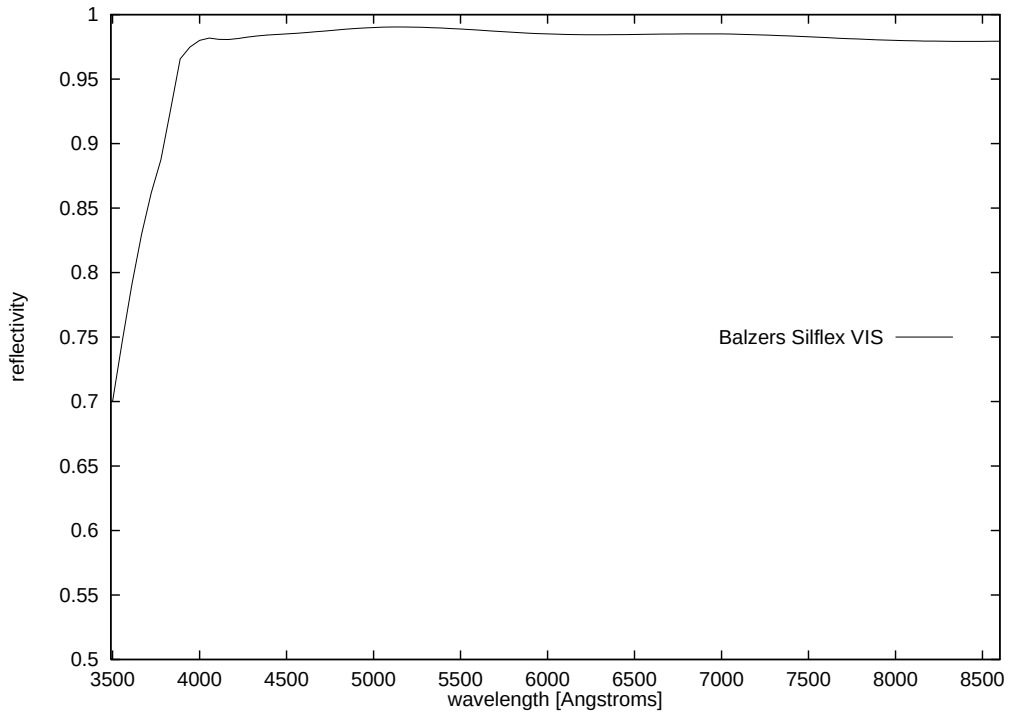

Figure 3.16: Guaranteed reflectivity of the single-layer mirror coating Silflex VIS from Balzers.

3.9.2 Lenses

The lenses of the F/N system and the entrance and exit surfaces of the image slicer will be coated with a multi-layer anti-reflection coating by Fa. Tafelmaier. The micro lenses, the crossdisperser prism, and the camera lenses will be coated by Balzers with optimized SuperTriolin multi-layer coatings.

The transmission of both coatings is shown in Fig. 3.17 for a low index glass. The average reflection losses will be about 1.5% per surface.

3.10 Straylight

A detailed straylight analysis of the instrument has not been and will not be carried out. As the camera cannot see directly neither the collimators nor the grating, straylight and lateral orders should be well suppressed. As the entrance

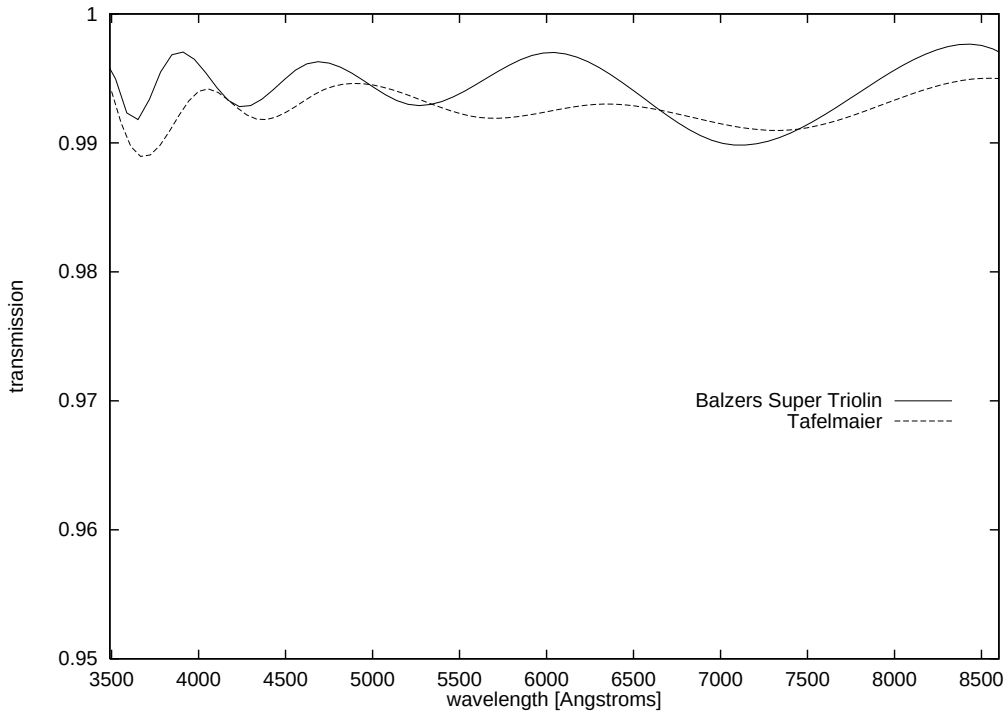

Figure 3.17: Transmission curves of the multi-layer lens coatings. The Balzers coating is measured on low-index glass ($n = 1.46$); the Tafelmaier curve is computed for a low-index glas ($n = 1.46$).

surface of the crossdisperser is near the pupil, a baffle could be implemented at this location. Further baffles will be introduced near the echelle grating.

Nevertheless, the tolerable amount of micro roughness of the mirrors and the lenses was estimated with respect to stray light.

3.10.1 Mirrors

According to Fig. 2 from [Elson, Bennett and Bennett, 1979, in 'Applied Optics and Optical Engineering', Vol. 7, p. 191], the amount of scattered light into one hemisphere will be up to about 1% per surface at the short wavelength limit of 350 nm for polishing with 25 Å rms micro roughness (i.e. '3 Rauten', DIN 3140). This means that up to 3% of the incoming light is scattered by the collimators and the folding mirror. But as this amount is scattered into one hemisphere each time, it is not critical concerning interorder straylight. It will only cause a loss in effective transmission.

3.10.2 Lenses

According to [Bennett, 1988, Optical Engineering, Vol. 17], the amount of scattered light into one hemisphere is less than about 1% for all glass – air surfaces

in the spectrograph at 350 nm with normal polishing. This amount is not critical (see previous Section).

3.10.3 Echelle Grating

The echelle grating will give the most serious contribution to the total interorder stray light. The amount of straylight has not been measured yet. The straylight will be partially blocked from the system via baffles in the echelle mounting.

3.11 Optical Tolerances for the Alignment of the CCD

The tolerances for the alignment of the 2kx4k CCD are given in the following table:

Flatness of detector	$\leq \pm$ 20 μm
Tilt (optical axis)	$\leq$ 1 arcmin
Distance to field lens	$\leq \pm$ 50 μm

3.12 Overall Efficiency of the FEROS Instrument

The efficiencies of the subcomponents of the instrument as well as the overall efficiency including the fibers and the CCD are given in the following table. The column "Fibers" includes the micro lens, the fiber, the F/N lens and the image slicer. For these four components transmission values are taken from the glas, fiber, and coating data sheets; for the coupling efficiency of the fiber a value of 75% and for the efficiency of the image slicer a value of 90% is assumed. With the image slicer prototype, the efficiency of the unit micro lens, fiber, F/N-system, and image slicer will be measured a.s.a.p. at ESO. The values in the column "Echelle" are taken from ESO document VLT-VTE-96/2152 (Echelle #1, catalogue no. Bausch & Lomb: 35.13.44.401). Cf. also Fig. 3.9. For the CCD the guaranteed minimum quantum efficiencies of the thinned and back-illuminated EEV chip are given.

λ	Fibers	Mirrors	Echelle	Crossd.	Camera	CCD	Total
(350)	0.50	0.24	0.73	0.55	0.70	0.50	0.017
370	0.52	0.52	0.73	0.79	0.80	0.58	0.07
400	0.56	0.92	0.73	0.90	0.85	0.72	0.21
450	0.57	0.94	0.73	0.91	0.85	0.85	0.26
500	0.58	0.96	0.73	0.91	0.85	0.85	0.27
600	0.59	0.94	0.73	0.89	0.85	0.85	0.26
700	0.60	0.94	0.73	0.88	0.85	0.78	0.24
800	0.60	0.92	0.73	0.87	0.85	0.55	0.16
900	0.60	0.92	0.73	0.86	0.85	0.28	0.08

3.13 Spot diagrams of the complete FEROS system

The spot diagrams of the complete FEROS system from fiber exit to detector (excluding the image slicer) are shown in the following figure. The box size is 2×2 pixels.

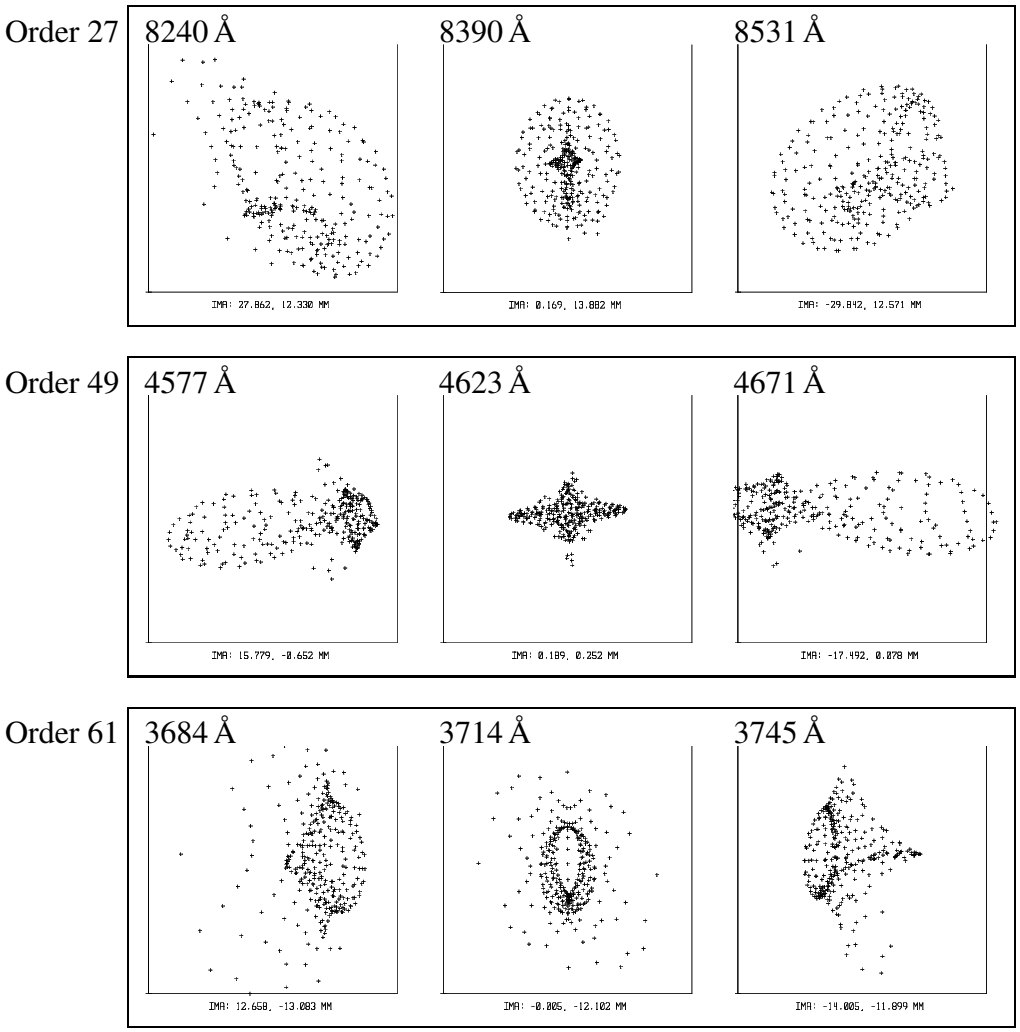

3.14 Image analysis of the complete FEROS system

An image analysis of the complete FEROS system has been performed with the following parameters:

- image size: 0.225 mm (image slicer moved to image plane)
- field position: 0.0 (center of obj. and sky)
- vignetting (in percent, upper right corner) is due to camera entrance (diam = 155 mm)
- length of scale bar: 0.225 mm = 15 pixels
- the tilt ω of the image is due to the tilt $\gamma = 0.6^o$ of the echelle grating with $\tan\omega = 2\tan\theta_b \tan\gamma$ and $\tan\theta_b = 2$ follows $\omega = 2.4^o$.

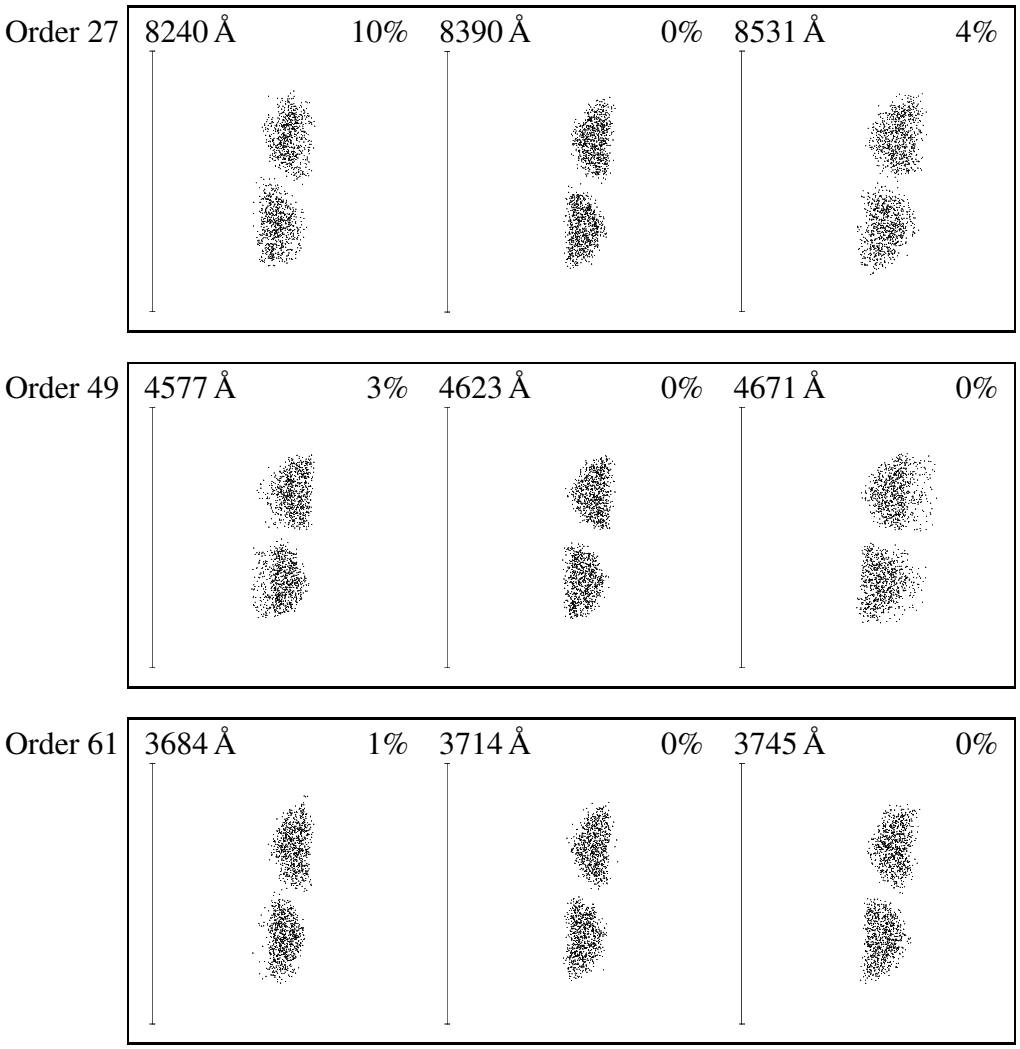

Chapter 4: Mechanical Design

4.1 General description

The mechanical parts of the spectrograph include:

- Vibration isolated optical bench
- Fiber entrance with fiber connectors
- Fiber link
- Fiber-exit unit with F/N system and image slicer
- Collimators and Folding Mirror supports
- Echelle grating support
- Crossdisperser prism support
- Camera housing with focussing unit, Shutter and CCD continuous-flow dewar on common support
- Removable enclosure

Figure 4.1 gives a top view on the bench-mounted part of the FEROS spectrograph. The set of detailed drawings of all components discussed in this chapter can be found in Appendix B.

4.1.1 Movable parts

During operation of the spectrograph no component has to be moved on the optical bench. A turning of the crossdisperser prism between to fixed positions in principle allows a change between two spectral ranges (default: $3700 - 8700$ Å, optional: $3500 - 6800$ Å). The reproducibility of this operation will be tested on the completed instrument. If the change of the spectral range still allows a fully automatic on-line reduction and does not degrade the long-term radial-velocity accuracy of the instrument, this feature could be offered to the user.

No focussing of the camera will be necessary in the thermally controlled environment. Further the camera is thermally stabilized and can compensate temperature variations up to ± 5 degrees.

The only remotely (i.e. electronically) controlled part of the system will be the shutter operated by the CCD controller.

4.1.2 Materials and Painting

Aluminum and stainless steel are used as materials for all mechanical components. With the thermal stabilization of the instrument no effects due to differential expansion are expected.

Mountings directly glued to Zerodur/Quarz-glass surfaces are made of Invar.

All mechanical components are foreseen to be black anodized. The highly reflective table top will be covered with a self-adhesive black velvet foil. For the baseplates of the components respective cuttings are foreseen.

4.1.3 Kinematic mounts

For each of the optical components Collimator 1 (Main Collimator), Collimator 2 (Transfer Collimator), and the Echelle a kinematic mount will be realized with 6 adjustable axial supports. These supports will be glued to the Zerodur/Quarz-glass components via 6 Invar plates. No Invar inserts are foreseen anymore because of the risk of drilling mounting holes into the components. The Invar plates will be glued to the glas surfaces with 3M Scotch-Weld 2216 B/A. The Invar plates are removable by screwing M3 screws into the three foreseen holes.

4.1.4 Miscellaneous

The optical axis of the spectrograph runs parallel to the optical table's surface in the whole instrument. The distance of this axis to the table top is 270 mm. It is defined by the components with the largest height (optics + supports), i.e. the Collimators.

Therefore, all mechanical components will have to be mounted on adequate aluminum basements. The ground plate of the basements will be positioned within ± 1 mm to their computed positions and clamped to the optical table. The positions of the basements are adjustable according to the requirements of the individual components.

For the adjustment of the components, a minimum of different tools is used. Most of the adjustments can be performed with two wrenches, one to turn the adjustment screw, the second to fix the screw with a nut.

The metric 25×25 mm grid of sealed M6 mounting holes on the optical tables is used as reference system.

The following nomenclature for the coordinate systems is used below:

coord.system	axis	direction
table system:	X	along the long table axis
	Y	along the short table axis
	Z	perpendicular to the table surface
optical system:	x	main dispersion, perpendicular to table surface ($\parallel$ Z)
	y	cross dispersion direction
	z	along the local optical axis

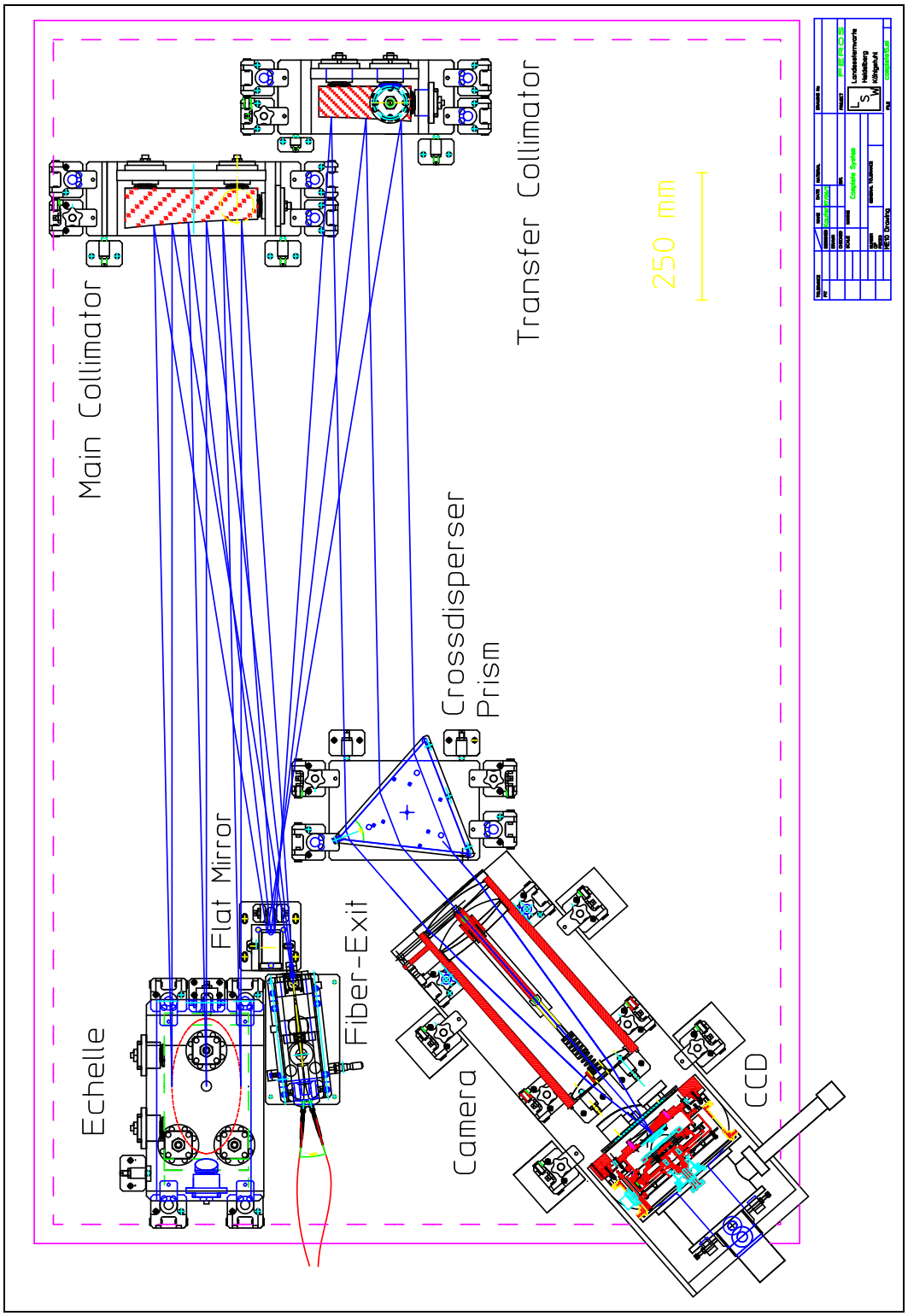

Figure 4.1: The FEROS complete system as seen from the top.

4.2 Optical Table

The spectrograph will be mounted on a $2400 \times 1500 \times 200$ mm optical table by Newport (model M-RPR-58-8) which guarantees sufficient static and dynamic stiffness for the still very moderate load of the FEROS's components. The table top has a metric 25×25 mm grid of sealed M6 mounting holes.

The table will be based on four passive vibration isolators by Newport (model PL-2000-4H-28) capable to damp floor vibrations generated by building vibrations due to e.g. dome rotation or micro earthquakes.

The levelling of the isolators has to be controlled manually (once per month); an automatic level control can be added but requires a permanent connection to compressed air and therefore is to date not foreseen (the FEROS optical bench set up in the LSW laboratory has not needed any refilling for 3 months).

With these components the surface of the table will have a working height of 914 mm above the floor (cf. Fig. 4.2).

The weight of the optical table with supports is ≈ 600 kg. Therefore, a total weight of the instrument of about 900 kg has to be expected.

4.3 Fiber entrance with fiber connectors

The light of object and sky will be coupled into the fibers via microlenses. Since the design and modification of the B&C unit to carry and position the fiber entrances is contributed by ESO, only the fiber entrance connector is described here.

Fig. 4.3 shows the layout of the fiber connectors. For the object/sky fiber a microlens will be used. Since the centering of the microlens is crucial, the connector type SMA906 is used, which has a strongly toleranced top of the ferrule. To center the microlens for each lens and connector an individually machined cap will reduce the diameter of the ferrule to the microlens diameter of 1.10 mm. The length of the microlens is 2.00 mm.

The microlens will be glued to the fiber with EpoTek 301 which has a very high transmission in the whole wavelength range.

The distance from the telescope focus to the surface of the microlens is 1.35 mm; from telescope focus to the mechanical stop of the connector is 13.15 mm.

At the ESO 1.5-m telescope focus a diaphragm with a diameter of 0.29 mm equivalent to $2.7''$ must be placed.

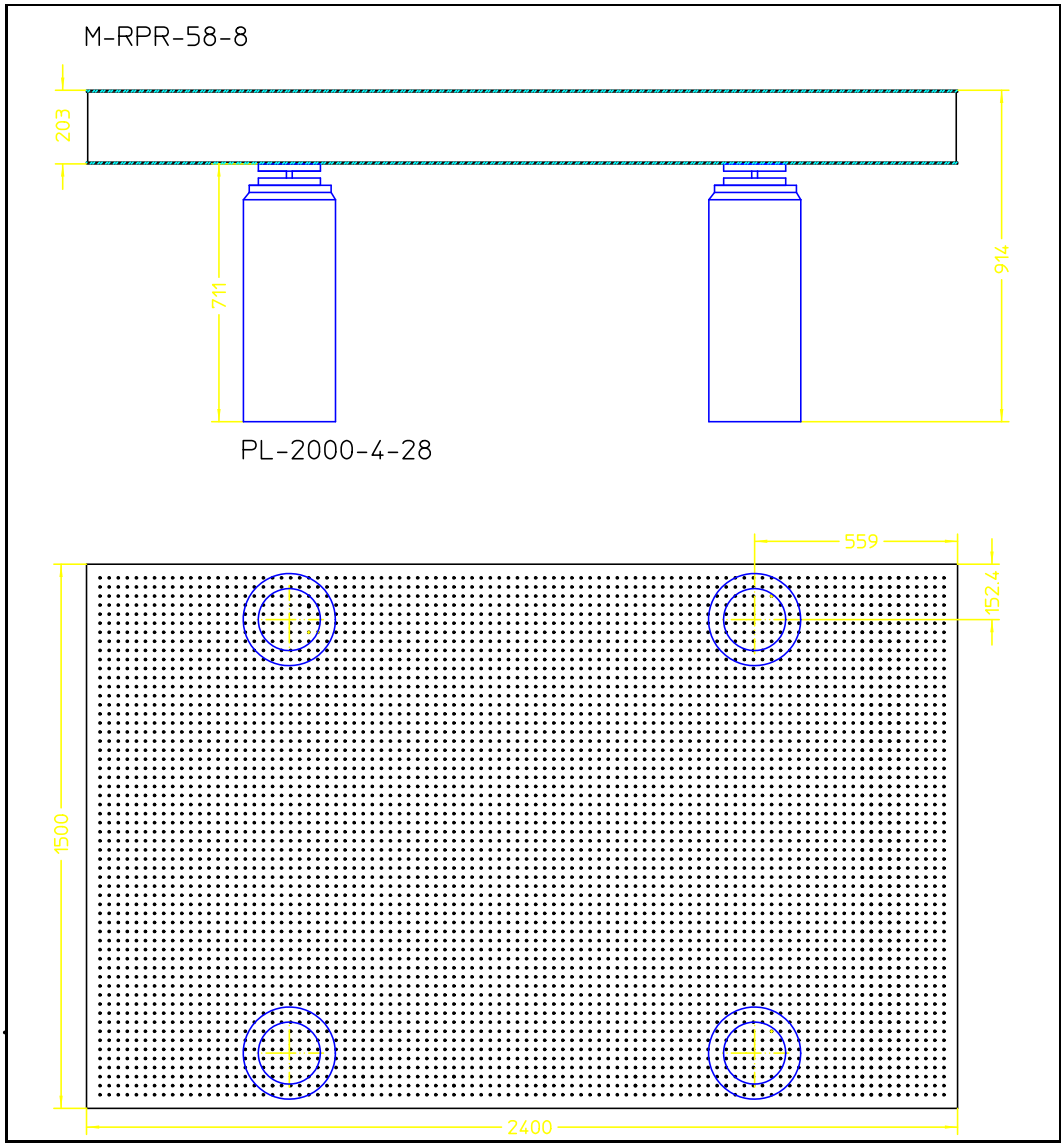

Figure 4.2: Dimensions of the optical table and the table support.

4.4 Fiber link

The fibers will be lead from the B&C adaptor through the telescope's polar axis to the spectrograph. Therefore, no additional connectors to remove the fibers during the turn-overs of the instrument ('change of pier')will be necessary. The length of the fiber link is **12** m. The two fibers coming from the telescope will be additionally protected by a common flexible tube.

The sky fiber will be led to a SMA fiber-fiber connector in the B&C calibration unit where the sky or calibration light can be selected manually.

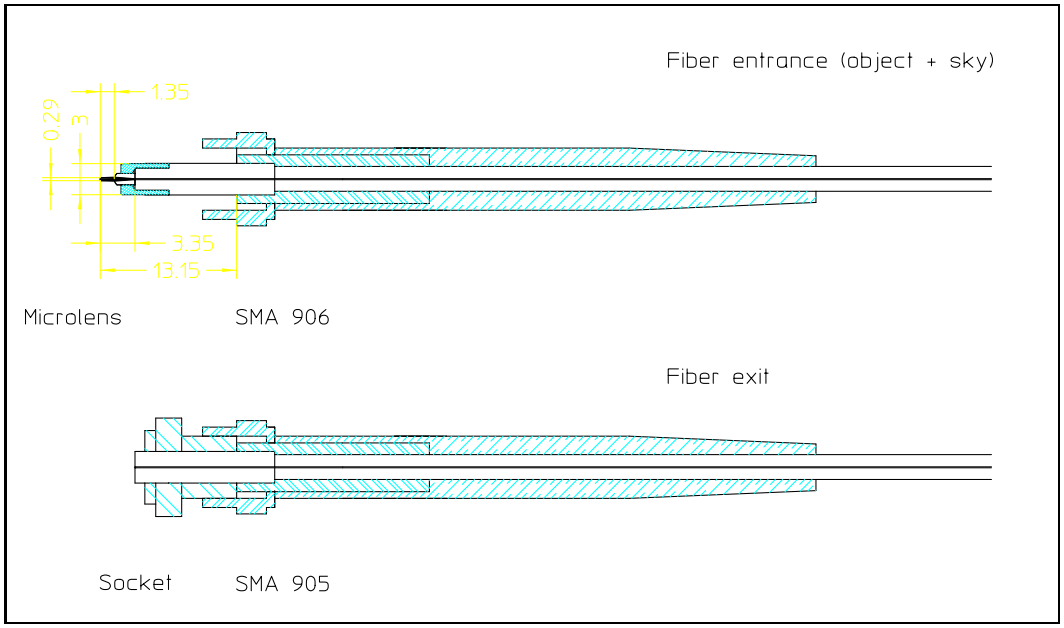

Figure 4.3: Layout of the fiber-entrance connectors with the microlens for object/sky fiber (top) and the fiber-exit connectors plugged into its socket (bottom).

4.5 Fiber-exit unit with F/N System and Image Slicer

The fiber-exit unit holds the pair of fibers ([object+sky/calibration]) from which the light is coupled into the spectrograph. Further, the F/4.6 at the fiber exit is converted via the F/N system to F/11 which is accepted by the spectrograph. At the 'slit' of the spectrograph, a two-beam two-slice image slicer is foreseen, which allows to exploit the maximum 2-pixel resolution of the system.

Figure 4.4 shows the complete fiber-exit unit, whose components are described below.

For the top part of the fiber-exit unit including the two fibers, the fiber-exit head, the F/N system, and the Image Slicer, a spare system will be manufactured. This part is called the fiber-exit head in the following. This spare will be completely pre-adjusted, which allows an easy exchange of the complete unit in case of failure of one of the subcomponents. After replacement of the fiber-exit head by the spare, no adjustment of the following instrument will be neccessary. The focussing and alignment in z-direction and the positioning in y-direction can be done at the basement of the fiber-exit unit (and has not to be done e.g. at the collimator!).

The beam from the fiber-exit unit enters the spectrograph with an angle of 6.466°, which is measured between the z- and X-axis. Therefore, the fiber-exit unit will be mounted with this angle on a ground plate whose mounting holes are fitted to the 25 mm grid of the optical table. Fine adjustment of the angle is foreseen in the basement of the fiber-exit unit with the axis of rotation in Z-direction through the

exit-slit plane (which lies within the image slicer). Further, an adjustment of all tilt-angles can be performed with the 3-point mounting shown in the figure. This 3-point mounting also allows a limited height adjustment of the fiber-exit head.

4.5.1 Fiber exits

The two incoming fibers are terminated with the above described SMA905 connectors which are plugged and screwed into a connector plate of the fiber-exit head. By this, the connectors prevent mechanical stress from the fibers. The unprotected fibers with their Polyamide cladding protude the connectors by about 75 mm. The fiber exits are mounted with a separation of 0.375 mm, respectively, and their axes are concentric to a 2.9 mm diameter stop placed 13.3 mm ahead. The angle between the two fibers is 1.61°. The fibers are guided over a few centimeters in precision milled grooves in a plate mounted on the turnable plate of the fiber-exit head. The adjusted fibers are clamped on their outer cladding over a distance as long as possible to reduce the pressure on the fiber core and avoid additional focal-ratio degradation.

For the alignment of the fiber pair, the fiber-exits are turnable around the vertical axis at the (non-turning) stop.

4.5.2 F/N System

The F/N system housing is adjustable against the stop in xyz-direction by the use of the Newport component M-LP1-XYZ. This allows an alignment with the fiber exits whose positioning capabilities are very limited. Focussing in z is done by translation of the F/N system which is offered by the standard component mentioned above.

4.5.3 Image Slicer

The two-beam two-slice image slicer will be mounted in a cylindrical tube between two multi-layer coated Quarz-glass windows (cf. Fig. 4.5). This reduces the risk of destroying the image slicer during the coating process; further it will be perfectly protected against dust and humidity, which is crucial because of the tiny optically active region.

The work with a 15:1 scale Acrylic model of the image slicer has shown, that a high degree of adjustability is required to simultaneously slice the images of the two fibers. Therefore, the image slicer housing is adjustable against the F/N system in xyz-direction again by the use of the Newport component M-LP1-XYZ. In this case rotation around the z-axis has to be provided and is used to align the fibers on the slice angle.

In case of general problems with the concept of the image slicer, a 2 hole exit-slit (0.24 mm hole diameters, 0.9 mm separation) can be positioned at this place using the same positioning component.

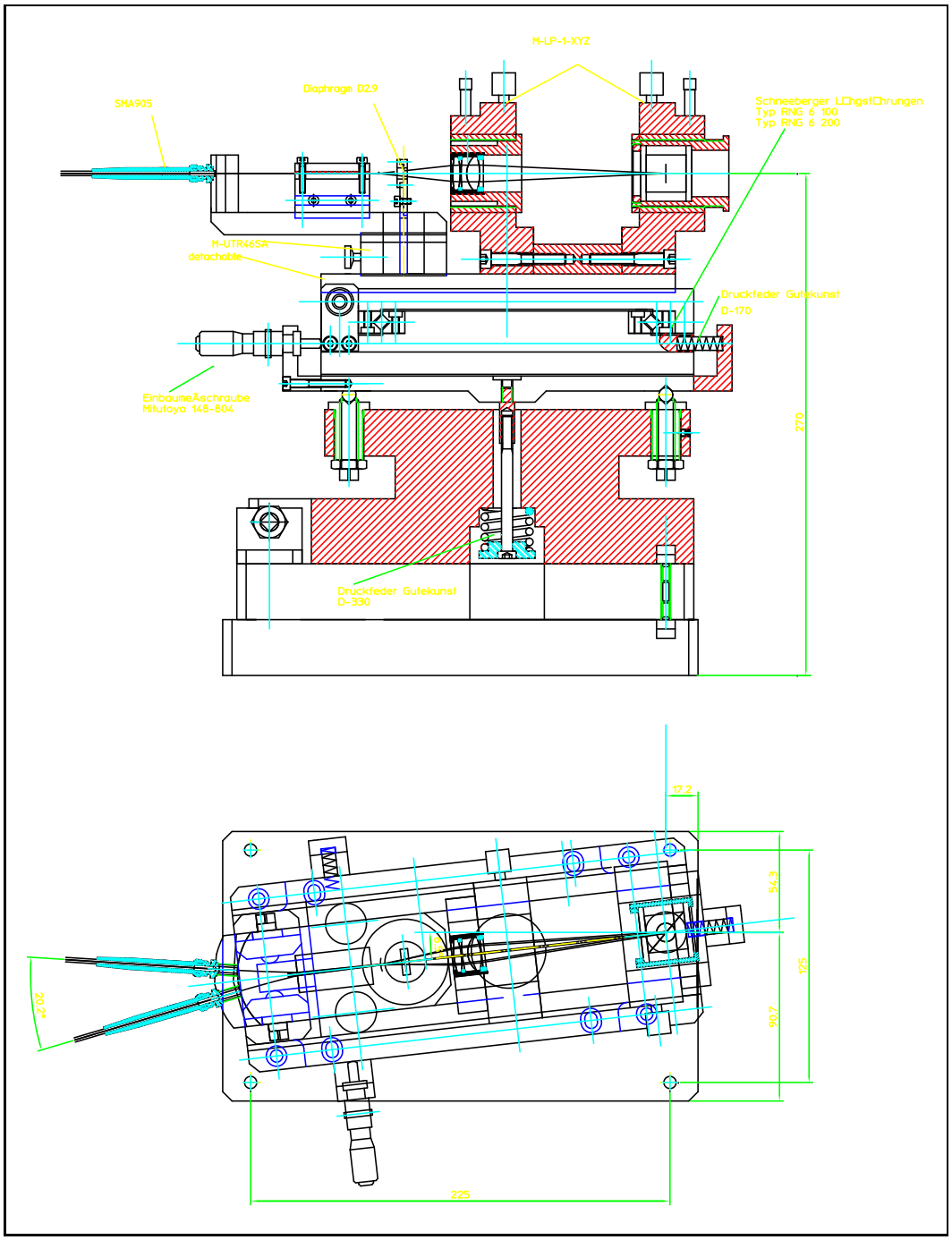

Figure 4.4: Layout of the fiber-exit unit with fiber-exit head carrying the fiber exits, the F/N system, and Image Slicer.

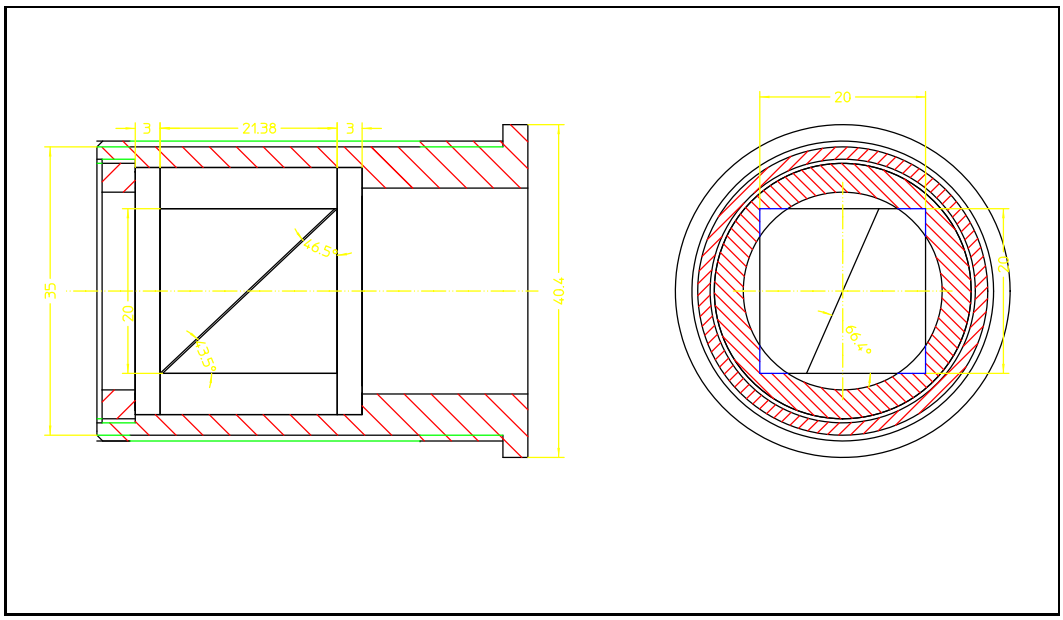

Figure 4.5: Layout of the housing of the image slicer.

4.6 Collimators

The Figs. 4.6 and 4.7 show the mountings of the two collimators (which are cut from one parent paraboloid). For this purpose a kinematic mount with 6 axial supports is used. The supports are mounted to the glass surfaces via glued Invar plates. This mount allows a fine adjustment of the components by ± 1 mm in all degrees of freedom. The positioning of the collimator mountings in the XY-plane

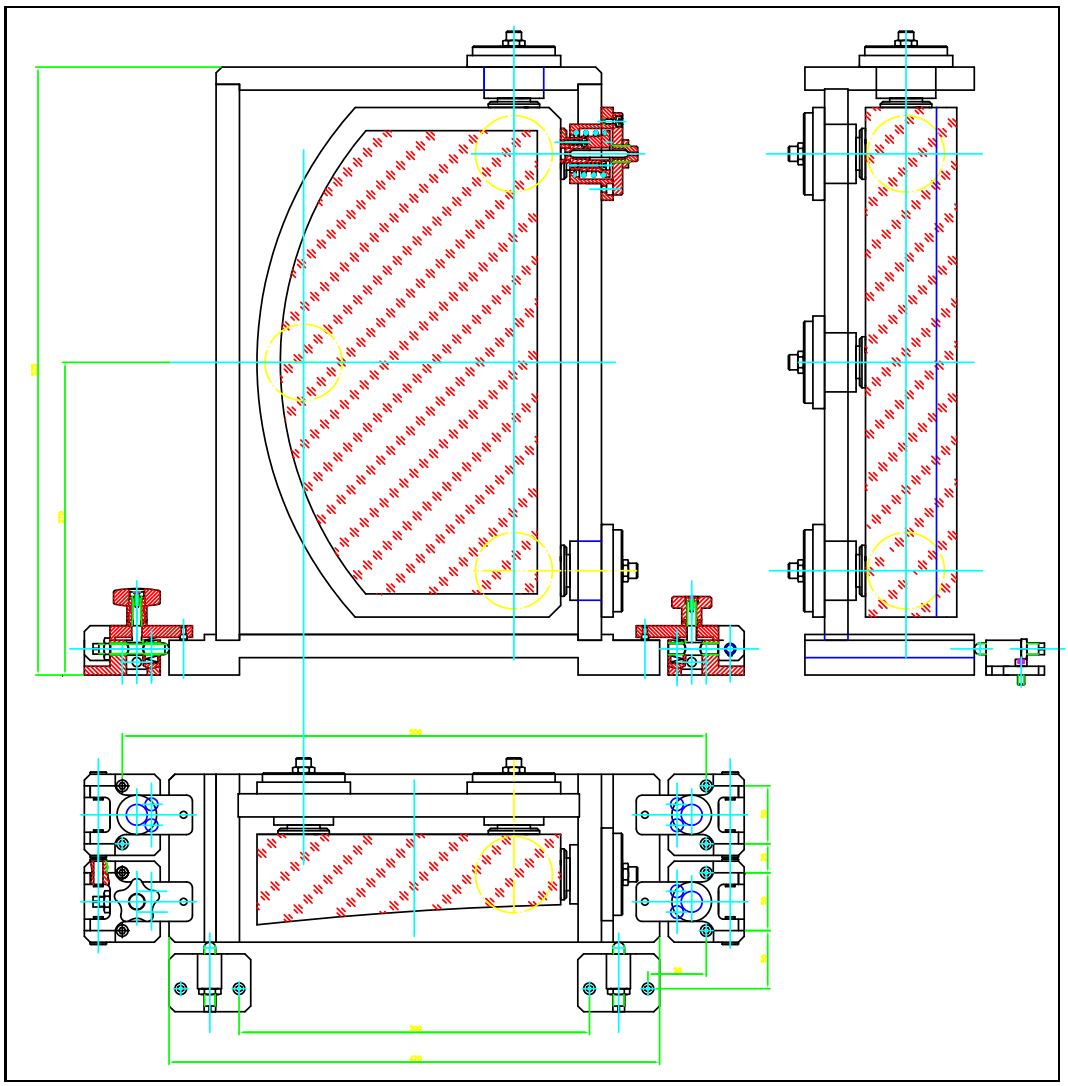

Figure 4.6: Mounting of the Main Collimator.

is done via adjustment screws in the clamps and stops, which hold the components on the optical table. The basement of the mountings and the clamps and stops are adapted to the 25 mm grid of the table surface to position the optical components to within ± 0.5 mm to the computed positions.

For storage and transport, the optically active surfaces will be protected from dust and mechanical influences by plastic covers (not shown in the drawings).

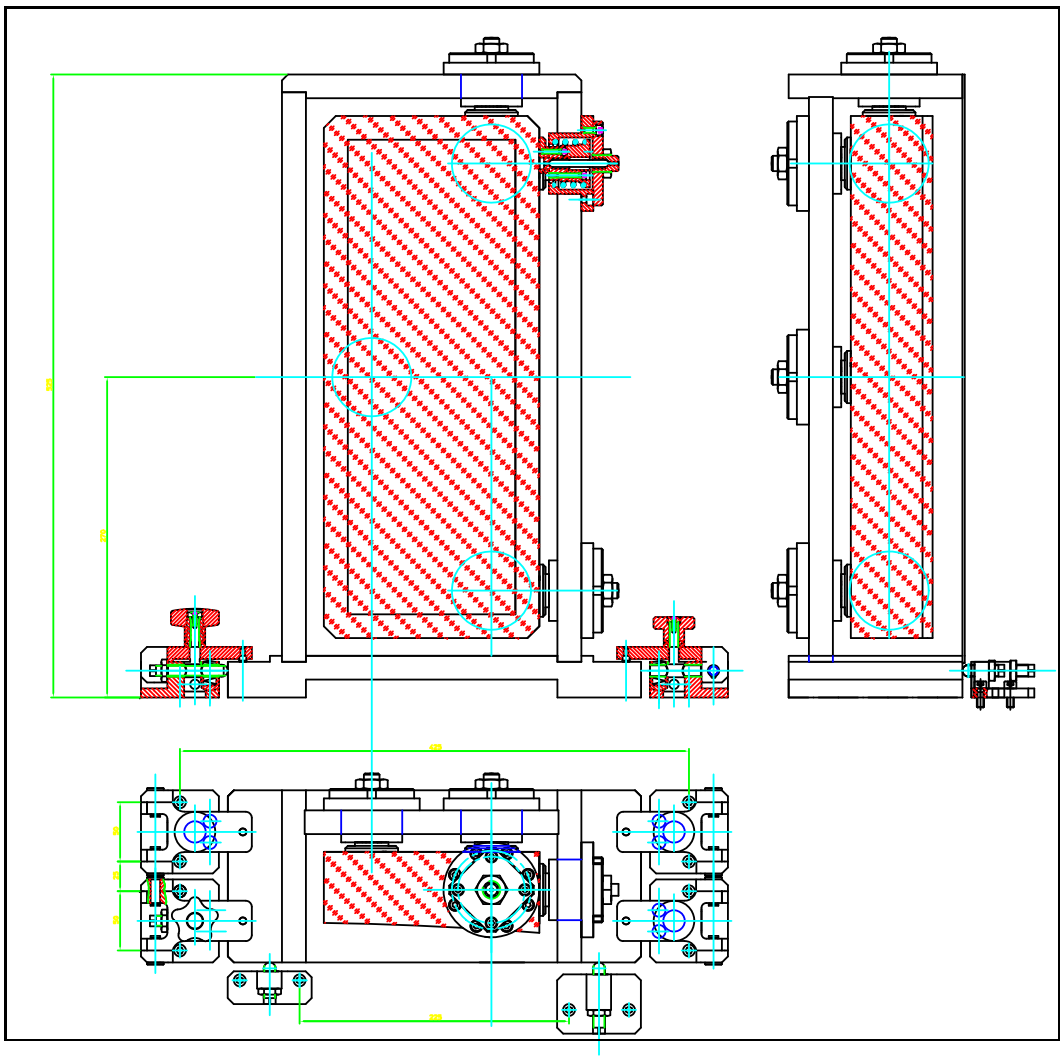

Figure 4.7: Mounting of the Transfer Collimator.

4.7 Folding Mirror

Figure 4.8 shows the layout of the Folding Mirror.

Since this component does not need any linear fine adjustment in xyz (=ZYX), a simple mounting is foreseen with the Zerodur component just standing upright in a protecting cage. This cage must not exceed a thickness of 50 mm in Y-direction not to obscure the beam coming from the fiber-exit unit.

Only a 3-point tilt table is foreseen for fine adjustment of the tilts, mainly the tilt between the x- and Z-axis. Further, a rotation around the Z axis through the reflecting surface will be available. The positioning on the 25 mm grid is realized through holes in the basement which are lengthened in X-direction.

For storage and transport, the optically active surface will be protected from dust and mechanical influences by plastic covers (not shown in the drawings).

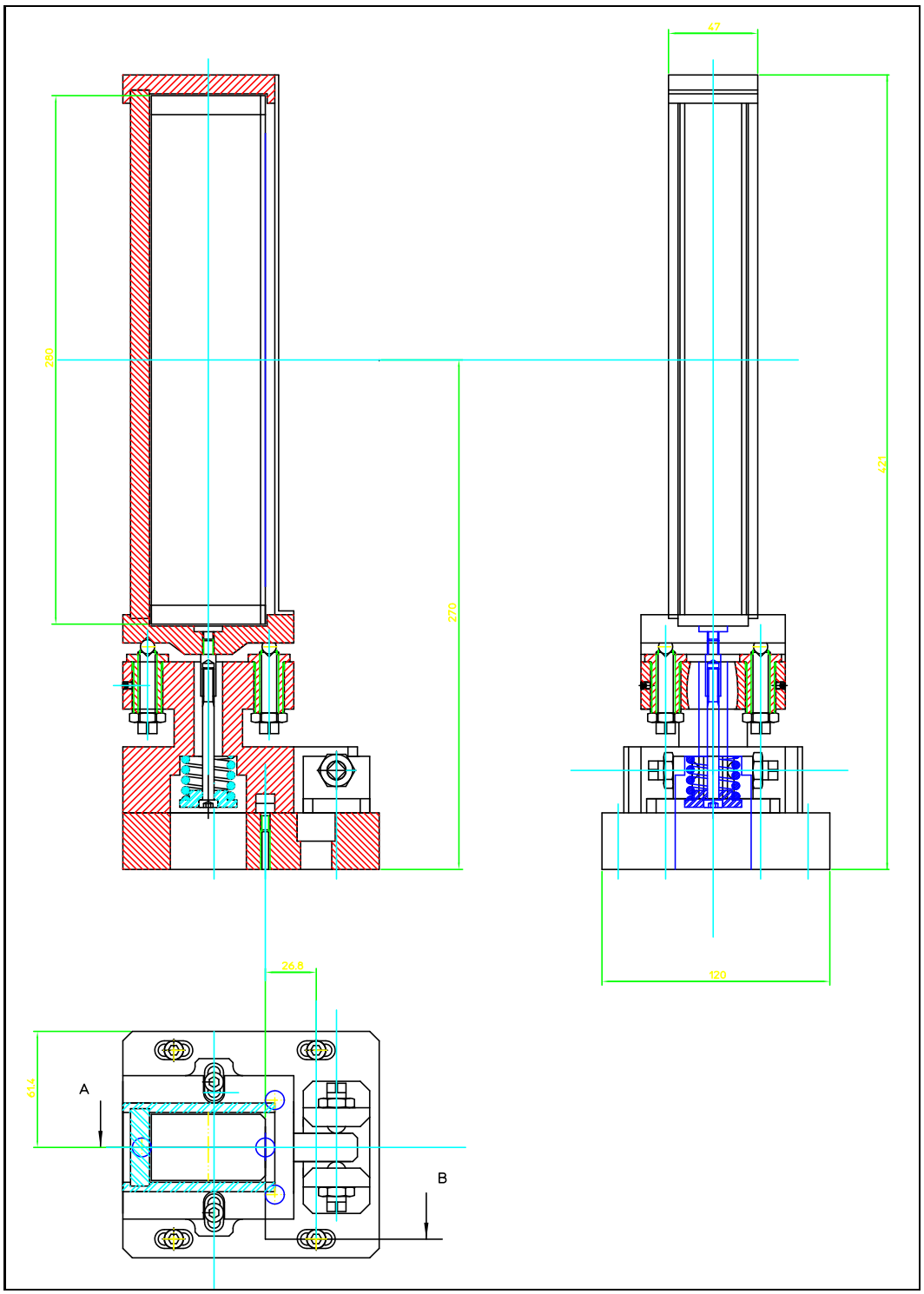

Figure 4.8: Mounting of the Flat Folding Mirror.

4.8 Echelle

The mounting of the echelle grating is basically identical to the mountings of the collimators and shown in Fig. 4.9.

For the axial supports, modified Invar plates have to be used, which account for the tilt angle of 63.4° of the R2 echelle grating.

Further, an additional adjustable stop is used for turning the echelle mounting $\gamma = 0.6^\circ$ (the off-Littrow angle) around the Z-axis through the center of the echelle grating.

To reduce the amount of straylight emerging from the echelle grating, baffles will be inserted below the defracting surface (not shown in the drawing).

For storage and transport, the optically active surface will be protected from dust and mechanical influences by plastic covers (not shown in the drawings).

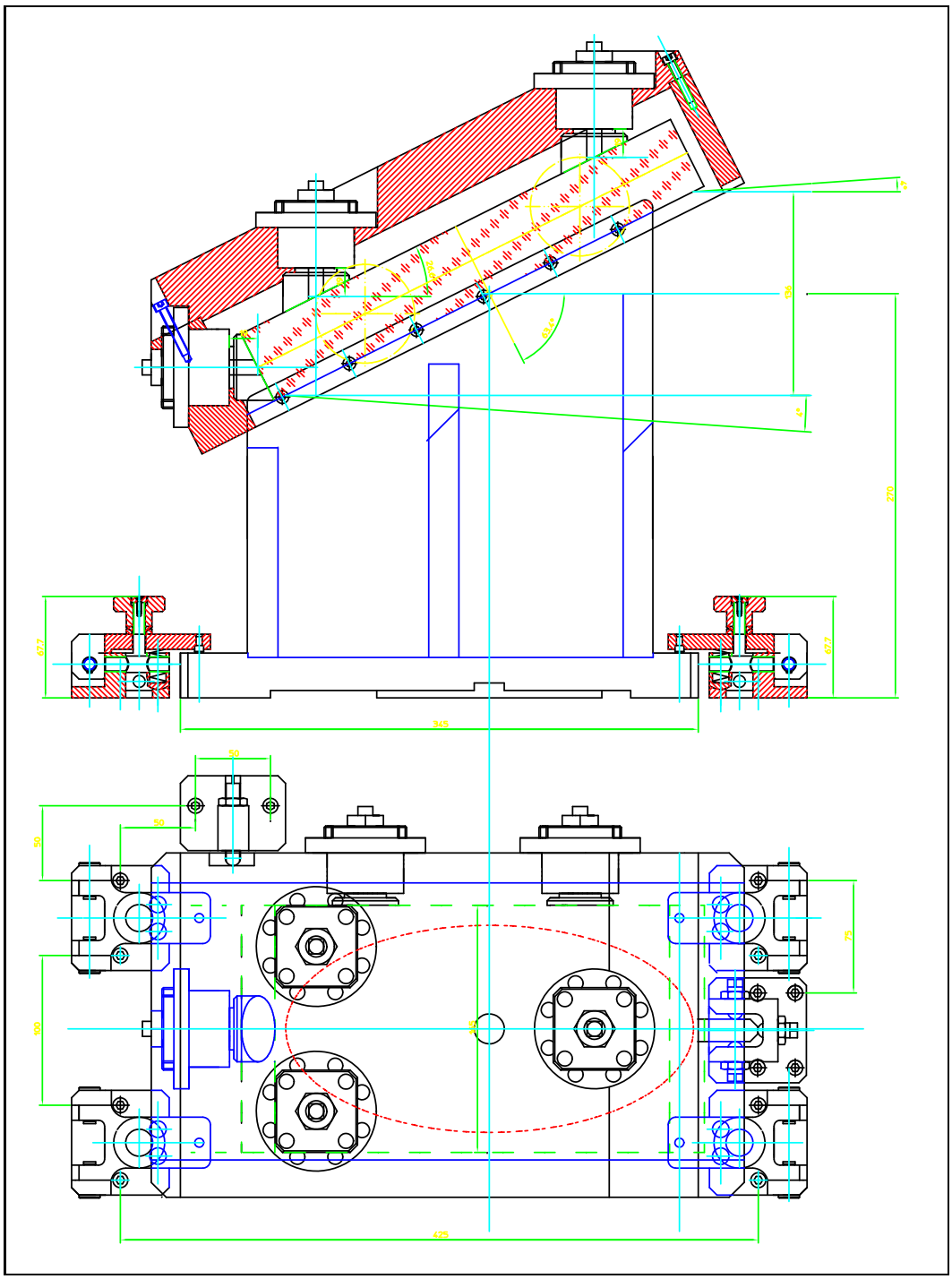

Figure 4.9: Mounting of the Echelle grating.

4.9 Crossdisperser Prism

Figure 4.10 shows the mounting of the Crossdisperser Prism on the Newport turntable M-UTR 160 which allows rotation of the prism around the Z-axis through the center of gravity.

The resolution of the turntable (1 arcmin) will be sufficient to re-position the echelle orders on the detector within 10 pixels after a turn of the prism, e.g., between two wavelength regimes.

For the positioning of the prism, the clamps and stops attached to the basement can be used.

For storage and transport, the optically active surfaces will be protected from dust and mechanical influences by plastic covers (not shown in the drawings).

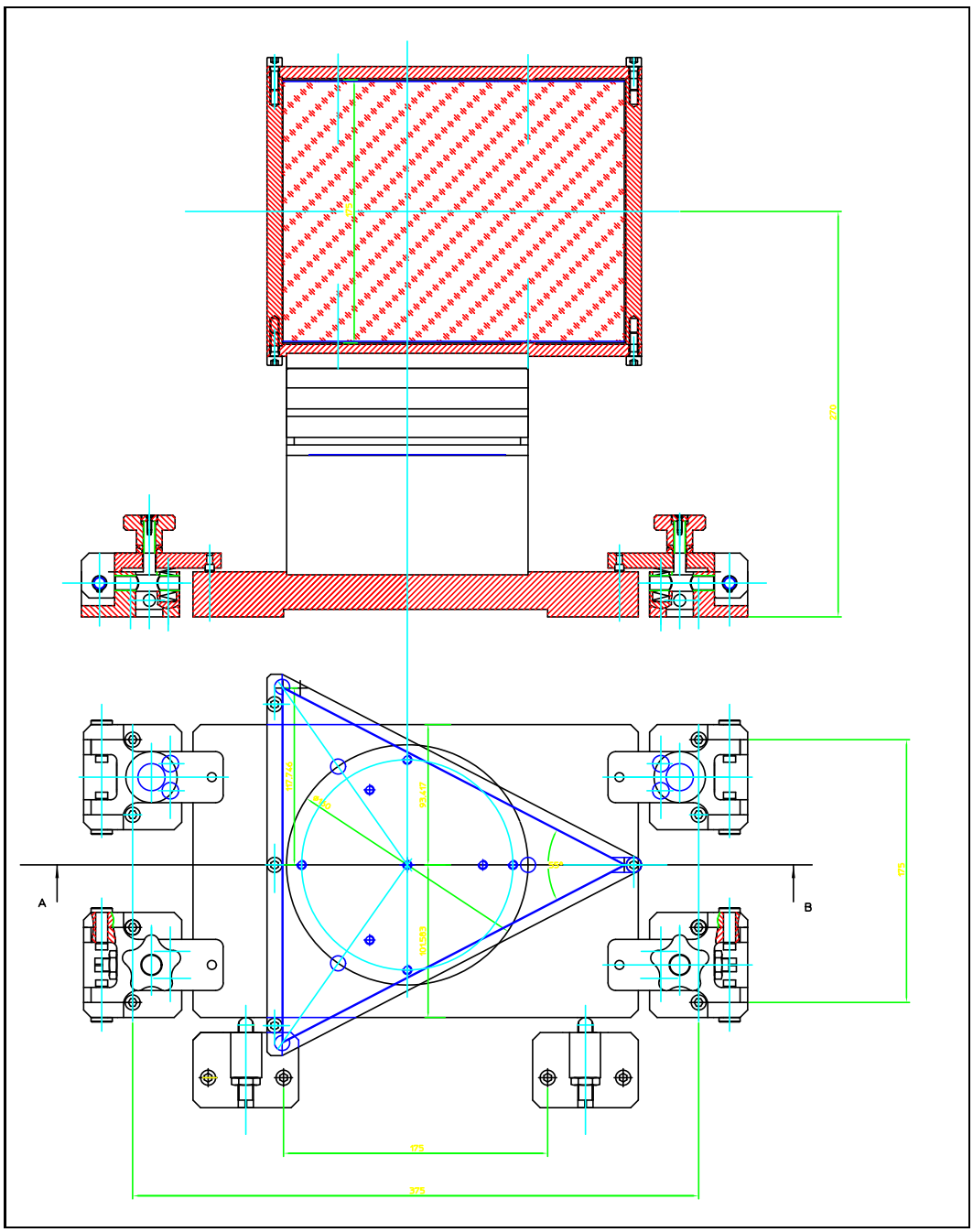

Figure 4.10: Mounting of the Crossdisperser Prism.

4.10 Camera, Shutter, and CCD Continuous-flow Dewar

The camera with its focussing unit will be mounted on a stable breadboard ($300 \times 900 \times 58$ mm, Newport M-XSN-13) together with the shutter and the CCD dewar to allow independent adjustment of this unit. The complete unit is shown in Fig. 4.11.

For the final adjustment of the breadboard relative to the crossdisperser and its fixing, adjustments screws will be mounted on the optical table.

4.10.1 Camera

The housing of the spectrograph camera will be delivered by the optics manufacturer. This component includes the fieldlens, which acts simultaneously as entrance window of the CCD dewar. For centering the fieldlens (and the CCD) to the focussing unit, a removable cylinder can be inserted. For the centering procedure, the focussing unit can be positioned with clamps and stops which fix the basement of the housing on the breadboard.

For focussing, the camera housing of the focussing unit will be mounted on a linear translation roll stage built with cross-roll bearings. This stage is manually adjustable via a micrometer screw with an accuracy of $5\ \mu$m to match the requirements derived from the optical layout. For passive temperature stabilisation a 200 mm Delrin rod was introduced in the focussing unit.

For fine focussing, Hartmann masks can be manually inserted at the front side of the camera housing where a simple sledge is foreseen for this purpose.

For storage and transport, the optically active surfaces will be protected from dust and mechanical influences by plastic covers (not shown in the drawings). In addition, the Hartmann sledge will be used to protect the sensitive CaF_2 front lens.

Note that the presented drawings of the camera only show the principal functions and maximum dimensions of the components. The detailed mechanical design of the camera unit is up to the manufacturer (FISBA) and will be available in week 25/1997. These drawings will be delivered to ESO as an attachment to the FDR including the necessary modifications of the complete Camera–CCD Unit.

4.10.2 Shutter

The shutter will be mounted to the CCD flange to produce an independent and light-tight unit. The Prontor shutter E100 with a free diameter of 100 mm will be used for this purpose. The shutter has to be removed for the centering of the focussing unit and the fieldlens to insert the centering tool ('the removable cylinder', cf. above). Therefore, the shutter itself can be mounted on a cylinder

which uses the same interface to the fieldlens. This allows a quick exchange of shutter and centering tool.

To avoid any heat development close to the field lens, the shutter's electro-magnet and power electronics will be dismounted and positioned outside the optical system. The magnet's movement will be transmitted through a mechanical cable release then.

The shutter electronics require a 24 V, 1.3 A DC signal to open the shutter blades. Pulse forming and voltage reduction for exposures longer than 40 ms is provided by the shutter electronics intrinsically. The shutter control is provided by the CCD controller (equipped with a driver for the 24 V, 1.3 A) to guarantee the optimum timing between the CCD and shutter operations.

4.10.3 CCD

The CCD will be supplied with a precisely machined flange and the integrated and adjusted field lens. Via this flange the dewar will be mounted to a flange on the breadboard. This flange allows precise tilts around the x- and y-axis and translation in x-direction for the centering of this component on the camera optics by the help of the removable cylinder.

Further, rotation around the z-axis for the alignment of the detector rows is foreseen. This is because of the off-Littrow angle of $\gamma = 0.6^\circ$ the image of the image slicer will be rotated by $\omega = \mathbf{2}.4^\circ$ ($\tan\omega = 2\tan\theta_B \tan\gamma$ and $\tan\theta_b = 2$).

The use of the ESO VLT-continuous flow cryostat to avoid any detector displacements due to the varying weight of the dewar during the observations or due to the refilling procedure is planned.

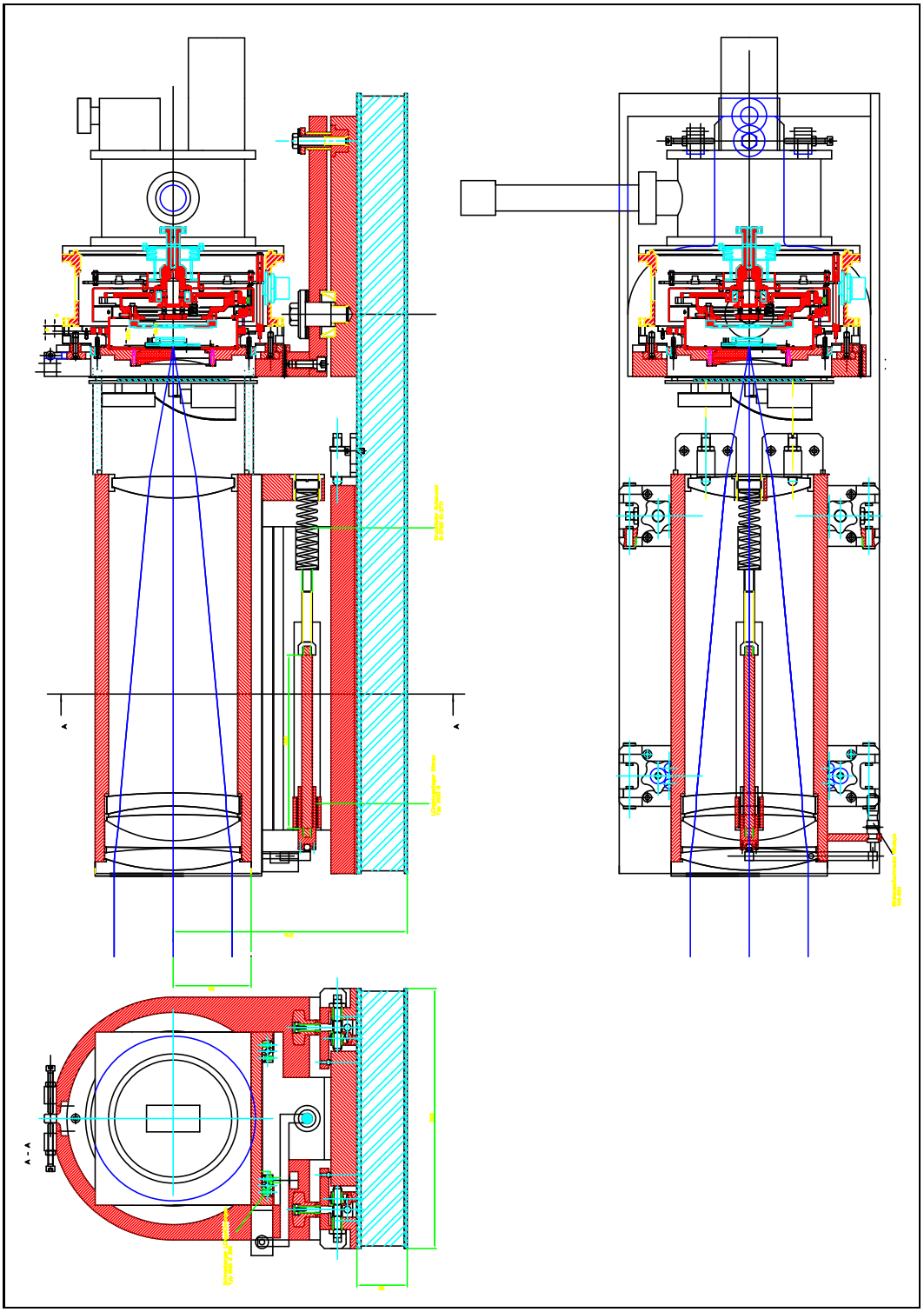

Figure 4.11: The Camera–CCD Unit.

4.11 Removable Enclosure

An easily dismountable and dust-tight cover made from 2 mm black anodized aluminum is foreseen and will be mounted around the optical table without any mechanical connection to the vibration stabilized table top (cf. Fig. 4.12).

The enclosure will be mounted on a free structure. Two removable doors on both short sides and four on both long sides are foreseen. So far, no additional thermal insulation is foreseen but can easily be provided inside the enclosure. The necessity will depend on the temperature stabilisation performance reached by the stabilized spectrograph room (see below, Section 4.12). The total weight of the cover without insulation will be about 50 kg.

From the size of this cover the minimum space requirements for the complete spectrograph are derived to 4 m in length, 2.8 m in width and 2 m in height.

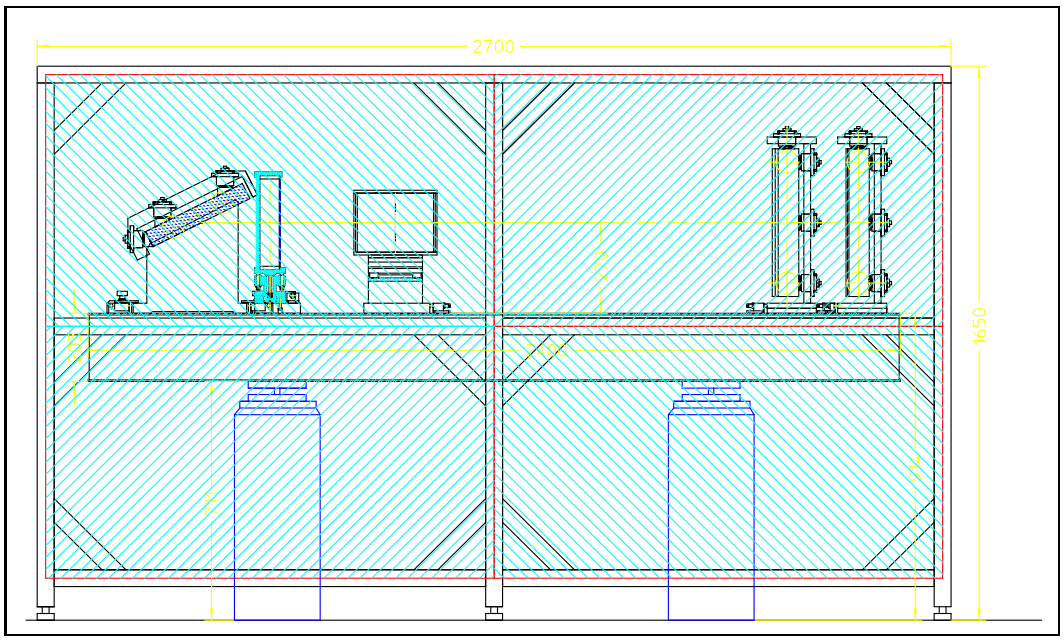

Figure 4.12: Design of the spectrograph's enclosure.

4.12 Spectrograph Room

The spectrograph will be housed in a temperature and humidity stabilized room inside the Coudé room of the ESO 1.52-m telescope. It will be located at the former place of the ECHELEC spectrograph close to the Coudé focus to minimize the fiber length.

This room will be provided by ESO.

The specified perfomances of this room are:

- temperature stability: $16.5 \pm 0.5^{\circ}$ C
- humidity control: always $< 65\%$

Chapter 5: CCD detector

The spectrograph will be equipped with a CCD camera incorporating a monolithic thinned and back-illuminated CCD chip by EEV with 2048×4096 pixels of $15 \times 15\,\mu$m size.

The chip will be mounted in a continuous-flow cryostat capable of maintaining any desired operating temperature in the range $-80°$ to $-130°$C to within $0.1°$C.

The CCD camera will be operated with the CCD controller developed by AOC and identical to that in operation at the Danish 1.54-m telescope on La Silla. The controller is capable of delivering the full performance of the CCD in terms of readout noise, CTE, immunity from interference, crosstalk, etc., and provides the image files with the necessary header information. Readout times will be of the order of 60 sec through two parallel signal chains.

CCD characteristics acc. to ESO	
Op. temperature	$-110°$ to $-120°$C
RON	3 e^- for 50 kpix/sec/port
Dark Current	4 e^-/h/pixel
CTE (par/ser)	0.99999/0.99999
Linearity	$< 1\%$ deviation up to full well
Full well capacity	150.000 e^-

5.1 CCD Detector

The camera will use an EEV CCD detector of the design specified for FEROS, i.e., 2048×4096 pixels of $15 \times 15\,\mu$m, mounted in a continuous-flow cryostat. The CCD can only be mounted with the columns in the main dispersion direction.

The thinned 2k×4k CCD and the standard ESO-VLT continuous-flow cryostat will be provided by ESO.

The CCD controller electronics (+ 1 spare) will be built by the AOC; also the integration and testing of the complete CCD system will be carried out at the AOC.

For the beginning, an engineering grade $13.5\,\mu$m EEV CCD has already been delivered by ESO at the end of March 1997. The first devices of this type have been tested at the Royal Greenwich Observatory. They show a good performance

with an on-chip noise of 4 e^- rms and a peak quantum efficiency of 85% at 550 nm and 27% (goal 50%) at 350 nm (the first measured Q.E. curve is shown in Fig. 5.1).

The minimum and goal quantum efficiencies for ESO's EEV CCD procurement are as follows:

wavelength [nm]	Guaranteed QE [%]	Goal QE [%]
320	22	50
350	50	65
375	58	72
400	72	78
450	85	85
500	85	85
600	85	85
700	78	80
800	50	70
900	28	50
1000	5	15

Throughout the FDR the above 'guaranteed minimum' is assumed.

The delivery of the science grade $15\,\mu$m EEV CCD to the FEROS consortium is planned for November 1997.

The completed CCD system will be delivered with comprehensive test reports as per the current ESO CCD test contract with AOC; monitoring of Q.E. stability will be done with flat field lamps and/or standard star observations.

The performance figures given above are based on experience at AOC and are typical measured figures, after optimising operational temperatures, clock waveforms, etc. They apply to CCDs operated at a pixel rate of 50 kpixels/sec and at a nominal temperature of $-110\ ^\circ$C. "Full well" is defined as the exposure limit to which no measurable departure from linearity occurs; the exposure level causing actual blooming is considerably higher.

5.2 CCD Mounting and Alignment

The alignment of the CCD chip, i.e., height, tip, tilt, and rotation will be done with a traveling microscope and accurate machining of the support base plate. Cross-check of the microscope results as well as final verification that alignment and focus errors are within specifications will be done by direct exposures of a variety of suitable test patterns. Adaptation to minor deviations from a flat optical focal plane can also be made. The minimum clearance between CCD chip and field lens is 4 mm, a back-focal distance of 4.5 mm is foreseen in the optical design.

5.3 Detector Head and Cryostat

The CCD detectors will be mounted in a standard ESO-VLT continuous-flow cryostat. Further, ESO has agreed to provide the mechanical parts for the detector head for mounting the CCD and the appropriate wiring for the inside of the detector head. This will be a copy of the parts being made for the UVES Blue detector system.

5.4 Interface to Spectrograph

The mechanical interface between the CCD camera and the spectrograph is via a precisely machined flange ensuring reproducible positioning of the camera in case removal should be necessary. The optical interface is via the cryostat window, which acts as the field lens of the spectrograph camera. For the alignment of the field lens with the focussing unit of the spectrograph camera, a centering tool will be provided by the manufacturer of the camera.

5.5 Controller

The controller will be of the type developed at AOC and which ESO has agreed to operate at the Danish 1.54-m telescope on La Silla. It is capable of reading out the chip through two parallel signal chains, in approx. 60 seconds with negligible crosstalk. Readout noise and CTE are limited only by the CCD detectors themselves. The entire detector system (including the shutter) is controlled by a Pentium type PC running under LINUX, i.e. with full UNIX multi-tasking and remote login features, and with sufficient on-board frame buffer capacity to hold an entire image during readout. The images are delivered directly onto the disk storage of the ESO-supplied workstation in a format ready for data reduction with MIDAS or other standard astronomical CCD reduction package. All necessary file header information on the status of the telescope and spectrograph will be included through links to the TCS (in ESO standard format), as established and tested for the system on the Danish 1.54-m telescope. Complete documentation will be provided as specified in the FEROS contract. A complete spare controller system (including a PC with all options) will be included in the delivery.

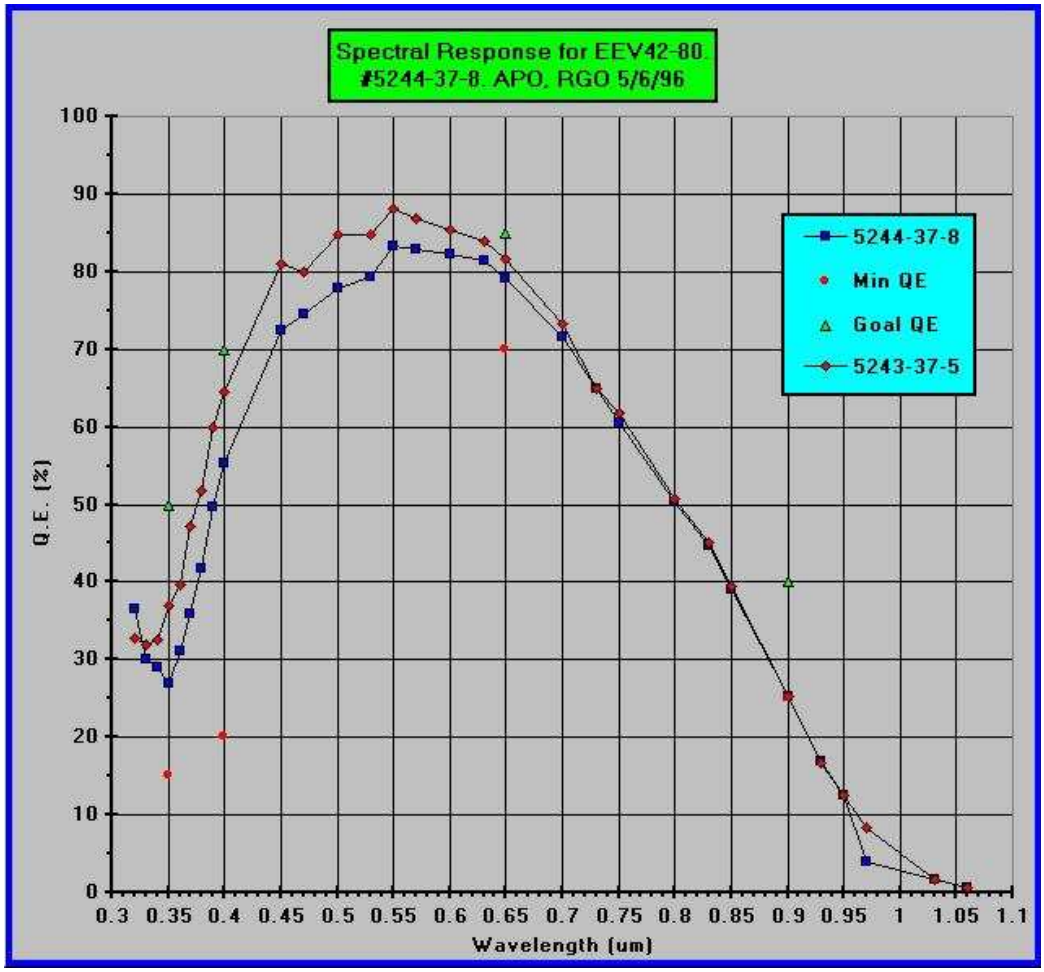

Figure 5.1: Quantum efficiency curve for the engineering 2kx4k chip EEV 42-80 (5243-37-5) measured at RGO.

Chapter 6: Calibration Unit

6.1 General Description

The calibration unit for the FEROS instrument will be used to feed the object and sky fiber entrances with emission line spectra for the wavelength calibration and a continuum-light source for flatfielding purposes. In an additional mode a line spectrum will be recorded instead of the sky spectrum simultaneously on the detector during the object exposure. [1]

The complete calibration unit will be housed in a seperate box, which will replace the existing B&C calibration unit. Therefore, the FEROS calibration unit (FCU) will also provide a Helium-Argon calibration lamp as normally used for the B&C instrument. The internal flatfield lamp can also be used for the B&C.

The already existing remotely controlled 'comparison source flip mirror', the neutral-densitiy filter in front of the diffuser, and the diffuser imaging optics will be used together with the FCU and have to be maintained at the B&C instrument.

The complete FCU with a manual control box will be provided by the FEROS Consortium. This control box provides simple digital (TTL) interfaces for remote control, e.g., by Camac/VME + DAISY (see below).

The design of the exchangeable FEROS and B&C slit units and the modification inside the B&C instrument are done by ESO (as defined in the FEROS contract).

6.2 Conceptional Design of the FCU

Figure 6.3 shows the optomechanical design of the FCU.

6.2.1 Components

The FCU contains the following functional components:

[1] So far (i.e., in the FCD and the FP) it was foreseen to provide this spectrum through a third fiber which is fed by an external calibration unit located in the telescope control room. In this case a manual fiber-pair selector was needed in the fiber-exit unit of the spectrograph. Further, an additional set of lamps and power supplies was needed. In the design presented here, the same calibration lamps will be used to feed the fibers in the different observation modes (cf. text) . Further, no fiber-pair selector is needed. The selection of calibration or sky feed of the scond fiber is done by plugging a fiber connector into the respective socket.

- **Flatfield Unit (FFU)**
  The FFU is optimized for the FEROS instrument and will provide a UV-enhanced continuum spectrum by the combination of two halogen lamps with an intensity ratio of 5:1. In front of the lamp with higher intensity a red-blocking filter combination (BG39 + BG24A + KG3(3 mm)) will make this halogen lamp look 'blue'. The light paths of the two lamps are combined with a 50:50 beamcombiner under 45° wherein the 'red' lamp uses the reflected lightpath and the 'blue' lamp the transmitted one.

  Figure 6.1 shows the computed outcoming intensity distribution of the FFU assuming a 3200 K blackbody distribution for the two halogen lamps. With this type of flatfield source, evenly exposed flatfields will be possible over the large wavelength range of FEROS. Of course, this source can also be used for internal flatfields of the B&C instrument.

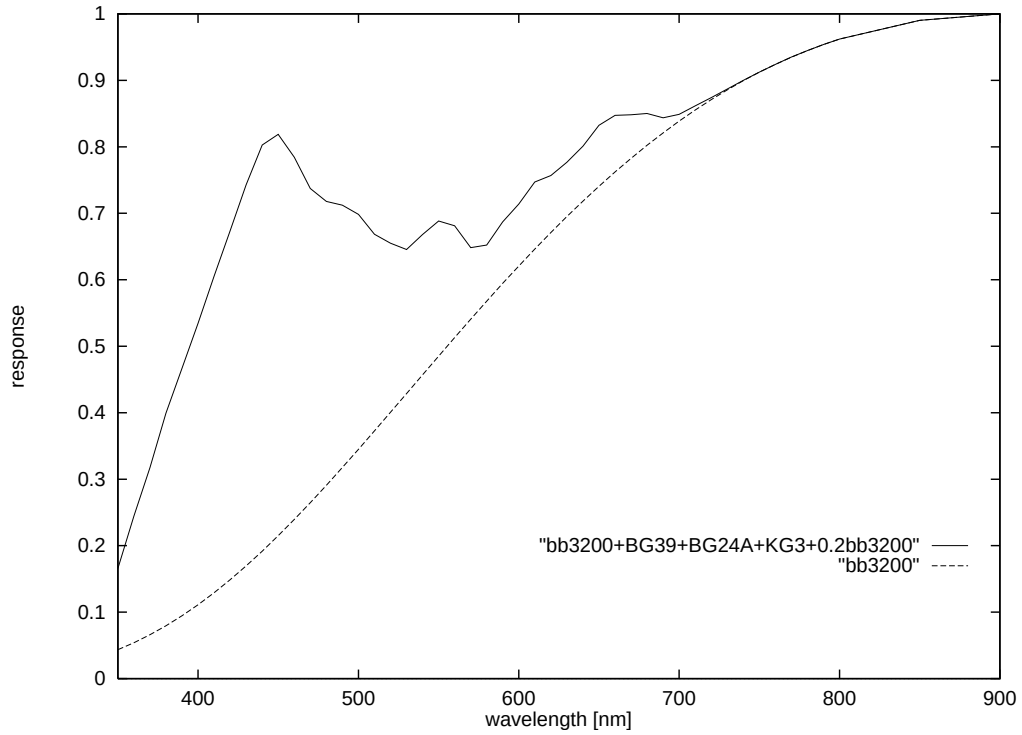

Figure 6.1: Output intensity distribution of the Flatfield Unit. The enhanced blue intensity over a normal halogen lamp (dashed line) is clearly seen.

Remotely controlled elements: 2 lamp power supplies
Possible states: ON/OFF/Remote

- **Wavelength Calibration Unit 1 (WCU1)**
  The WCU1 is foreseen to provide a line spectrum for the wavelength calibration of the FEROS spectra. In principle, an ordinary hollow cathode Thorium–Argon lamp seems to be sufficient for this purpose. This kind

of spectral lamps is needed to provide numerous lines per order over the wide spectral range of FEROS. The filling gas Argon shows very strong lines in the red beyond 6700 Å. The strongest lines are about a factor of 80 stronger than lines used for the calibration. Due to this high dynamic range, the detector is saturated in these lines and strong blooming features are discernible along the channel stops, i.e., along the detector columns with 4096 pixels. Usually, this is ignored and the lines are omitted from the calibration procedure.

In the case of FEROS two major complications occur:

1. The channel stops in the foreseen three-side buttable 2k×4k CCDs are aligned along the main dispersion direction. Therefore, the overexposed blooming Argon lines will destroy considerably large spectral regions within the orders (and due to the strong tilt of the orders also neighbouring orders).

2. In the Object + Calibration mode, the simultaneously exposed wavelength-calibration spectrum will destroy the object spectrum due to the blooming effect discussed in point 1.

For these reasons, the WCU1 will use the combination of a Thorium–Argon hollow-cathode lamp with the spectral region above 6700 Å blocked by an edge filter to a level of 1% and a Neon lamp to provide additional spectral lines in this red spectral region. As for the FCU, both beams are combined with a beam combiner.

Figure 6.2 shows the red part of the spectra of such a combined calibration lamp in comparison with a standard single Thorium-Argon lamp. The saturation level of the CCD is at unity.

Control elements: 2 lamp power supplies
Possible states: ON/OFF/Remote

- **Calibration Fiber + Neutral-Density Filter Wheel (NDFW)**
In the above mentioned Object + Calibration mode a comparison spectrum will be recorded through the sky/calibration fiber over the whole exposure time necessary for the object. For this purpose, the sky/calibration fiber has to be manually plugged into the respective socket.

  The length of the fiber from the slit unit to the socket in the FCU is **75 cm**. Therefore, the sky/calibration-fiber has to be **75 cm** longer than the object fiber.

  As light source for the comparison spectrum, the output of the WCU1 will be directed onto the sky/calibration fiber. To adjust the intensity of the WCU1 source to the exposure of the object, a variable circular neutral-density (ND)

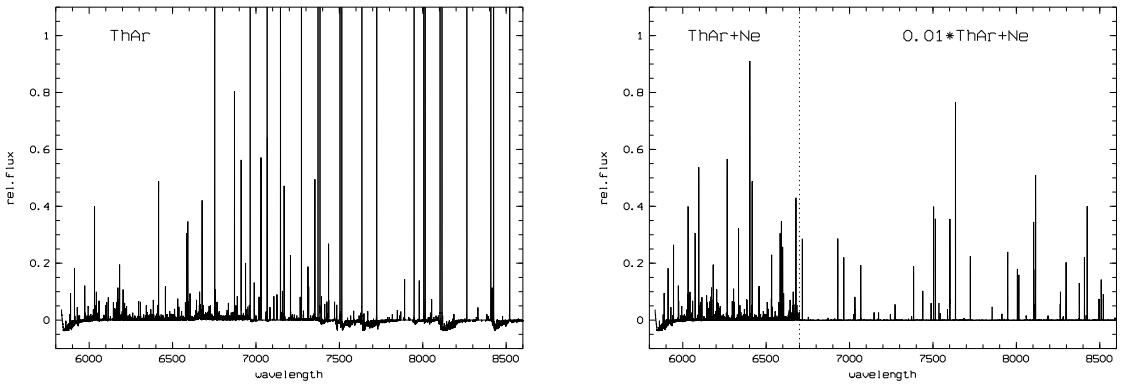

Figure 6.2: Red spectral region of a standard Thorium-Argon lamp (left) and the proposed Thorium-Argon blocked to 1% above 6700 Å and combined with a Neon lamp (right). The CCD saturation is a rel.flux=1; the saturated Argon lines at the left side reach values up to rel.flux≈80.

filter is used. An ND filter with an optical density range from 0–3 (100–0.1% transmittance) would allow exposure times up to two hours assuming that a good quality comparison spectrum can be obtained in about 7 sec exposure without additional damping. Once calibrated, the filter angle position can be automatically set according to the chosen object exposure time.

Control elements: Linear motor with potentiometer as position sensor, two limiting switches $S_{\max}$, $S_{\min}$
Possible states: 0–360°, Local/Remote

- **Wavelength Calibration Unit 2 (WCU2)**
  The WCU2 provides the same Helium-Argon line spectrum as already used in the existing B&C calibration unit.

  Control element: 1 lamp power supply
  Possible states: ON/OFF/Remote

- **Rotating Source-Selection Mirror (RSM)**
  To select the calibration light sources described above and direct the light onto the difuser, a rotating mirror with four working positions (0,90,180,270 degrees) is foreseen. The rotating unit will also cover the unused calibration sources.

  Control elements: Linear motor with 4 position switches
  Possible states: $S_1 = 0^o$, $S_2 = 90^o$, $S_3 = 180^o$, $S_4 = 270^o$ Local/Remote

Inside the B&C instrument, the already existing **comparison source flip mirror (CFM)** is used.

Remote control to flip the mirror does already exist
Possible states: IN/OUT, Local/Remote

6.2.2 Operational Modes

Between the two fundamental operational modes

- Object – Sky (OS)
- Object – Calibration (OC)

the observer has to switch manually (cf. above).

The table below gives the necessary states of the FCU components for the 4 operational modes of the instruments:

Exposure type	Mode	CFM	RSM	FFU	WCU1	NDFW	WCU2
Object+Sky	OS	OUT	0°	OFF	OFF	—	OFF
Object+Calib.	OC	OUT	270°	OFF	ON	$0-360^o$	OFF
Internal Flatfield	OS	IN	90°	ON	OFF	—	OFF
FEROS Wavelength Calib.	OS	IN	180°	OFF	ON	—	OFF
B&C Wavelength Calib.	—	IN	0°	OFF	OFF	—	ON

Since for flatfielding and wavelength calibration in the OC mode it can be desirable to illuminate object and calibration fiber with the same light source, the following sequences have to be performed:

OC Wavelength Calibration

time	⊢	−−	−−	−−	−−	−−	−−	−−	−−	−−	⊣
WCU1	⊢	−−	ON	−−	OFF	−−	ON	−−	−−	OFF	⊣
RSM	⊢	180	−−	−−	−−	270	−−	−−	−−	−−	⊣
Shutter	⊢	−−	open	−−	−−	−−	−−	−−	−−	close	⊣

OC Flatfield

time	⊢	−−	−−	−−	−−	−−	−−	−−	−−	−−	⊣
FFU	⊢	−−	ON	−−	OFF	−−	ON	−−	−−	OFF	⊣
RSM	⊢	90	−−	−−	−−	0	−−	−−	−−	−−	⊣
Shutter	⊢	−−	open	−−	−−	−−	−−	−−	−−	close	⊣

6.3 Opto-mechanical layout of the FCU

Figure 6.3 shows the opto-mechanical layout of the the FCU. The main body, which is mounted to the existing B&C calibration-unit flange, contains the rotating source mirror (RSM) for the selection of the different light sources to be imaged onto the diffuser. The RSM also allows to direct the light from the FFU and WCU1 via the NDFW onto the calibration fiber.

The different light sources and the neutral density filter wheel NDFW are mounted as modules on this body which allows easy exchange of the lamps or even the complete modules. The FFU and WCU1 modules both contain a combination of two lamps + filters + beamcombiner. All modules include their imaging optics.

6.4 Mechanical and Optical Interfaces between FCU and B&C

To mount the FCU to the B&C instrument, the existing flange of the B&C will be used.

The only optical interface is the diffuser, which will be illuminated by the FCU and imaged onto the respective slit unit by the already existing transfer optics.

Therefore, **no opto-mechanical modifications at the B&C are necessary** for the integration of the FCU.

6.5 Electronic Interface

All described modes of the FCU will be 'manually' selectable with a switch and control box in the telescope control room. This control box will be provided by the FEROS Consortium since it will already be needed for the integration of the instrument at the LSW.

Figures 6.5, 6.6, and 6.4 show the electronical layouts of the 3 lamp controls (FFU, WCU1, WCU2) circuits, of the neutral density filter control (NDFW), and the control circuit of the rotating source mirror (RSM). Figure 6.7 shows the layout for the wiring of the FCU on the telescope's side.

This control box provides simple digital (TTL) interfaces for the remote control, e.g., by Camac/VME + DAISY:

Component	Input Port	Output Port	Status	Remarks
FFU	A3		1 = OFF 0 = ON	
WCU1	A4		1 = OFF 0 = ON	
WCU2	A5		1 = OFF 0 = ON	
RSM	A6,A7		0,0 = 0° 0,1 = 90° 1,0 = 180° 1,1 = 270°	
		A12	1 = busy 0 = on position	
NDFW	A8,A9		1,1 = STOP 0,1 = increase density 1,0 = decrease density	
		C6	$0 - 5$ V = position	analog port to ESO ADC

Note, that for the logic 'active low' is used.

The digital ports are activated by setting the individual switches on the the control box in `remote` mode.

It should be noted that this simple interfacing via TTL ports is independent of ESO's final choice between a VME or CAMAC based instrument-control system.

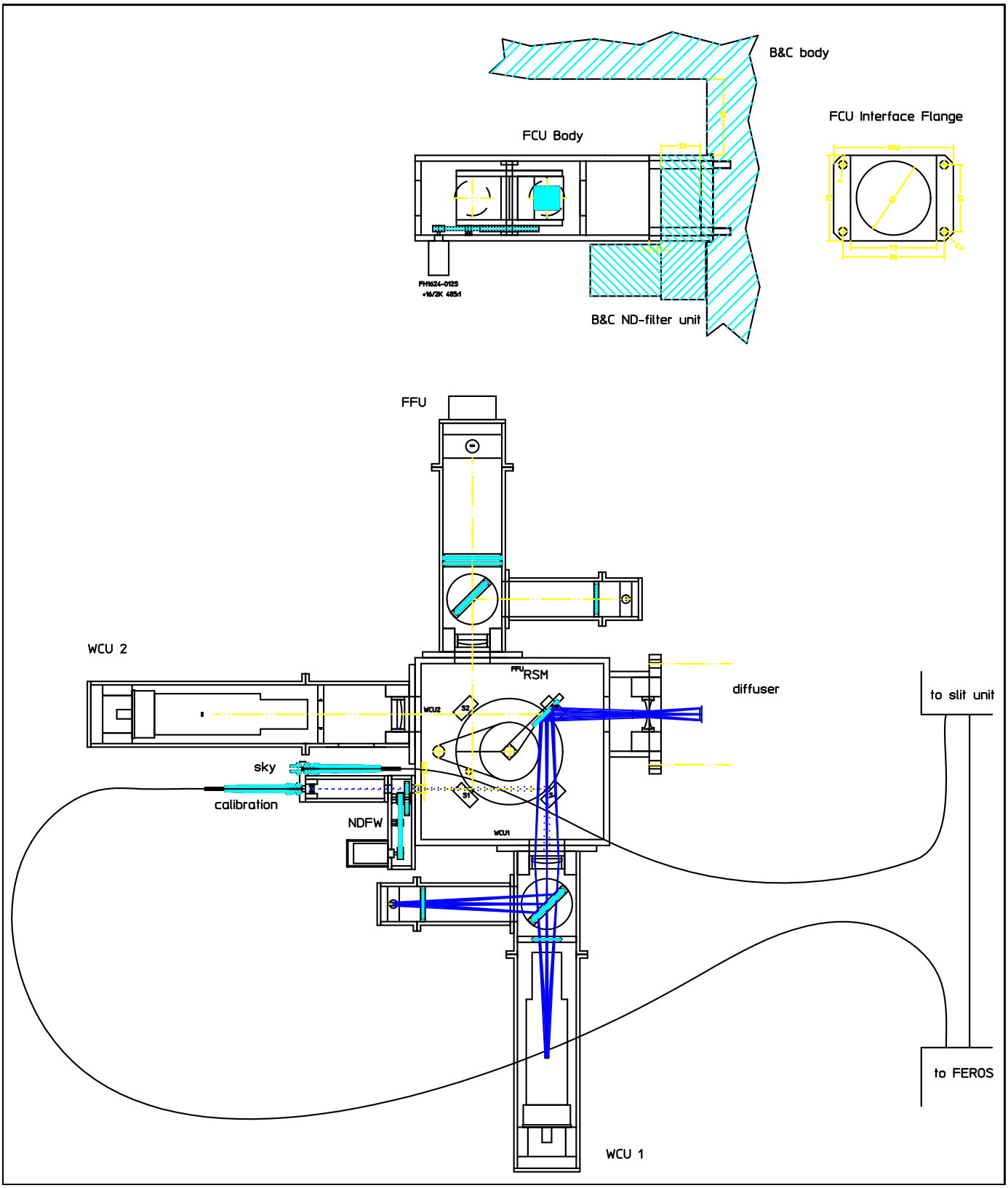

Figure 6.3: Opto-mechanical layout of the FEROS calibration unit (FCU).

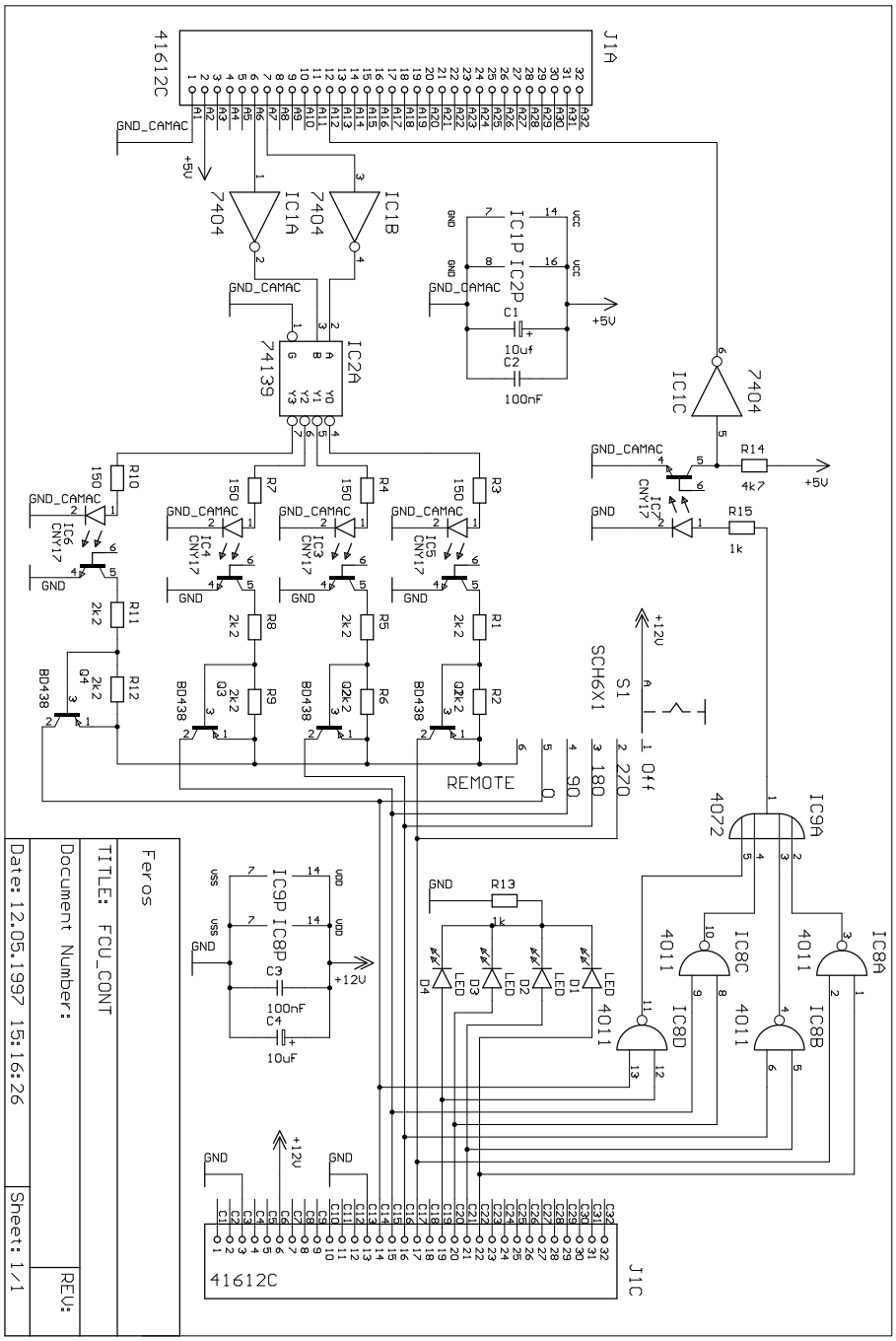

Figure 6.4: Electronical layout of the RSM control.

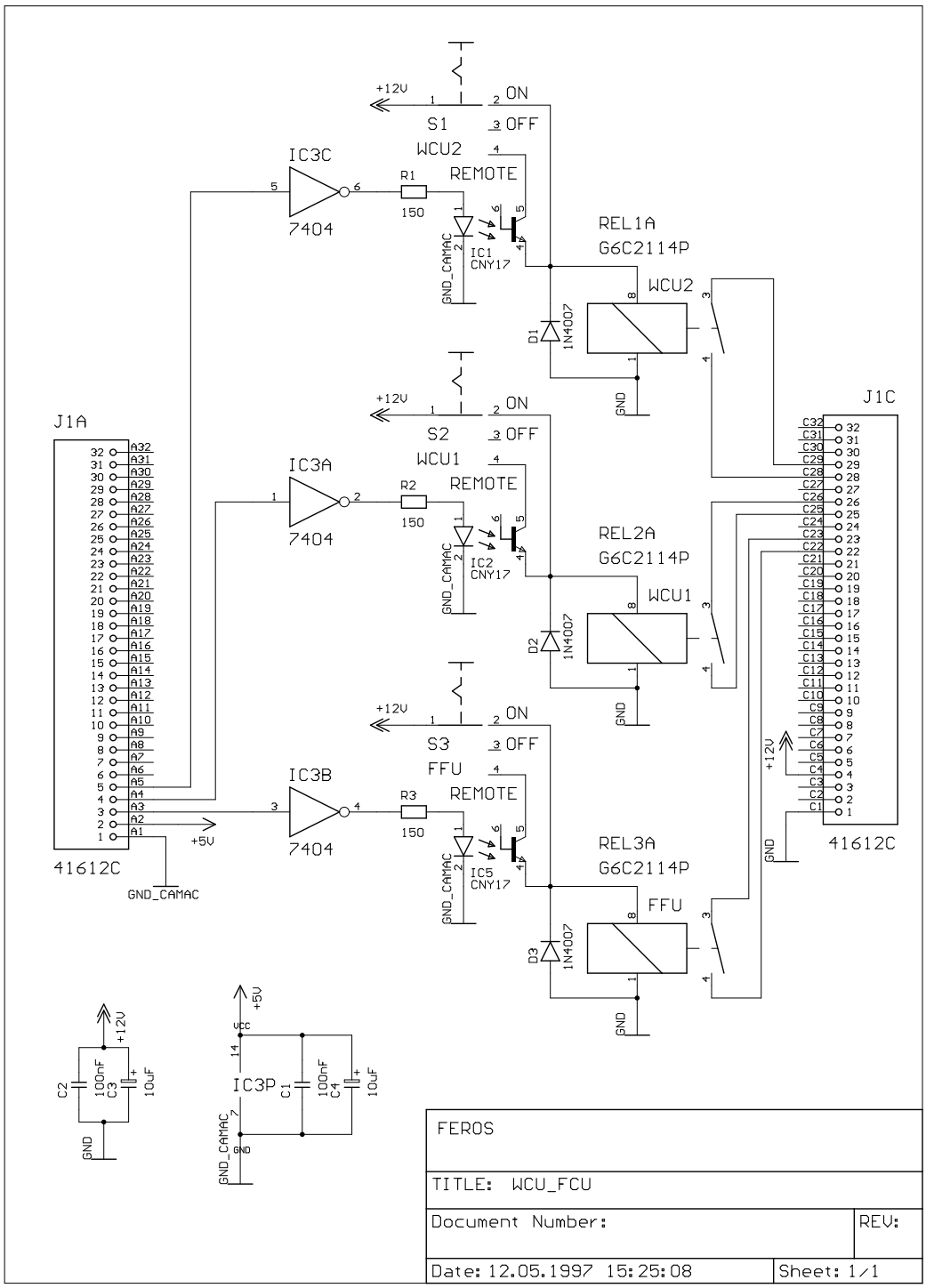

Figure 6.5: Electronical layout of the WCU1, WCU2, FFU control.

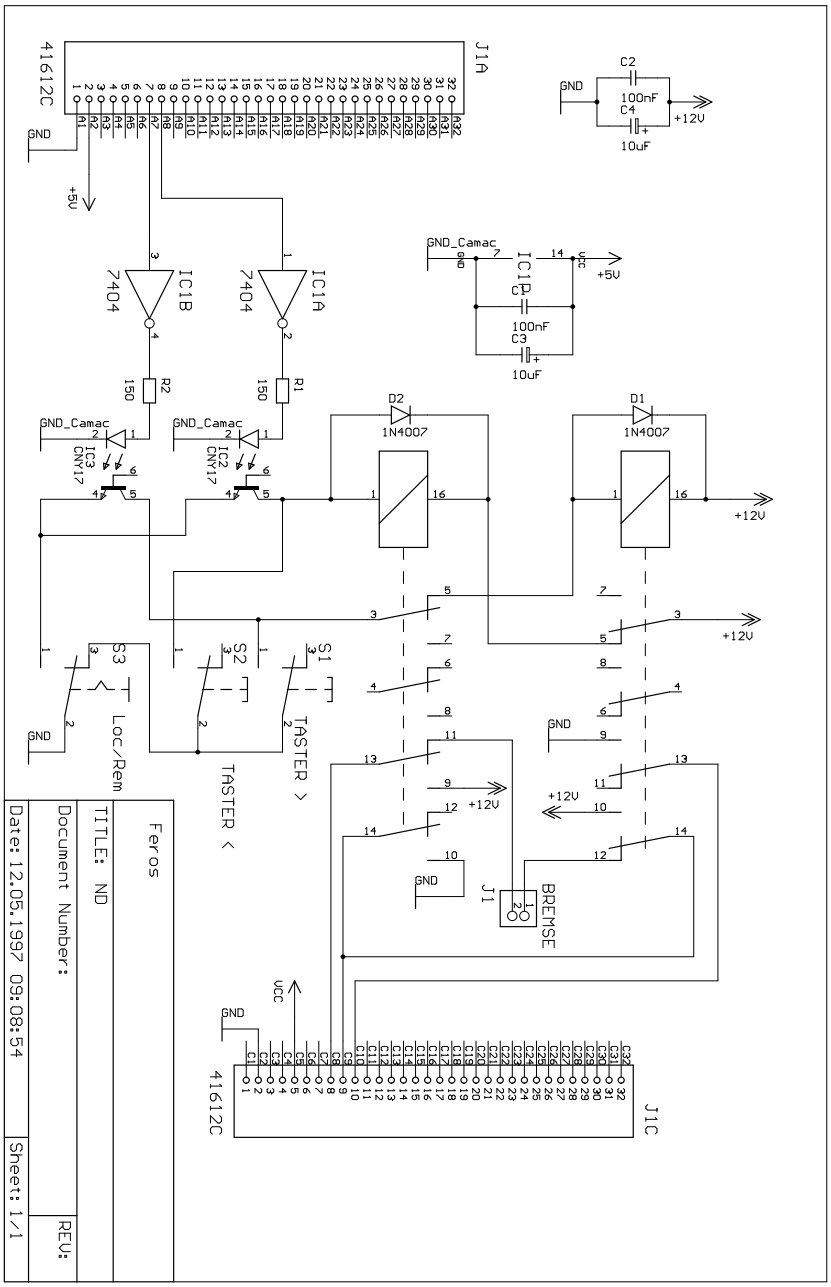

Figure 6.6: Electronical layout of the NDFW control.

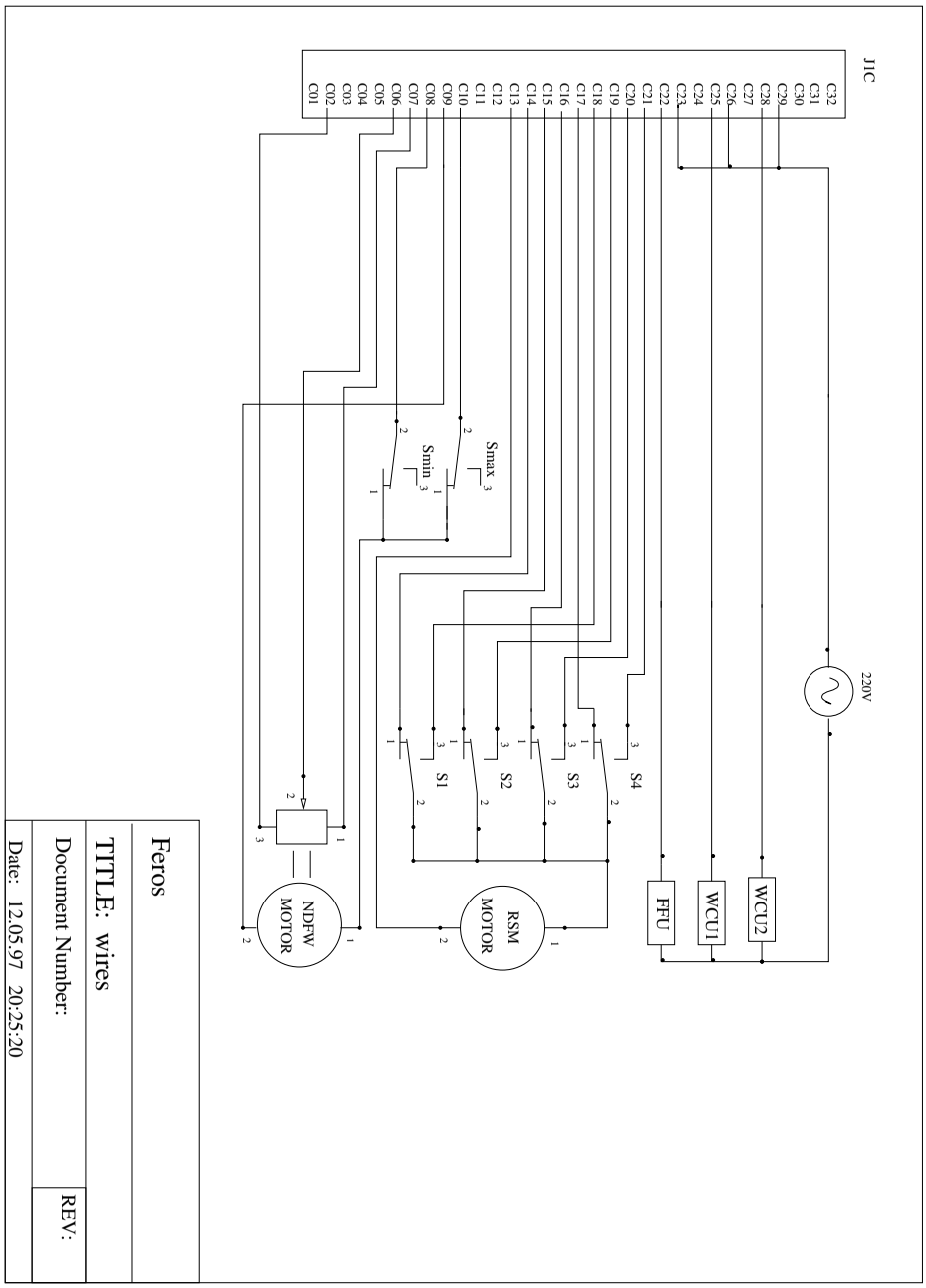

Figure 6.7: Electronical layout for the wiring of the FCU components on the telescope's side.

Chapter 7: Instrument Control: DAISY

A DAISY software frontend is foreseen for the 1.52-m instrument control, which will commonly operate the B&C and the FEROS instruments.

The FEROS shutter will be controlled by the CCD controller by the AOC. Communication between DAISY and this type of CCD controller has already been established at the Danish 1.54-m telescope and will be identical for FEROS.

All additional control functions refer to the FEROS calibration unit (FCU) and are described in Chapter 6.

Derived from this, the DAISY frontend should include the minimum of follwing functions:

- **define instrument:** FEROS or B&C
- **define exposure type:**
  - **FEROS**: Object+Sky
    → Internal Flatfield (FFU)
    → FEROS Wavelength Calib.(WCU1)

    Object+Calib.
    → Internal Flatfield (FFU sequence)
    → FEROS Wavelength Calib.(WCU1 sequence)
    → position of NDFW: τ [1]

    dark
    bias
  - **B&C**: Object
    Internal Flatfield (FFU)
    B&C Wavelength Calib. (WCU2)
    dark
    bias
- **define identifier:** `ident`

[1] if not computed from exposure time

- **define exposure time:** `t[sec]`
- **exposure:** start
  pause
  continue
  cancel

For the FEROS on-line data reduction software it is essential to save all these definitions in the FITS header of the CCD frames as descriptors.

In addition, the date, the universal time UT, and the siderial time ST at begin and end of exposure together with the telescope position as right ascension RA and declination DE should be passed to the image descriptors.

For standard reductions with a 'master flatfield' and a 'master wavelength calibration' frame, the instrument control system should be able to pass a corresponding flag to the data-reduction system.

Chapter 8: Instrument Simulation

Several tools for the simulation of the FEROS instrument have been developed. The purposes of these software tools are to provide

- raw data input for the development of the data reduction software (DRS),
- a 'physical model' of the instrument to cope with special problems inherent to the FEROS instrument (to be used during alignment, monitoring of the performance, development of the DRS)
- an exposure time calculator for the preparation of the observations

8.1 Raw-Data Simulator

The raw-data simulator runs in the MIDAS enviroment and produces a 2D MIDAS frame with the size of the detector (2k×4k pixels, 18 bit) showing the FEROS echellogram. For two examples of a Flatfield and a calibration-lamp exposure cf. Fig. 2.1 in Chapter 2.

The MIDAS pogramm to run the simulators shows the necessary input parmeters:

```
! @@ echgramm.prg
! ++++++++++++++++++++++++++++++++++++++++++++++++++++++++++++
!
! MIDAS procedure  echgramm.prg
! A. Kaufer     970404
!
! use via
!       echgramm frame
!       echgramm frame spectrum texp,mag flags
!
!   with
!       frame    : result frame
!       1d-spec  : 1-dim input spectrum
!       texp     : exposure level
!       flags    : Sky/Straylight/Noise flags [Y/N]
! ++++++++++++++++++++++++++++++++++++++++++++++++++++++++++++
!
define/par p1 ?   IMA  "Enter result frame : "
define/par p2 ?   IMA  "Enter 1D input spectrum: "
define/par p3 0.5,0 C  "Exposure time [sec], vis.Magnitude : "
define/par p4 YNN   C  "Sky/Straylight/Noise: [Y/N] "
!
write/key OUT_A {p1}
```

```
write/key INPUTR/R/1/2 {p3}
!
run MIDEXEC:echgramm_FEROS_M
!
read/descr {p1} *
crea/disp 0 415,830
load/lut idl4
load {p1} sc=-5
!
end:
```

The 1D input spectrum has to represent the wavelenth dependent flux distribution of the light source and, in the case of a stellar spectrum, should be normalized to unity at 5550 Å.

This model then includes:

- the wavelength dependent transmission of the instrument
- models for the grating and prism dispersions
- a model for the blaze function
- a model for the cross-dispersion profile due to the image slicer
- a model for the straylight distribution
- models for photon and detector noise
- data sampling

This modeling is of crucial importance for the development of the data-reduction software, which has to cope with, e.g., the strong curvature of the echelle orders and the complicated cross-profile of the orders.

Basically this model could also be used to derive the reachable S/N of the spectra by using the DRS routines to completely reduce the spectra. A more direct approach for the estimation of the expected quality of the spectra will be given by the exposure-time calculator (cf. below).

8.2 Physical Model

Based on the opto-mechanical design of the FEROS system, a basic physical model of the system is available. The influence of deviations of the real optical system to the designed system onto the instrument performance can be evalutated easily with this model. This will be of importance during the integration and alignment phase of the instrument.

The result of an application of this model is shown in Fig. 8.1: the lengths of the vertical bars show the field and color dependent deviations between the

positions on the detector according to the analytical grating dispersion equation and the centroids of the raytraces computed by the physical model (enlarged by a factor 2). These data are now used to find an optimized global representation of the dispersion of the FEROS instrument which is crucial for the data reduction software. With this model it was possible to improve the RMS values of the global wavelength fit from 25 mÅ to 2 mÅ which is needed for the high precision studies to be performed with FEROS.

8.3 Exposure-Time Calculator

For the preparation of an observing run, the user will be equipped with an exposure-time calculator (accessible via the WWW).

For the given input parameters

- visual magnitude or flux of the object in one of the UBVRI bands,
- spectral type (or effective temperature) of the object,
- observing date and time, RA, DE (to compute phase of the moon and airmass, and possibly pointing restrictions at the ESO 1.52),
- seeing,
- CCD binning factor

the necessary exposure time to reach a specified S/N (or vice versa) at a given wavelength will be computed.

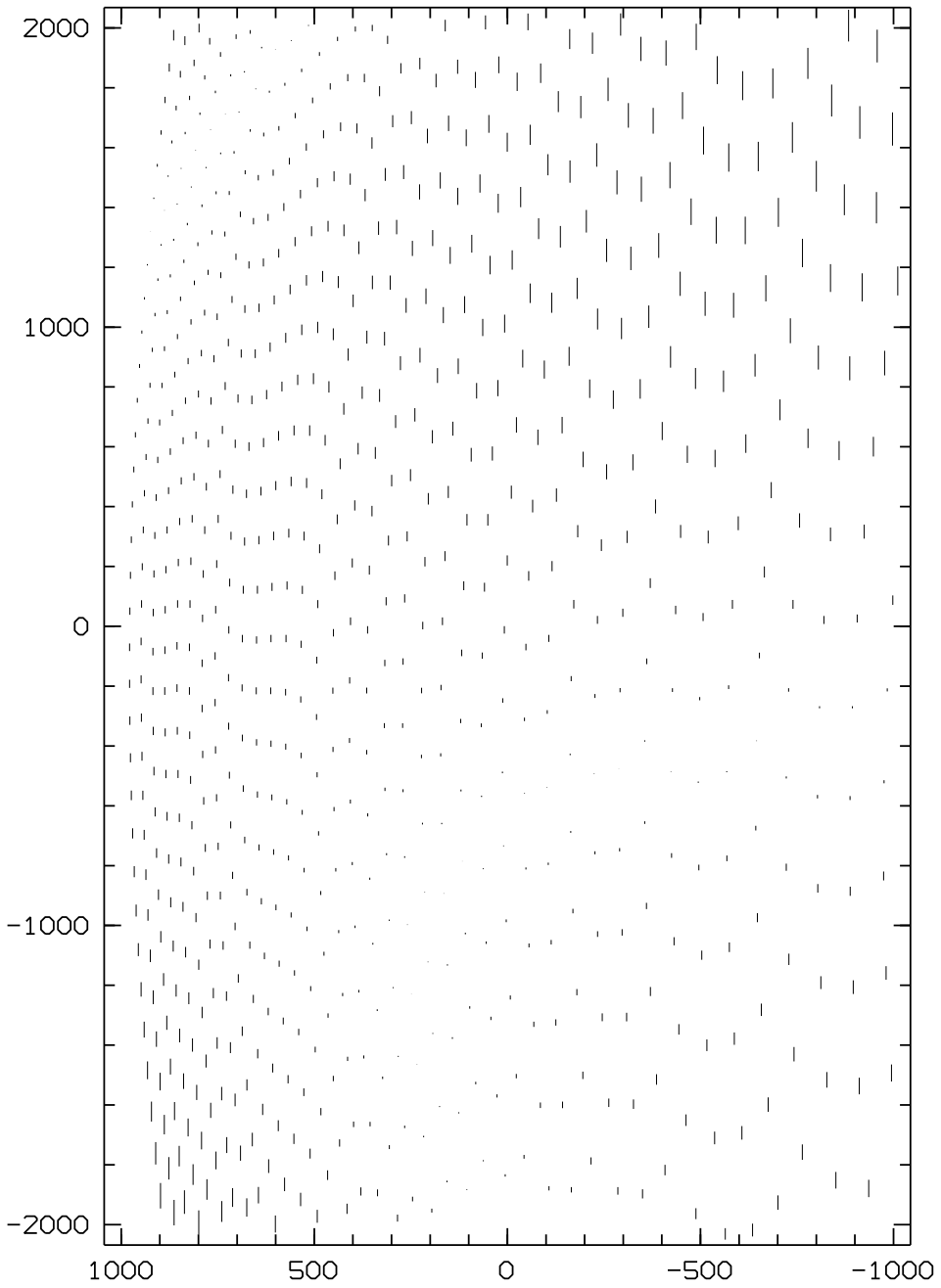

Figure 8.1: Distortion of the echellogram on the detector due to the 'real' optical system (cf. text).

Chapter 9: Data Reduction Software

The FEROS data reduction software (DRS) will run in the MIDAS environment under UNIX. As far as possible, existing MIDAS code will be used for the reduction.

The standard MIDAS echelle package has to be modified in a few areas since it is not optimized for fiber data and the strong curvature of the spectra in FEROS. We have already developed a modified version of the MIDAS echelle package for the fiber-coupled echelle spectrograph of Heidelberg (HEROS), which deals with many of the problems which are specific to fiber-linked echelle spectrographs. We can build the FEROS DRS on this package.

The software will be completely automatic if the results of a previous reduction session are available. The results of a reduction session (calibration tables and parameters) can be saved and recalled later as guess parameters for the automatic reduction. This is basically already working with standard MIDAS, if reproducible standard setups are used, which will be the case with FEROS.

The DRS will be available at the telescope workstation and allow on-line data reduction. This requires efficient coding of all routines working with the large 2k$\times$4k frames.

The reduction package will include:

1. **Precise order definition**. The standard MIDAS procedures will not be optimal for FEROS due to the strong curvature of the spectra and the complex slit crossprofile due to the use of an image slicer. Since the location of the orders will be very stable, it is sufficient to trace the orders on a well-exposed flat-field spectrum, which makes order detection and definition fairly simple.

   FEROS will possibly allow to switch between two wavelength ranges. The reproducibility of the setting ($<$ 10 pixel in cross-dispersion direction) will be sufficient to allow full on-line reduction also in this case.

2. **Precise wavelength calibration**. This is especially critical in the red part, where in some orders only a few lines will be available for wavelength calibration. This can be overcome with "global" dispersion formulae, which combine several orders for the fit. This increases the robustness of the fit substantially.

   For the highest precision, a calibration lamp spectrum will be exposed simultaneously with the object spectrum through the "sky" fiber. With this

procedure, small wavelength shifts during the exposure can be corrected for. The systematic errors of the wavelength calibration are then limited by the stability of the *relative* position of both fibers only.

3. **Background subtraction**. This is a critical point for all echelle spectrographs, especially when little space is available between the orders, which in our case is in the red part of the spectrum. However, sufficient inter-order space is available with FEROS (minimum 5 pixel) even with the use of a sky-fiber. Spline interpolation of the interorder background will be used to approximate the background.

4. **Flat-field correction**. For fiber spectrographs, division by the flat-field removes also most of the echelle blaze function. For fiber spectrographs, flat-fielding has to be done (and can be done), with the extracted 1-D spectra, and not with the 2-D data.

5. **Optimal order extraction** requires precise order definition. Optimal extraction algorithms can then be used to optimize the S/N ratio.

6. **Rebinning** to constant wavelength steps in linear and logarithmic scale. Logarithmic scale is required for cross-correlation techniques. The rebinning corrects the heliocentric velocity also, so that rebinning is required only once.

7. **Order merging** requires previous removal of the echelle blaze function. With fiber spectra, this can be done with good precision with flat-fielding only. Small residual curvatures can be removed with the use of standard stars.

8. **Correction for the instrument response function**. A standard response function can be built by observing spectrophotometric standards which have a proper wavelength sampling. If the echelle ripple can be removed by flat-fielding, no particularly dense sampling is required for the standard star tables.

9. **Sky subtraction**. This is not foreseen within the standard MIDAS echelle package. With FEROS it can be done if the "sky" fiber is used. Object and sky spectra will be extracted in the same way and the wavelength-calibrated 1-D spectra will be subtracted.

10. **Graphical user interface**. The FEROS DRS will have many parameters. Although most of these are filled on start-up with reasonable "default" values which allow completely automatic reduction, a GUI will be supplied to ease the operation for inexperienced users.

11. **Cross correlation facilities** to achieve relative radial velocity measurements with an accuracy of 50 m/s, which corresponds to about 1/50 pixel on the

detector.

12. **Time-series analysis facilities**. Time series spectroscopy will be an important application with FEROS. Several tools to analyze and display such data (2-D time series spectra) will be provided.

13. **Data-archive facilities**. 2-D raw data, 2-D extracted (pixel-order space) data, 2-D rebinned (wavelength-order space) data 1-D merged spectra can all be archived.

Chapter 10: Alignment Concept

10.1 General

This concept shows in which way the different optical components of the FEROS instrument will be integrated and aligned.

The following nomenclature for the coordinate systems is used below:

coord.system	axis	direction
table system:	X	along the long table axis
	Y	along the short table axis
	Z	perpendicular to the table surface
optical system:	x	main dispersion, perpendicular to table surface ($\parallel$ Z)
	y	cross dispersion direction
	z	along the local optical axis

The optical bench on which the spectrograph is set up has a 25-mm grid of mounting holes which is used as a reference system on which all components can be positioned to within ± 1 mm to the computed positions.

The optical axis of the complete system is parallel to the table top with a distance of 270 mm.

10.2 Alignment tools

The following main alignment tools are needed:

1. 1 Auto-Collimator + Achromat producing a F/11 beam (AC+F/11).
2. 1 Flat Mirror, 20 mm diameter (M1)
3. 2 Flat Mirrors, 140 mm diameter (M2 and M3)
4. 1 HeNe Laser
5. Masks with computed beam positions and sizes for the Laser wavelength.
6. (Microscope+CCD–imager, only at LSW)
7. Removable cylinder for Fiber-exit head
8. Removable cylinder for Fieldlens (delivered by manufacturer of the Camera)
9. Hartman-masks for the Camera focussing

For the fine alignments of the individual components of the instrument, the following steps are neccessary (in chronological order):

10.3 Centering of the Microlens on the Fiber

The fiber-entrance surfaces are glued and polished in standard SMA906 connectors. This connector type offers a strongly toleranced top of the ferrule. To center the microlens, for each lens and connector an individually machined cap will reduce the diameter of the ferrule to the microlens diameter of 1.10 mm.

The fiber connectors of object and sky have to be carefully positioned in the B&C adaptor against the entrance diaphragms with 0.294 mm hole diameter by the use of precision fiber positioners. The distance from the diaphragm in the telescope focus to the surface of the microlens is 1.35 mm.

10.4 Internal alignment of the Fiber-exit heads

Figure 10.1 shows a layout of the Fiber-exit unit consisting of the Fiber-exit head and the basement.

The two exchangeable Fiber-exit heads have to be aligned separately before mounting onto the basement, which is pre-installed on the optical table (see below). The incoming two fibers are mounted on the Fiber-exit head for which the following alignment steps are required:

1. Distance of fiber exits to pupil stop.
   The two fibers have to be mounted on the Fiber-exit head in guidings which position the fibers' axis within mechanical accuracy. The fibers are movable within the guidings in z-direction and are aligned to the nominal distance to the pupil stop of 13.3 mm. For this purpose, a cylinder of 13.3 mm radius can be inserted at the place of the stop. Then the exit surfaces of the fibers have to be brought in contact with the cylinder's surface. The cylinder can be removed then and leaves the fiber-exit surfaces concentric to the stop.

2. Alignment of the F/N system to the fiber-exit surfaces.
   Position of F/N system within mechanical accuracy with the help of the xyz-positioner. The images of the fiber pairs will be inspected at the F/11 focus with the AC+F/11 system to check the conformity with the computed spot diagrams, the computed image diameter of 0.240 mm, and the distance of 0.900 mm. This is important to match the geometry of the image slicer.

3. Alignment of the image slicer.
   The image slicer has to be positioned at the F/11 focus within mechanical accuracy with the help of the second xyz-positioner. Then the slicer prism has to be aligned with the fiber pair in y-direction by rotating the image

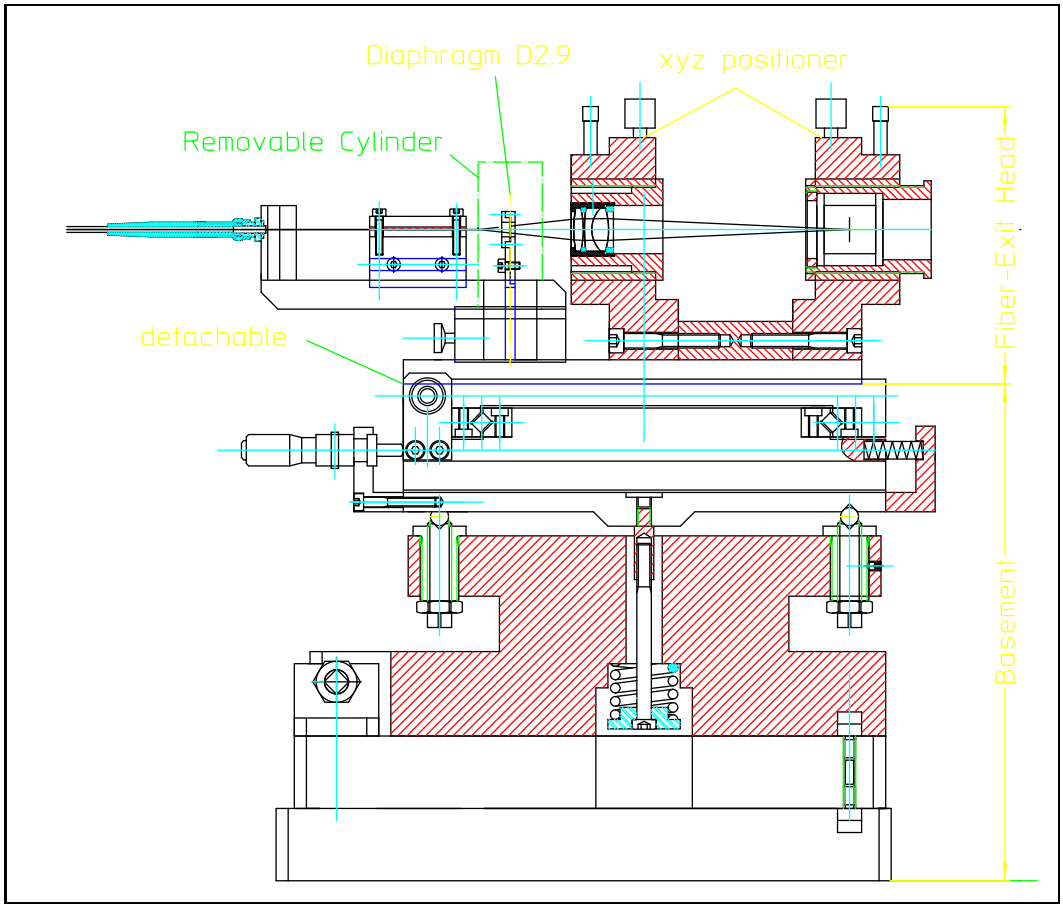

Figure 10.1: The Fiber-exit unit with the detachable Fiber-exit head mounted on its basement. Further, the xyz-positioners, the micrometer screws and the removable cylinder are indicated (cf. text).

slicer around the z-axis. By translating in xy the full images have to be converted into the sliced images of the fiber images. The work with a 15:1 scale image-slicer model has shown that the best alignment can be well judged from the geometry of the sliced images. This can be done with the AC+F/11 system already installed in the previous step. Further, the signal from the unsliced image has to be distributed equally in the two sliced 'half moons'. Both, geometry and intensity distribution can be well-measured with the microscope+CCD imager at LSW for the prealignment of the two Fiber-exit heads. Figure 10.2 shows the outputs from the Acrylic (!) 15:1 scale image-slicer model.

4. Mounting of the Fiber-exit head on the basement on the optical table will be conducted after the alignment of the Collimator–Echelle unit.

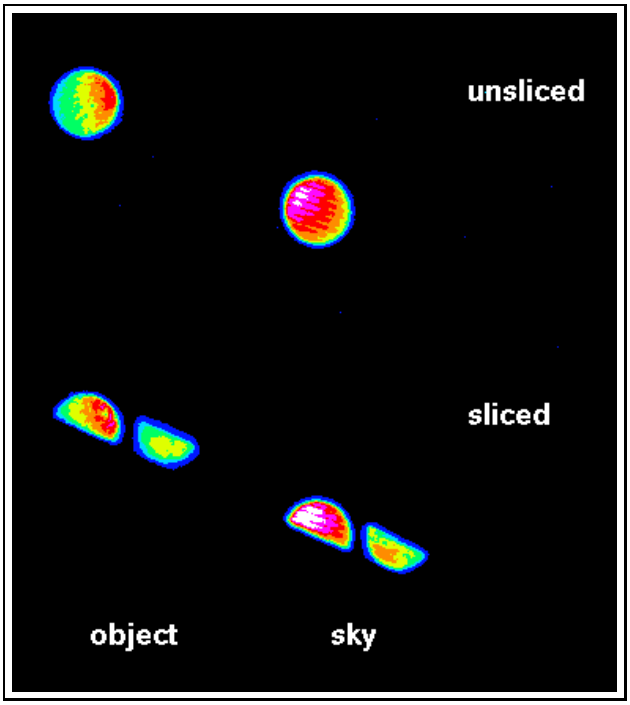

Figure 10.2: CCD images of the unsliced and sliced outputs of the scaled image-slicer prototype. The inhomogeneous intensity distributions within the images is due to the low polishing quality and inhomogeneity of the Acrylic's surfaces.

10.5 Pre-alignment of the basement of the Fiber-exit unit

Position and angle of the basement of the Fiber-exit unit with mechanical accuracy on the optical table. The exact off-axis angle of 6.466° can be aligned with the help of the turning device foreseen in the basement.

For the further alignment steps, the AC+F/11 system is installed on the basement of the Fiber-exit unit. The focus of the F/11 achromat is defined by autocollimation by inserting mirror M1 (Fig. 10.3, step 1). This focus position is moved to the nominal slit position of the FEROS system with the help of the positioning elements of the basement.

10.6 Position and focus of Collimator 1

Position on the optical table with mechanical accuracy.

The focus of the Main Collimator is checked with the AC+F/11 system by inserting mirror M2 at the nominal position of the Echelle grating in the parallel beam (Fig. 10.3, step 2).

10.7 Position of Folding Mirror

Position on the optical table with mechanical accuracy is sufficient. Alignment of small tilts and rotation around the Z-axis through the reflecting surface is foreseen and can be used in the next alignment step.

10.8 Focus of Collimator 2

Position on the optical table with mechanical accuracy.

The focus of the Transfer Collimator is checked with the AC+F/11 system by inserting mirror M3 at the nominal position of the prism cross disperser. (Fig. 10.3, step 3).

For this purpose, mirror M2 has to be turned around the vertical Z-axis by 0.6° (as later the Echelle) until it points via Collimator 1, the Folding Mirror, and Collimator 2 to mirror M3.

10.9 Mounting and alignment of Fiber-exit unit

For the alignment of the Fiber-exit unit the position of the focus ahead of the Folding Mirror (about 100 mm) has to be determined. Therefore, mirror M1 is inserted again at the previously determined position and turned by 180°. The AC+F/11 system is removed from the basement of the Fiber-exit head and placed at the intermediate focus position (Fig. 10.3, step 4). The alignment and focus is checked with auto-collimation.

Now, having fixed the slit position of the system with the AC, M1 can be removed and the Fiber-exit head can be mounted on its basement (Fig. 10.3, step 5).

The Fiber-exit head with the spectrograph 'slit' within the image slicer must be focussed now to the already set-up Collimator–Echelle–system. For this purpose, the basement of the Fiber-exit unit can be aligned internally in z- and y-direction with micrometer screws (cf. Fig.10.1). The focus (z-direction) and the image position (xy-direction) has to be checked at the intermediate focus behind the Folding Mirror with the previously aligned AC+F/11 system.

10.10 Position and tilt of Echelle grating

For this step, the AC+F/11 system, M2 and M3 can be removed. Now, the Fiber-exit head is fed by the light of a He-Ne laser through one fiber. This provides a sufficiently bright beam to follow through the system.

Then, the Echelle is positioned on the optical table with mechanical accuracy (Fig. 10.3, step 6).

The correct alignment of the blaze angle 63.4° (y-axis), the off-Littrow angle of 0.6° (x-axis) and the z-axis of the Echelle is checked by following the reflected and dispersed F/11 laser beam. The computed positions will be indicated on masks which can be inserted in front of the Collimator 1, the Folding Mirror and the Collimator 2.

10.11 Position of crossdisperser prism

Mechanical accuracy is sufficient. The angle of minimium deflection of 48.6° is sufficiently aligned with the turntable which gives a resolution of better than 1 arcminute (≈ 10 pixels on the detector).

10.12 Alignment of the unit Camera – Fieldlens – CCD

Camera, Fieldlens and CCD have to be aligned separately as one unit before mounting onto the optical table.

1. Position of CCD chip relative to fieldlens.
   The precise alignment of the fieldlens which also acts as the entrance window of the CCD dewar and the CCD chip is carried out by the supplier of the CCD, i.e., the AOC.

2. Centering of the fieldlens on the Camera.
   The centering of the fieldlens and the front part of the Camera has to be better than 50 μm. Therefore, between the Camera housing and the fieldlens mounting a reference cylinder supplied by the manufacturer can be introduced. Therefore, the Camera's focussing unit has to be movable perpendicular to the optical axis in y-direction against the fieldlens+CCD. Alignment in x-direction is available at the CCD-flange. After the centering procedure, the cylinder is removed and the shutter can be mounted at the CCD flange forming a light-tight unit.

3. Focussing of the Camera.
   Linear translation along the z-axis is foreseen. For focussing the linear resolution is better than 5 μm. Manual focussing is foreseen with passive thermal compensation. For the focussing procedure, an operating CCD system is required. For fine focussing of the Camera, Hartman masks can be inserted at the front of the focussing unit using the provided sledge.

4. Alignment of Echelle orders.
   For the final alignment of the CCD rows and the slit images, the CCD has to be rotated by 2.4° around the z-axis.

10.13 Position of Camera–CCD unit

The prealigned Camera–CCD unit will be positioned with mechanical accuracy on the optical table. The support of this unit is alignable in XY on the optical table to allow for the alignment of the optical axis of the Camera–CCD unit and the outgoing beam of the crossdisperser prism (Fig. 10.3, step 7).

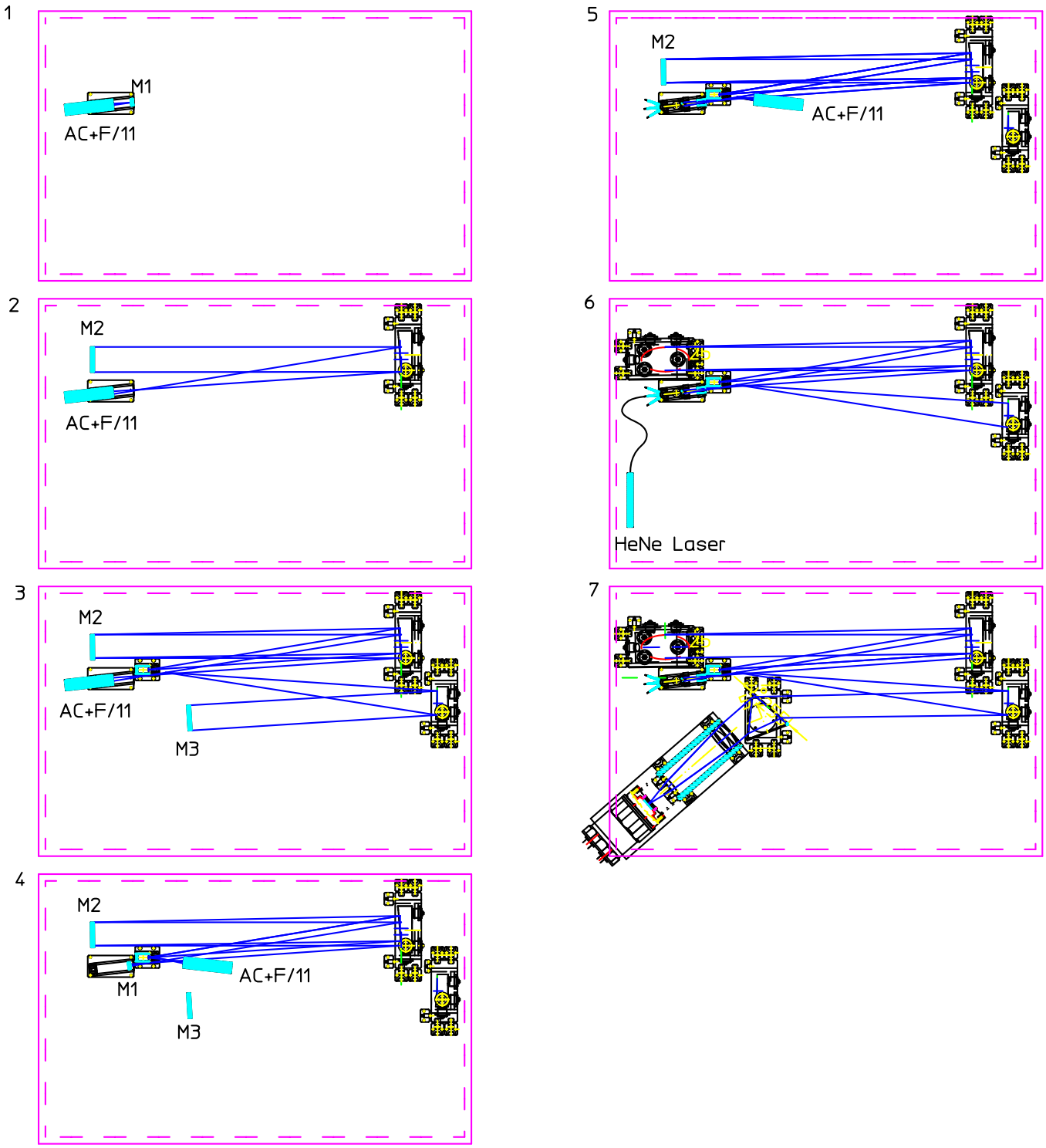

Figure 10.3: Alignment steps for the FEROS system.

Chapter 11: Concept for Verification Tests

The conformance with the requirements and the reached performance will be first tested in the laboratory in Heidelberg. The acquisition of CCD frames and the on-line data reduction in the MIDAS environment are prerequisites for any of the further tests. Therefore, the following tests are simultaneously tests for the CCD controller hard and software and the on-line data reduction software.

1. The **spectral range** will be the first result of the on-line reduction of an obtained spectrum.
2. The **resolving power** and its **degradation over the detector** by measuring over the full spectral range the FWHMs of spectral lines in raw (2-D) and fully reduced (1-D) Thorium-Argon calibration spectra.
3. The **degradation of the resolving power due to temperature variations** by monitoring the (unstabilized) room temperature and measuring simultaneously the FWHMs as described above.
4. The **line asymmetry** by computing the skewness (third moment) of the light distribution within Thorium-Argon emission lines all over the detector.
5. The **interorder scattered light level** by measuring the background over the detector in flatfield exposures.
6. The **radial-velocity accuracy** and therefore the stability of the configuration by exposing several daylight sky (i.e. solar) spectra with exposure times of about an hour spread over several hours and days. The scatter in the derived radial velocities will be measured.
7. The **efficiencies of the subcomponents** of the instrument are tested at the following locations:

• Fiber-exit head (Micro lens + fiber + F/N system + image slicer)	ESO laboratory
• CCD	AO Copenhagen or ESO
• All other components	Manufacturers

8. The **total efficiency** of the FEROS instrument under realistic conditions will be measured at the 1.52-m telescope during the commissioning phase with spectrophotometric standard stars.

Chapter 12: Maintenance Concept

FEROS is bench-mounted in a separate room in the Coudé room of the ESO 1.52-m telescope. No mechanical instrument change-overs are needed at the ESO 1.52-m telescope to change between the operation of the B&C and FEROS. Since the FEROS instrument works in a fixed configuration without any movable parts on its bench-mounted part, no time for the instrument setup is required.

Therefore, to maintain the performance of FEROS during operation at La Silla, a comparatively small amount of maintenance work is needed.

In the following a tentative list of items for a maintenance plan is given:

- Cleaning of object and sky fiber end surfaces, twice per year
- Cleaning of surfaces of the calibration fiber connectors
- Check of the pressure in the vibration control system, once per month
- Re-filling of LN_2 tank, once per two weeks
- Check of temperature/humidity control system, once per month
- Check of the calibration lamps, once per year
- Continuous monitoring of the instrument performance

The latter is of crucial importance for a long-term stability of the instrument. For the verification of the instrument performance during the comissioning phase a set of mainly software based verification procedures will be provided and, therefore, are available for this task, too. These performance checks should be carried out on a timescale of several months.

A monitoring of the major performance parameters like the resolution and the efficiency of the instrument should also be carried out and reported by the observers.

Chapter 13: Safety Aspects

During the setup of the instrument, the operation, and the maintenance work, a small number of safety aspects have to be considered to avoid hazards to the human personal.

In this sense, the following list refers to items with critical handling:

- The optical bench is a heavy (600 kg) and large ($2500 \times 1500 \times 200$ mm) component and therefore requires a particularly careful handling during the set-up phase. Especially the transport up to the Coudé room has to be considered.
- Further heavy and sensitive optical components: Echelle + mounting (50 kg), Main collimator + mounting (50 kg), Transfer collimator + mounting (50 kg), Camera–CCD unit (100 kg)
- The handling of liquid nitrogen for the continuous-flow dewar must be in accordance with the common operation instructions.
- High voltages are used in connection with the calibration lamps in the FEROS Calibration Unit (FCU) attached to the B&C adapter. Critical points on the FCU will be adequately labeled.
- Earthquakes: all components of the bench-mounted part of the spectrograph are permanently fixed onto the bench with clamps. The vibration-control system of the bench itself is clamped to the table top, too. Therefore, no moving or dropping heavy mechanical components will be encountered during potential earthquakes.

Chapter 14: Planning and Management

14.1 Strategy

The four institutes building FEROS are:

- Landessternwarte (State Observatory) Heidelberg–Königstuhl (LSW)
- Astronomical Observatory Copenhagen University (AOC)
- Institut d'Astrophysique de Paris (IAP)
- Observatoire de Paris/Meudon (OPM)

The strategy followed in this project aims on putting FEROS into operation for the astronomical community as soon as possible. Therefore, a tight schedule for the procurement, manufacturing, integration, and tests of the subcomponents is indispensable. In this time schedule the most critical part is the manufacturing of the camera which will have the longest delivery time of all subcomponents.

In the following first the division of areas of responsibilities between the consortium members are briefly described. Then the members of the key personnel are introduced. Finally, the individual work components with their time schedule are described, the required actions are defined, and manpower estimate and responsibilities are given.

14.2 Responsibilities

Most of the construction work will be carried out in the workshops of the LSW and the instrument will be set up in the laboratory of the LSW. The CCD system will be supplied by the AOC. Items which cannot be manufactured in our workshops will be procured from outside suppliers. The IAP/OPM will contribute services for the commissioning phase, evaluation of performances, and writing of documentation.

One scientist is permanently engaged to coordinate the project (A. Kaufer, LSW). The organigram of Fig. 14.1 shows the responsibilities of the key personnel (see next chapter) for the project.

14.3 Key Personnel

The following scientists and technicians are nominated for key functions within the management structure of the FEROS project (in alphabetical order). For their responsibilities see also Fig. 14.1.

Name	Johannes Andersen
Education	Ph.D. and D.Sc., University of Copenhagen
Position	Associate Professor and Deputy Director, AOC
Research	Stellar and Galactic astrophysics, instrumentation
Function	Overall coordination of CCD camera, liaison
Experience	25 years experience in spectroscopic observations, instrument design (including CES, CASPEC), and project coordination
Availability	15%

Name	Immo Appenzeller
Education	Dr. rer. nat. University of Göttingen
Position	Professor for Astronomy, University of Heidelberg and Director, Landessternwarte Heidelberg–Königstuhl
Research	Stellar and extragalactic astrophysics
Function	Advisor
Experience	About 25 years of experience in developing polarimetric, photometric, and spectrographic instrumentation
Availability	Advisor

Name	Roger Cayrel
Education	Dr. of the University of Paris
Position	Senior Astronomer at Paris Observatory
Research	Chemical composition of stars, spectroscopy
Function	Coordinator for the Paris Observatory group (M. and F.Spite, P.Francois, S.Grenier). Methods of data reduction, user's manual
Experience	Associate director if INAG (1968-72); project officer and director of CFHT telescope (1974-81); extensive experience in observations
Availability	15% to 25%, depending on the stage of the project

Name	Michel Dennefeld
Education	Dr. of University of Paris
Position	Maitre de Conferences at Paris University
Research	Chemical evolution of galaxies, spectroscopy
Function	Coordinator of the IAP group (M.Gerbaldi, A.Vidal-Madjar, R.Ferlet); tests, data reduction methods, user's manual
Experience	Head of the instrumentation group of INSU; extensive experience in observational spectroscopy
Availability	15%

Name	Claus Hartlieb
Education	"Meister" of precision mechanics
Position	Technical staff, Landessternwarte Heidelberg–Königstuhl

Function	Construction and manufacturing
Experience	Over 40 years of professional experience
Availability	45%

Name	Andreas Kaufer
Education	Dr. rer. nat. University of Heidelberg
Position	Research Scientist, Landessternwarte Heidelberg–Königstuhl
Research	Variability in hot luminous stars, the chemical evolution of the Galaxy, instrumentation for high-resolution spectroscopy
Function	Instrument responsible
Experience	5 years of experience in astronomical observation especially with (fiber-linked) echelle spectrographs; development and comissioning of HEROS.
Availability	100%

Name	Jens Klougart
Education	Electronics Engineer, Technical University of Denmark
Position	Project Engineer, Telescope and Instrument Control
Function	High-level controller programming; interface to telescope and spectrograph controllers; MIDAS file interface; documentation
Experience	Over 15 years of experience in design and construction of telescope control and data acquisition systems; also upgrade and management of computer and workstation networks and communications
Availability	15%

Name	Anton Malina
Education	Pre-graduate in physics, University of Heidelberg
Position	Graduate student, Landessternwarte Heidelberg–Königstuhl
Research	Data-Reduction Software (DRS)
Function	Online DRS
Experience	Experience in software design, C, Fortran, MIDAS
Availability	100%

Name	Holger Mandel
Education	Dr. rer. nat. University of Heidelberg
Position	Research scientist, Landessternwarte Heidelberg–Königstuhl
Research	Stellar astrophysics, high-resolution spectroscopy, instrumentation
Function	Optical design, adjustment
Experience	More than 10 years of experience in development of ground-based (FLASH/HEROS) and space instrumentation (ORFEUS)
Availability	25%

Name	Preben Nørregaard

Education	Electronics Engineer, Technical University of Denmark
Position	Project Engineer, CCD camera system at AOC
Function	Design, construction, and test of CCD camera and controller
Experience	10 years of experience with design and construction of telescope control and data acquisition systems, 5 years with CCD cameras
Availability	15%

Name	Ludwig Schäffner
Education	"Meister" of precision mechanics
Position	Technical staff, Landessternwarte Heidelberg–Königstuhl
Function	Construction and manufacturing
Experience	Over 25 years of professional experience
Availability	55%

Name	Walter Seifert
Education	Dr. rer. nat. University of Heidelberg
Position	Research scientist, Landessternwarte Heidelberg–Königstuhl
Research	Extragalactic astrophysics, instrumentation
Function	Optical design
Experience	Experience in astronomical observations and optical design (FORS project)
Availability	Advisor

Name	Otmar Stahl
Education	Dr. rer. nat. University of Heidelberg
Position	Staff scientist, Landessternwarte Heidelberg–Königstuhl
Research	Stellar astrophysics, high-resolution spectroscopy
Function	Head of the science support software group
Experience	More than 10 years of experience in astronomical observations and astronomical data processing. Head of scientific applications software development at the LSW
Availability	20%

Name	Bernhard Wolf
Education	Dr. rer. nat. University of Munich
Position	Director of Astronomy at the Landessternwarte Heidelberg–Königstuhl, Professor at the University of Heidelberg
Research	Stellar astrophysics, high-resolution spectroscopy
Function	Principal Investigator
Experience	About 30 years of experience in astronomical observations and use and development of spectroscopic instrumentation
Availability	30% to 50% depending on the stage of the project.

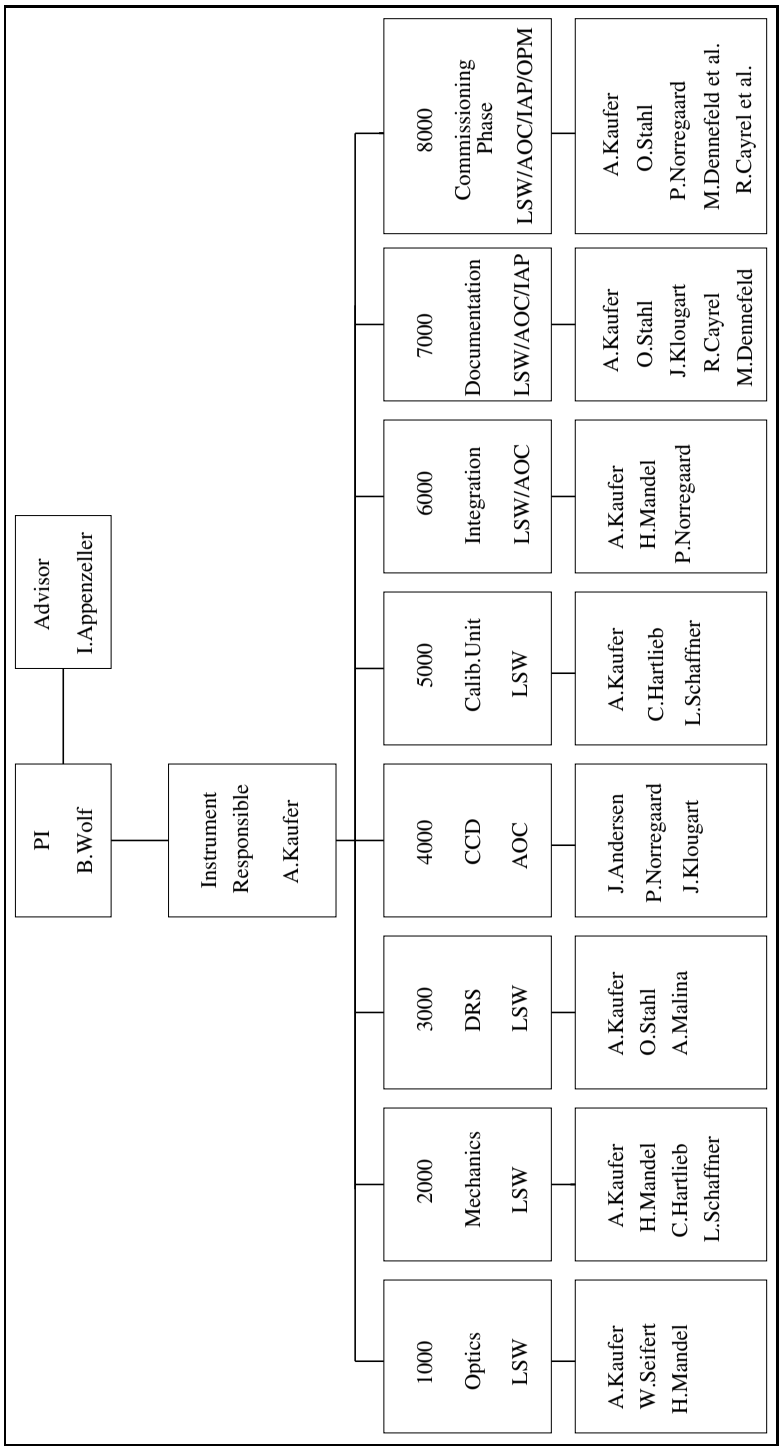

Figure 14.1: Organigram showing the responsibilities of the key personnel.

14.4 Description of Work Components

1000 Optics

Description:
Design of complete optical system, procurement, assembly and testing of individual components

Work to perform:
1001 Final Optical Design
1002 Prototype Image Slicer
1003 Procurement of optical parts

Manpower: 24 weeks

Dependencies:

Support:
A. Kaufer (design, procurement, testing, assembly)
W. Seifert (design)
H. Mandel (procurement)

Status (24/97):
1001 done
1002 work in progress
1003 all components ordered

Remarks: does not include the fiber link

2000 Mechanics

Description:
Design of complete mechanical system, procurement, manufacturing, assembly of individual components

Work to perform:
2001 Final Mechanical Design
2002 Procurement of parts
2003 Manufacturing of parts

Manpower: 46 weeks

Dependencies: 1001, 1003

Support:
A. Kaufer (design drawings)
H. Mandel (procurement)
L. Schäffner (construction, drawings, manufacturing)
C. Hartlieb (manufacturing)

Status (24/97):
2001 done
2002 started
2003 started

Remarks:

3000 Data Reduction Software

Description:

Science data reduction sofware, online DRS, graphical user interface (GUI)

Work to perform:

3001 Implementation

3002 Tests with exisiting and simulated data

3003 Tests with FEROS data

Manpower: 28 weeks

Dependencies: 1001

Support:

A. Kaufer (instrument simulation, DRS, GUI)

O. Stahl (DRS)

A. Malina (Online DRS)

Status (24/97):

3001 work in progress

3002 started

3003

Remarks:

4000 CCD

Description:

Design and procurement of CCD controllers, delivery of engineering and science CCDs, test and integration of CCDs

Work to perform:

- 4001 Purchase of Controllers
- 4002 Delivery of engineering CCD + cryostat by ESO
- 4003 Integration of Camera
- 4004 System Test
- 4005 Delivery of science CCD by ESO
- 4006 Integration of Camera
- 4007 System Test
- 4008 Delivery to LSW

Manpower: 40 weeks

Dependencies: delivery of CCDs and cryostat by ESO

Support:

J. Andersen
P. Nørregaard (system design)
J. Klougart (controller, interfacing)

Status (24/97):

- 4001 done
- 4002 done
- 4003
- 4004
- 4005
- 4006
- 4007
- 4008

Remarks: Work carried out at AOC. ESO has agreed to provide the mechanical parts for the detector head for mounting the CCD and the appropriate wiring for the inside of the detector head. This will be a copy of the parts being made for the UVES Blue detector system.

5000 Calibration Unit

Description:
Design of opto-mechanical system and control electronics, procurement, manufacturing, and assembly

Work to perform:
- 5001 Final optical, mechanical, and electronics design
- 5002 Procurement of parts
- 5003 Manufacturing of parts

Manpower: 6 weeks

Dependencies:

Support:
A. Kaufer (design drawings, procurement)
L. Schäffner (construction, drawings, manufacturing)
C. Hartlieb (manufacturing)

Status (24/97):
- 5001 partially done
- 5002 started
- 5003

Remarks: does not include B&C fiber-slit unit

6000 Integration

Description: Integration of the system components, integration into the complete instrument, alignement, tests

Work to perform:
- 6001 Fiber-exit Unit
- 6002 Calibration Unit
- 6003 Camera – CCD Unit
- 6004 Complete Instrument

Manpower: 28 weeks

Dependencies: 1000, 2000, (3000), 4000, 5000

Support:
A. Kaufer (integration, assembly, alignment)
H. Mandel (alignment)
P. Nørregaard (CCD, controller)

Status (24/97):
- 6001
- 6002
- 6003
- 6004

Remarks: at LSW

7000 Documentation

Description:
Documentation of the opto-mechanics, the CCD system, the data reduction software, and the complete system. Supply of operation and user manuals.

Work to perform:
7001 Draft Versions
7002 Final Versions

Manpower: 32 weeks

Dependencies: 1000, 2000, 3000, 4000, 5000, 6000, 8000

Support:
A. Kaufer (Optics, Mechanics)
O. Stahl (DRS)
J. Klougart (CCD)
R. Cayrel (Operation)
M. Dennefeld (User)

Status (24/97):
7001
7002

Remarks:

8000 Commissioning

Description: Comissioning of the instrument at the ESO 1.52-m telescope

Work to perform:
8001 1. Run: setup of instrument and DRS, integration to B&C, implementation of instrument control
8002 2. Run: verification of performance
8003 3. Run: optimization

Manpower: 18 weeks

Dependencies: 6000, 7000

Support:
A. Kaufer (Instrument)
O. Stahl (DRS)
P. Nørregaard (CCD)
M. Dennefeld (Operation)
R. Cayrel (Operation)

Status (24/97):
8001
8002
8003

Remarks:

14.5 Time Schedule

The time schedule for the execution of the individual tasks defined in the work components above is given by the bar chart on the following page. The used symbols read as follows:

$\triangle$ = Milestone

$\triangle\!\!\!\!\bigcirc$ = Reached Milestone

$\vdash$ = Begin of Period

$\dashv$ = End of Period

Work Package	Item	1996 J A S O N D	1997 J F M A M J J A S O N D	1998 J F M A M J J A S O N D	1999 J F M A M J J A S O N D	2000 J F M A M J J A S O N D
1000	**Optics**	⊢ – – – –	– – – – – – – – – – – –	– – – – – – – – – – – – ⊣		
1001	Final Optical Design	⊢ – – ⊣				
1002	Prototype Image Slicer		⊢ – – ⊣			
1003	Procurement of opt. parts	⊢ –	– – – – – – – – – – – –	– – – – – – – – – – – – ⊣		
	Reserve			⋆		
	Optical Design Review	◬				
2000	**Mechanics**		⊢ – – – – – – – – – – – –	– – – – – – – – – – – – ⊣		
2001	Final Mechanical Design		⊢ – – – – ⊣			
2002	Procurement of parts		⊢ – – – – ⊣			
2003	Manufacturing of parts		⊢ – – – – ⊣			
	Reserve			⋆		
	Final Design Review		△			
3000	**DR Software**		⊢ – – – – – – – – – – – –	– – – – – – – – – – – – ⊣		
3001	Implementation		⊢ – – – – ⊣			
3002	Tests with exist. data			⊢ – – ⊣		
3003	Tests with FEROS			⊢ – – ⊣		
	Reserve			⋆		
4000	**CCD**		⊢ – – – – – – – – – – – –	– – – – – – – – – – – – ⊣		
4001	Purchase of Controllers		⊢ – – – – – – ⊣			
4002	Delivery of eng. CCD		◬			
4003	Integration of Camera		⊢ – – ⊣			
4004	System Test		⊢ – – – ⊣			
4005	Delivery of sci. CCD			△		
4006	Integration of Camera			⊢ ⊣		
4007	System Test			⊢ ⊣		
4008	Delivery to LSW			△		
	Reserve			⋆		
5000	**Calibration Unit**		⊢ – – – – – – – ⊣			
5001	Design		⊢ – ⊣			
5002	Procurement		⊢ – – – – ⊣			
5003	Manufacturing			⊢ ⊣		
	Reserve			⋆		
6000	**Integration**			⊢ – – – – – – – ⊣		
6001	Fiber-exit unit			⊢ – ⊣		
6002	Calibration unit			⊢ ⊣		
6003	Camera – CCD unit			⊢		
6004	Complete instrument			⊢ ⊣		
	Reserve			⋆		
	Preliminary Acceptance			△		
7000	**Documentation**			⊢ – – – – – – – – – – ⊣		
7001	Draft Version			⊢ – – – – ⊣		
7002	Final version			⊢ – – – – ⊣		
8000	**Commissioning**			⊢ – – ⊣		
8001	1. Run			⊢		
8002	2. Run			⊢		
8003	3. Run			⊢		
	Provisional Acceptance			△		
	Guarantee Period				⊢ – – – – – – – – – – – –	– – – – – – – – – – – – ⊣
	Final Acceptance					△

14.6 Manpower Estimate

A summary of the total manpower in man-weeks for the work components is given in the following table. Here, the manpower estimates from the work components above are splitted into the years and scientific and technical manpower requirements.

Work	1996		1997		1998		1999	2000
Package	Sci.	Tech.	Sci.	Tech.	Sci.	Tech.		
1000 Opt.	14		8		2			
2000 Mech.	4	2	8	28		4		
3000 DRS.			20		8			
4000 CCD			12	20	4	4		
5000 Calib.			2	4				
6000 Integ.			8		20			
7000 Doc.			10	12	10			
8000 Com.					16	2		
Guarantee Period							$*$	$*$

During the guarantee period (marked with $*$ in the table above), manpower will be available for necessary improvements (on request) and has to be available for the execution and reduction of the observing programs during the guaranteed observing runs.

The manpower commitment for the technical tasks will be supplemented by a few scientists of the associated institutes who will participate in the test phase (3 times 10 nights comissioning time) and the scientific program (45 nights guaranteed observing time). This group, headed by the PI, will be responsible for working out the details of the observing program, for preparing of the observations and for ensuring rapid analysis and scientific use of the data collected. It will closely cooperate with the technical groups to optimize the scientific use of the observing time.

14.7 Procurement Plan

Table 14.1 gives a list of the provider and manufacturers of the major FEROS components, which were selected by the consortium. The expected delivery dates of the components are given in week/year. Note that all the optical and many of the supplementary components are already ordered to keep the time schedule of the project.

Table 14.1: *FEROS Procurement Plan.* r = received, dn = delayed by n weeks

Component	Manufacturer/Provider (Country)	Delivery	Status
Echelle Grating	ESO (Milton Roy, USA)	50/1996 (1976)	r
Micro lenses	Fisba Optik (CH)	03/1997	r
Fibers	ESO (CeramOptec)	40/1997	
Fiber-exit focal reducer	Sill Optics (D)	15/1997	d8
Image Slicer Prototypes	H. Kaufmann (D) [a]	22/1997	d6
Off-axis Collimators	Optical Surfaces Ltd. (UK)	22/1997	d8
Flat Folding Mirror	Optical Surfaces Ltd. (UK)	25/1997	d2
Crossdisperser Prism	Optical Surfaces Ltd. (UK)	25/1997	d8
Dioptric Camera	Fisba Optik (CH)		
Glas Data	Fisba	19/1997	d3
Final Optical Design	LSW	21/1997	d3
Final Opto-mech. Design	Fisba	25/1997	d3
Complete System	Fisba	02/1998	d3
Coatings	Balzers AG (LIE)	(on components)	
Continous-flow cryostat	ESO	14/1997	r
CCD chip, engineering grade	ESO (EEV, USA)	14/1997	r
CCD chip, science grade	ESO (EEV, USA)	48/1997	
CCD controllers	AOC (DK)	22/1997	
Optical Bench, Breadboard	Newport (USA)	08/1997	r
Bench mounting Components	Newport (F)	20/1997	r
Mechanical Components	LSW workshop (D)	18–52/1997	
Shutter	Prontor (D)	20/1997	r
Calibration Lamps	Juniper (GB)	20/1997	r
	LOT-Oriel (D)	20/1997	r
Calibration Unit Control	TH-Darmstadt (D)	42/1997	

[a] alternatively by Fisba Optik (CH)

Chapter 15: Critical Items

15.1 Image Slicer

To achieve the high resolution of FEROS a novel concept of a two-beam, two-slice image slicer has been proposed. In the following the feasibility and efficiency of such an image slicer is discussed:

- Feasibility:
  - At the LSW a 15:1 scale Acrylic model was built in the mechanical workshop to test the principle geometry, the function, the manufacturing tolerances, and the alignment requirements of such a device. These tests were carried out successfully and lead to the final design of the device presented to the possible manufacturers.
  - A Quarz prototype will be built by Kaufmann Präzisionsoptik in May 1997.
  - Independently, an offer to build the image slicer was received from FISBA Optik.
  - To have the possibility to select the device with the best performance, a small number of image slicers (2-5) will be finally built.
- Efficiency:
  - The efficiency that will be reached by the image slicer mainly depends on how close the manufacturer will match the tolerances set by the design. We expect that a minimum efficiency of 80% can be reached.
  - No coating is foreseen directly on the surfaces of the image slicer because the heating during the coating process could destroy the optical contact between the individual components of the device. But as discribed in the mechanical design, the device with the best performance will be glued between two multi-layer coated windows.

In case of invincible problems with the concept of the image slicer, a 2 hole exit-slit (0.24 mm hole diameters, 0.9 mm separation) will be positioned at the intermediate f/11 focus. This will lower the resolution of FEROS to 25 000, which is still in accordance with the FEROS contract.

15.2 Camera

The time critical component of the FEROS project is the camera due to its long delivery time. This delivery time mainly depends on the delivery times for the special glases used in the design. In the schedule contracted with the manufacturer, the date of delivery of the glas is defined as the starting point of the manufacturing of the camera:

- Start point: delivery of the glas; passing of glas data to LSW
- + 2 weeks: delivery of the final optical design which is adapted to the real glas data and the manufacturer's radii tools
- + 4 weeks: delivery of the final opto-mechanical design to LSW, design review
- + 1 week: start of manufacturing
- + 6 months: delivery of complete system to LSW

As starting point week 19/1997 is planned which results in a delivery of the complete system in the first weeks of 1998.

15.3 Fiber-Flatfield stability

Recently, problems with the flatfield stabilty of high-resolution fiber-fed spectrographs like FOCES (Universitätssternwarte München) and FUEGOS for the VLT were reported. Small-scale variations with amplitudes of several percent are observed in subsequent flatfield exposures when the fiber cables are moved (e.g., by the telescope motion) in between. No explanations for this phenomenon are known to date.

Since these problems could considerably affect the performance of FEROS, we carried out tests with the proposed fiber link used in the HEROS spectrograph of the LSW:

A prototype fiber link of the FEROS fiber was built with the identical components: BK7 microlens: $r = 0.7$ mm, $l = 2.0$ mm glued to an Optran WF 100/110 P fiber of 12 m length, fiber exit polished. This fiber link was used at the ESO 1.52-m telescope to feed the HEROS echelle spectrograph ($R = 20000$, $350 < \lambda < 870$ nm).

Figure 15.1 shows a representative section of all reduced flatfield spectra of the night from 18./19.04.97, normalized by their mean spectrum. The spectra were taken with the telescope pointing at different sky regions observed throughout the whole night. In these spectra none of the described problems with the flatfielding

stability of the fiber link is observed within a 0.5% peak-to-peak level throughout the wavelength range of the instrument.

The S/N of the raw flatfield spectra is approx 490 in the center of this order. The S/N of the displayed reduced spectra is approx 450. The degradation of the S/N is only due to the normalization of the individual flatfields by the average of the 6 flatfields. Therefore, we conclude that all spectra are compatible with pure photon noise.

From this test of the fiber link we are optimistic to obtain stable flatfield exposures with FEROS, too. Of course, special attention will be given to this question during the tests of the FEROS instrument.

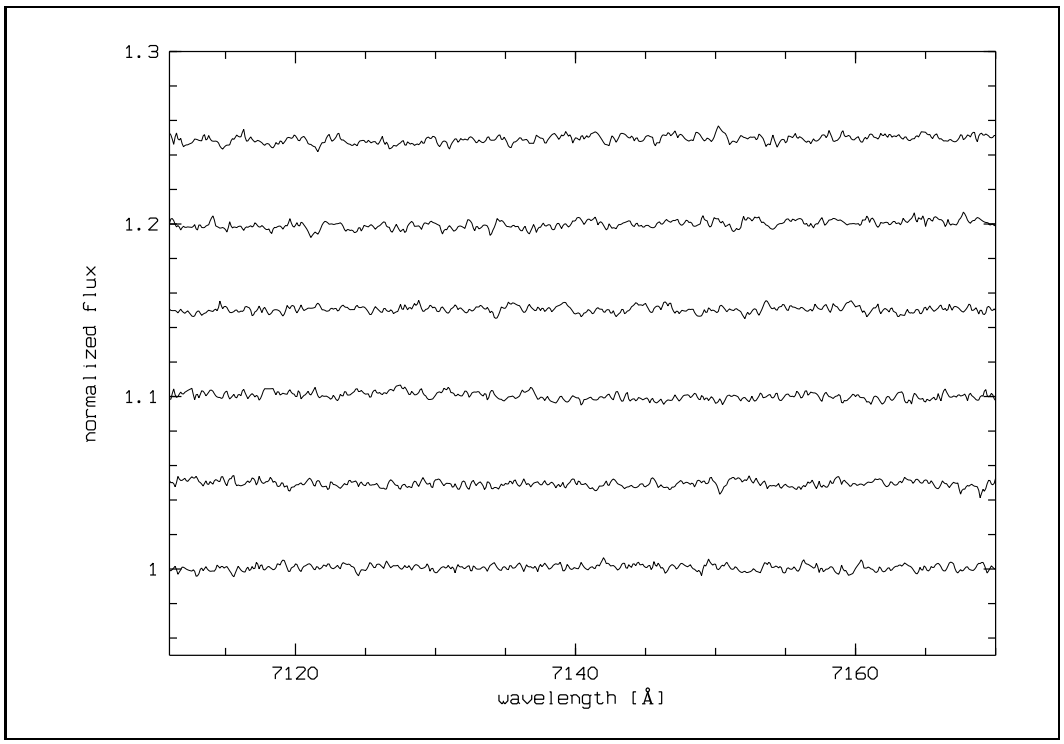

Figure 15.1: Flatfield spectra taken with the FEROS fiber link feeding the HEROS spectrograph at the ESO 1.52-m telescope. Between the exposures, the telescope and therefore the fiber cable was moved to different positions. All spectra are compatible with pure photon noise.

Chapter 16: User/Operational Manual (Draft)

16.1 Introduction

FEROS, the **F**iber fed **E**xtended **R**ange **O**ptical **S**pectrograph is a fiber-fed bench-mounted prism-crossdispersed echelle spectrograph at the ESO 1.52-m telescope at La Silla. It works in quasi Littrow mode and in white pupil configuration. For the object and the nearby sky, the complete optical spectrum from $370 - 860$ nm is recorded in one exposure with a resolving power of $R = 48\,000$ by the use of a two-beam, two-slice image slicer.

The main parameters and the expected performance for FEROS are summarized in Table 16.1:

Table 16.1: *Main parameters of FEROS.*

Wavelength range	
in one exposure (object+sky)	$3700 - 8600$ Å (40 orders, 2 fibers)
Resolving Power (with 2-slice image slicer)	$\lambda/\Delta\lambda = 48\,000$
Entrance Aperture	2.7 arcsec
Fiber Input/Output Focal Ratio	F/4.6
Spectrograph Beam Size	136 mm diameter
Off-axis Collimators	F/11, cut from one parent paraboloid
Echelle	R2, 79 lines/mm, 154 mm by 306 mm
Crossdisperser Prism	LF5 glass, 55° apex angle
Dioptric Camera	
Wavelength Range	$350 - 900$ nm
F/#	F/3.0
Focal Length	410 mm
Field Diameter	69 mm
Image Quality (E_{80})	< 25 μm
Efficiency	$> 85\%$
CCD	2048×4096, 15 μm, thinned
Expected Detection Efficiency (without telescope)	7% (3700 Å), 27% (5000 Å), 8% (9000 Å)
Expected Limiting Magnitudes at the ESO 1.52	16 mag in V ($S/N = 15$, 2 h)
	12.5 mag in V ($S/N = 100$, 2 h)
Expected Radial-Velocity Accuracy	< 25 m/s, < 5 m/s with iodine cell
	(contract: < 50 m/s)

The schematic layout of the FEROS instrument is shown in Fig. 16.1.

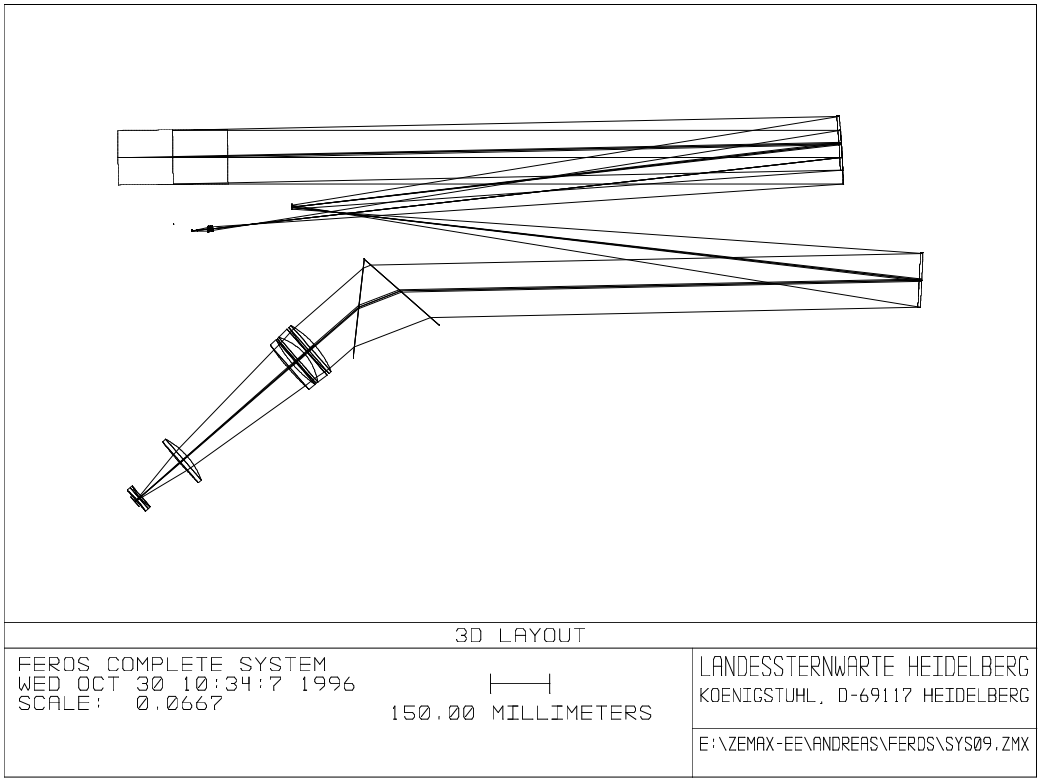

Figure 16.1: FEROS optical system from fiber exits to detector.

Two fibers are coupled to the Cassegrain focus of the telescope by micro lenses. In the coudé room, the fiber exit is converted to the F/11 focal ratio accepted by the spectrograph via a F/N lens system. A two beam, two-slice image slicer in the F/11 focal plane halves the width of the image of the fiber in the direction of dispersion. The fibers are re-imaged on the Echelle grating through the first collimator, the Main Collimator. Then, the light goes back to the Main Collimator and is reflected by the Folding Mirror to the second collimator, the Transfer Collimator. The entrance surface of the prism crossdisperser is located near the pupil image and the light is finally imaged by the dioptric camera on the detector.

The detector used is a monolithic 4096×2048 15 μm pixel CCD aligned with the long side in direction of dispersion.

The beam of the spectrograph is 136 mm. The fiber input/output focal ratio is F/4.6, the collimators focal ratio is F/11 and that of the camera is F/3.

16.2 Instrument Configurations / Observing Modes

The bench-mounted part of the spectrograph contains *no* movable or remotely controlled components besides the CCD shutter. Therefore, FEROS works in a fixed configuration only to gurantee the best possible long-term stability of the

spectrograph.

All changes between the operational modes are carried out with/at the FEROS Calibration Unit (FCU) attached to the B&C instrument.

The two fibers simultaneously recorded on the detector allow basically two fundamental observing modes:

- Object – Sky (OS)
- Object – Calibration (OC)

Between these two modes, the observer has to switch manually (cf. below).

In both modes, the internal flatfield (FF) and wavelength calibration (WC) light sources are available for the two fibers via remote control of the FCU:

fiber	mode	light sources
1 (object)	OS/OC	object, FF, WC
2 (sky)	OS	sky, FF, WC
2 (calibration)	OC	FF, WC (along with object exposure)

16.2.1 The Object + Sky Configuration

In the OS mode two fibers record the star light and the nearby sky background simultaneously. For this mode, the second fiber has to be plugged into the fiber connector named 'sky' at the FCU.

Both fibers have a projected entrance aperture of 2.7 arcsec; this keeps slit losses below 12 % for a seeing of 1.5 arcsec and keeps the effect of differential atmospheric refraction up to $z = 60^\circ$ ($\mathrm{airmass} = 2$) negligible.

For calibration purposes, the internal flatfield or the wavelength calibration source are recorded through the two fibers.

16.2.2 The Object + Calibration Configuration

In the OC mode the object fiber is used as in the OS mode described above. The second fiber has to be plugged into the fiber connector named 'calibration' at the FCU.

Then, the light of the calibration source (WC) can be recorded throughout the whole object exposure to monitor the stability of the spectrograph. The position of the neutral density filter wheel has to be set according to the exposure time.

With the OC observing mode and the software techniques described below, a long-term radial velocity accuracy of < 25 m/s is reached for sharp-lined solar-like stars.

16.3 FEROS Spectral Characteristics

16.3.1 Spectral Coverage

For the two fibers, the complete wavelength range from $3\,700 - 8\,600$ Å is recorded in 40 orders on the detector without gaps.

16.3.2 Spectral Resolution

By the use of the two-slice image slicer, the resolving power of FEROS is 48 000 with a degradation less than 10% over the whole wavelength range.

16.3.3 Efficiency and Limiting Magnitudes

FEROS has a high throughput with 27% peak efficiency, 7 (1.7)% in the extreme blue at 3 700 (3 500) Å and 8% in the extreme red at 9 000 Å. With these efficiencies and an efficiency of 60 % for the 1.52-m telescope, a spectrum of a 10th magnitude star can be taken in 15 minutes with a $S/N \approx 100$ per wavelength bin in V (Fig. 16.2). Within one hour for a star of 16th magnitude still a S/N of 10 is reached.

16.3.4 Instrument Simulation and Exposure-Time Calculator

To prepare the observations, an exposure-time calculator is available for FEROS which takes into account instrumental and environmental conditions to compute for a given object either the necessary exposure time to reach a specified S/N or the S/N which is reached in a given exposure time. (. . .)

16.4 Observations

(. . .)

16.4.1 The DAISY Instrument Control

16.4.2 Selection of the Observing Mode

16.4.3 Object+Sky Exposures

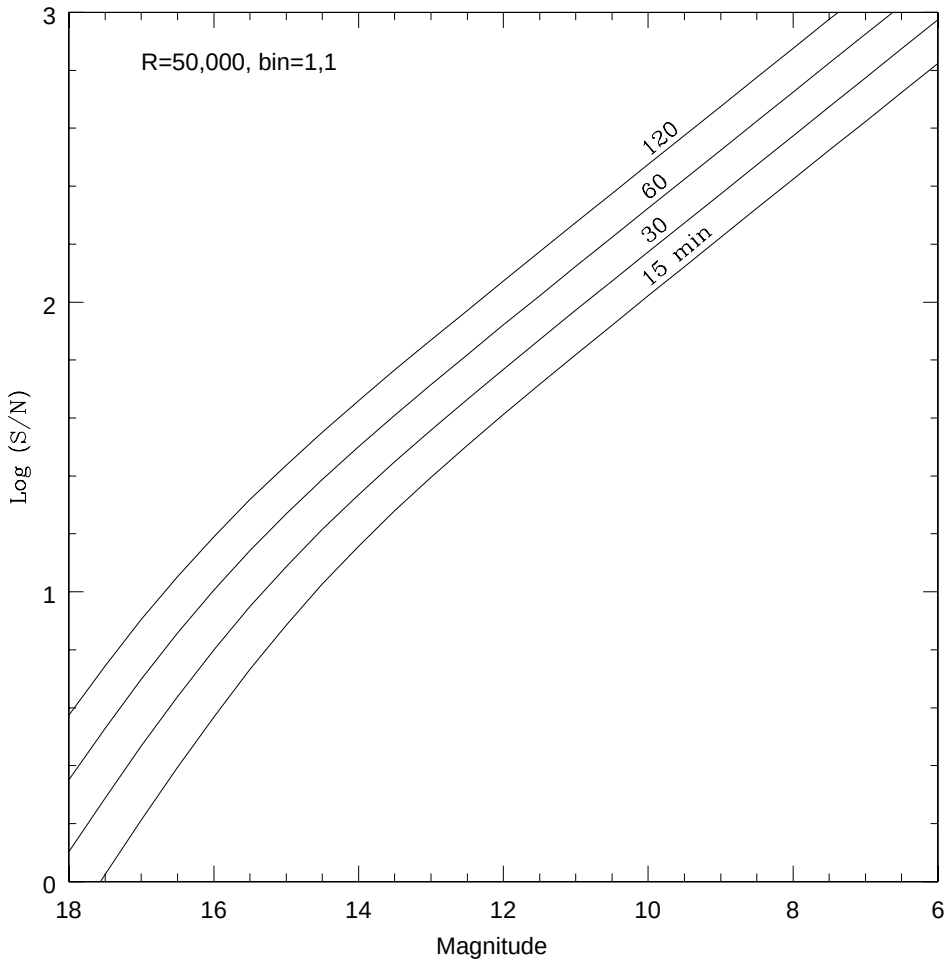

Figure 16.2: Reachable S/N ratio per wavelength bin for different exposure times.

16.4.4 Object+Calibration Exposures

16.4.5 Flatfield Exposures

16.4.6 Wavelength-Calibration Exposures

16.4.7 Dark Exposures

16.5 Observing run: Example and Advice

(. . .)

16.5.1 Preparation of the Observations

Instrument Simulation

16.5.2 Preparation of the Instrument

Before Sunset

Pointing and Focusing

16.5.3 Object+Sky Exposures

16.5.4 Object+Calibration Exposures

16.5.5 High-accuracy Radial-Velocity Observations

16.6 The CCD detector

The FEROS detector is a thinned, back-illuminated, monolithic 2k$\times$4k EEV CCD chip with $15\,\mu$m pixel size. It is LN_2 cooled with a continuous-flow cryostat.

The CCD characteristics are as follows:

Op. temperature	-110° to -120°C
RON	3 e^-
Dark Current	4 e^-/h/pixel
CTE (par/ser)	0.99999/0.99999
Linearity	$< 1\%$ deviation up to full well
Full well capacity	150.000 e^-
Quantum efficiency [nm : %]	350 : 50
	370 : 58
	400 : 72
	450 : 85
	500 : 85
	600 : 85
	700 : 78
	800 : 55
	900 : 28

(. . .)

16.7 (On-line) Data Reduction Software

(. . .)

16.7.1 Purposes

16.7.2 Requirements

16.7.3 Capabilites

16.8 Data Archiving

(. . .)

Appendix A: Optical System Data

A.1 ZEMAX system data for the FEROS complete optical system

```
System/Prescription Data

File : C:\ZEMAX\ANDREAS\FEROS\Sys09.zmx
Title: FEROS complete system
Date : MON MAY 5 1997

GENERAL LENS DATA:

Surfaces        :          36
Stop            :           2
System Aperture : Entrance Pupil Diameter = 2.9
Ray aiming      : Off
Apodization     :Uniform, factor =     0.000000
Eff. Focal Len. :     8.43832 (in air)
Eff. Focal Len. :     8.43832 (in image space)
Total Track     :     2130.26
Image Space F/# :     2.90976
Para. Wrkng F/# :     2.99523
Working F/#     :     3.07255
Obj. Space N.A. :     0.10838
Stop Radius     :        1.45
Parax. Ima. Hgt.:    0.973515
Parax. Mag.     :   -0.649964
Entr. Pup. Dia. :         2.9
Entr. Pup. Pos. :           0
Exit Pupil Dia. :      77.136
Exit Pupil Pos. :     229.917
Field Type      : Object height in Millimeters
Maximum Field   :      1.4978
Primary Wave    :    0.462000
Lens Units      : Millimeters
Angular Mag.    :  -0.0375959

Fields          : 1
Field Type: Object height in Millimeters
#        X-Value        Y-Value         Weight
 1       0.000000      -1.497800       1.000000

Wavelengths     : 1
Units: Microns
#          Value         Weight
 1       0.462000       1.000000
```

SURFACE DATA SUMMARY:

Surf	Type	Radius	Thickness	Glass	Diameter	Conic
OBJ	TILTSURF	--------	13.3		2.9956	--------
1	COORDBRK	--------	0		0	--------
STO	STANDARD	Infinity	26.3		2.917362	0
3	STANDARD	46	4	FK54	18	0
4	STANDARD	-39.6	0.5		18	0
5	STANDARD	73.1	3	LLF6	18	0
6	STANDARD	12.7	7	FK54	18	0
7	STANDARD	-31	100.6845		18	0
8	COORDBRK	--------	0		0	--------
9	STANDARD	Infinity	1500		0.1235196	0
10	STANDARD	-3000	-1700	MIRROR	477.4539	-1
11	COORDBRK	--------	0		0	--------
12	DGRATING	Infinity	0	MIRROR	490.1453	0
13	COORDBRK	--------	0		0	--------
14	COORDBRK	--------	0		0	--------
15	COORDBRK	--------	1700		0	--------
16	STANDARD	-3000	-1400	MIRROR	547.9828	-1
17	STANDARD	Infinity	1600	MIRROR	96.60169	0
18	STANDARD	-3000	-1325	MIRROR	421.5239	-1
19	COORDBRK	--------	0		0	--------
20	STANDARD	Infinity	-100	LF5	203.2386	0
21	COORDBRK	--------	0	LF5	0	--------
22	STANDARD	Infinity	-100		203.261	0
23	COORDBRK	--------	0		0	--------
24	STANDARD	-240.7799	-25	CAF2	158	0
25	STANDARD	622.6922	-1		158	0
26	STANDARD	-4761.222	-8	PSK3	158	0
27	STANDARD	-139.2893	-30	FK54	153	0
28	STANDARD	1003.717	-10		153	0
29	STANDARD	313.5372	-15	BK7	153	0
30	STANDARD	711.9877	-340.4111		153	0
31	STANDARD	-195.9967	-25	FK5	141	0
32	STANDARD	1020.826	-134.3496		141	0
33	STANDARD	135.6392	-2	LAK16A	74	0
34	STANDARD	Infinity	-10	SILICA	74	0
35	TOROIDAL	Infinity	-4.5		74	0
IMA	STANDARD	Infinity	0		69	0

```
SURFACE DATA DETAIL:

Surface OBJ     : TILTSURF
 X Tangent      :             0
 Y Tangent      :       -0.1133
Surface   1     : COORDBRK
 Decenter X     :             0
 Decenter Y     :             0
 Tilt About X   :        -6.466
 Tilt About Y   :             0
 Tilt About Z   :             0
 Order          : Decenter then tilt
Surface STO     : STANDARD
Surface   3     : STANDARD
 Aperture       : Circular Aperture
 Minimum Radius :             0
 Maximum Radius :           7.5
Surface   4     : STANDARD
 Aperture       : Circular Aperture
 Minimum Radius :             0
 Maximum Radius :           7.5
Surface   5     : STANDARD
 Aperture       : Circular Aperture
 Minimum Radius :             0
 Maximum Radius :           7.5
Surface   6     : STANDARD
 Aperture       : Circular Aperture
 Minimum Radius :             0
 Maximum Radius :           7.5
Surface   7     : STANDARD
 Aperture       : Circular Aperture
 Minimum Radius :             0
 Maximum Radius :           7.5
Surface   8     : COORDBRK
 Decenter X     :             0
 Decenter Y     :             0
 Tilt About X   :         6.466
 Tilt About Y   :             0
 Tilt About Z   :             0
 Order          : Decenter then tilt
Surface   9     : STANDARD
Surface  10     : STANDARD
 Aperture       : Rectangular Aperture
 X Half Width   :            70
 Y Half Width   :            70
 Y- Decenter    :         170.3
Surface  11     : COORDBRK
 Decenter X     :             0
 Decenter Y     :             0
 Tilt About X   :          -0.6
 Tilt About Y   :         -63.4
 Tilt About Z   :            90
 Order          : Decenter then tilt
```

```
Surface  12     : DGRATING
 Lines / Micron :          0.079
 Diffract Order :            -49
 Aperture       : Rectangular Aperture
 X Half Width   :       69.14024
 Y Half Width   :       155.4887
 X- Decenter    :      170.2955
 Y- Decenter    :  -0.001163251
Surface  13     : COORDBRK
 Decenter X     :              0
 Decenter Y     :              0
 Tilt About X   :              0
 Tilt About Y   :              0
 Tilt About Z   :            -90
 Order          : Decenter then tilt
Surface  14     : COORDBRK
 Decenter X     :              0
 Decenter Y     :              0
 Tilt About X   :              0
 Tilt About Y   :           63.4
 Tilt About Z   :              0
 Order          : Decenter then tilt
Surface  15     : COORDBRK
 Decenter X     :              0
 Decenter Y     :              0
 Tilt About X   :            0.6
 Tilt About Y   :              0
 Tilt About Z   :              0
 Order          : Decenter then tilt
Surface  16     : STANDARD
 Aperture       : Rectangular Aperture
 X Half Width   :            200
 Y Half Width   :             70
 Y- Decenter    :          205.9
Surface  17     : STANDARD
 Aperture       : Rectangular Aperture
 X Half Width   :            120
 Y Half Width   :            7.5
 Y- Decenter    :           43.8
Surface  18     : STANDARD
 Aperture       : Rectangular Aperture
 X Half Width   :            200
 Y Half Width   :             70
 Y- Decenter    :       -142.544
Surface  19     : COORDBRK
 Decenter X     :              0
 Decenter Y     :         -169.6
 Tilt About X   :          -48.6
 Tilt About Y   :              0
 Tilt About Z   :              0
 Order          : Decenter then tilt
```

```
Surface  20     : STANDARD
 Aperture       : Rectangular Aperture
 X Half Width   :          87.5
 Y Half Width   :         127.5
 Y- Decenter    :          -4.5
Surface  21     : COORDBRK
 Decenter X     :             0
 Decenter Y     :            52
 Tilt About X   :            55
 Tilt About Y   :             0
 Tilt About Z   :             0
 Order          : Decenter then tilt
Surface  22     : STANDARD
 Aperture       : Rectangular Aperture
 X Half Width   :          87.5
 Y Half Width   :         127.5
 Y- Decenter    :          -4.5
Surface  23     : COORDBRK
 Decenter X     :             0
 Decenter Y     :          -109
 Tilt About X   :         -47.5
 Tilt About Y   :             0
 Tilt About Z   :             0
 Order          : Decenter then tilt
Surface  24     : STANDARD
 Aperture       : Circular Aperture
 Minimum Radius :             0
 Maximum Radius :          77.5
Surface  25     : STANDARD
 Aperture       : Circular Aperture
 Minimum Radius :             0
 Maximum Radius :          77.5
Surface  26     : STANDARD
 Aperture       : Circular Aperture
 Minimum Radius :             0
 Maximum Radius :          77.5
Surface  27     : STANDARD
 Aperture       : Circular Aperture
 Minimum Radius :             0
 Maximum Radius :            75
Surface  28     : STANDARD
 Aperture       : Circular Aperture
 Minimum Radius :             0
 Maximum Radius :            75
```

```
Surface  29     : STANDARD
 Aperture       : Circular Aperture
 Minimum Radius :             0
 Maximum Radius :            75
Surface  30     : STANDARD
 Aperture       : Circular Aperture
 Minimum Radius :             0
 Maximum Radius :            75
Surface  31     : STANDARD
 Aperture       : Circular Aperture
 Minimum Radius :             0
 Maximum Radius :            69
Surface  32     : STANDARD
 Aperture       : Circular Aperture
 Minimum Radius :             0
 Maximum Radius :            69
Surface  33     : STANDARD
 Aperture       : Circular Aperture
 Minimum Radius :             0
 Maximum Radius :          35.5
Surface  34     : STANDARD
 Aperture       : Circular Aperture
 Minimum Radius :             0
 Maximum Radius :          35.5
Surface  35     : TOROIDAL
 Rad of rev.    :      230.9204
 Coeff on y^2   :             0
 Coeff on y^4   :             0
 Coeff on y^6   :             0
 Coeff on y^8   :             0
 Coeff on y^10  :             0
 Coeff on y^12  :             0
 Coeff on y^14  :             0
 Aperture       : Circular Aperture
 Minimum Radius :             0
 Maximum Radius :          35.5
Surface IMA     : STANDARD
 Aperture       : Rectangular Aperture
 X Half Width   :         30.72
 Y Half Width   :         15.36
```

```
MULTI-CONFIGURATION DATA:

 Configuration   1:
 Wave wgt    1 :           0.5
 Param 2    12 :           -27
 Wavelength  1 :        0.8522

 Configuration   2:
 Wave wgt    1 :           0.5
 Param 2    12 :           -27
 Wavelength  1 :        0.8384

 Configuration   3:
 Wave wgt    1 :           0.5
 Param 2    12 :           -27
 Wavelength  1 :        0.8229

 Configuration   4:
 Wave wgt    1 :             1
 Param 2    12 :           -49
 Wavelength  1 :        0.4667

 Configuration   5:
 Wave wgt    1 :             1
 Param 2    12 :           -49
 Wavelength  1 :         0.462

 Configuration   6:
 Wave wgt    1 :             1
 Param 2    12 :           -49
 Wavelength  1 :        0.4573

 Configuration   7:
 Wave wgt    1 :           0.5
 Param 2    12 :           -61
 Wavelength  1 :        0.3741

 Configuration   8:
 Wave wgt    1 :           0.5
 Param 2    12 :           -61
 Wavelength  1 :         0.371

 Configuration   9:
 Wave wgt    1 :           0.5
 Param 2    12 :           -61
 Wavelength  1 :        0.3681
```

Appendix B: Mechanical drawings

B.1 Optical Table

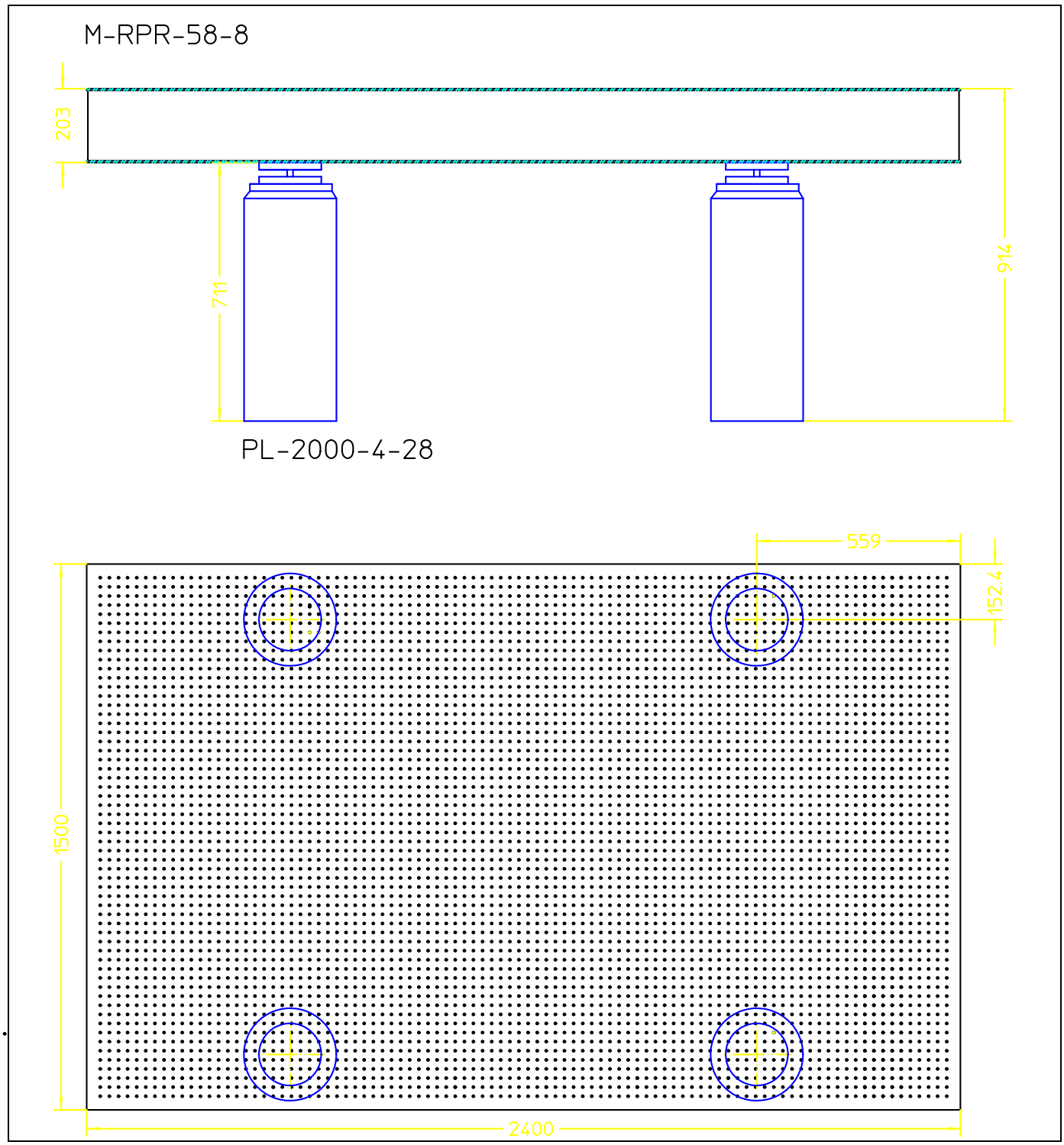

B.2 Microlens

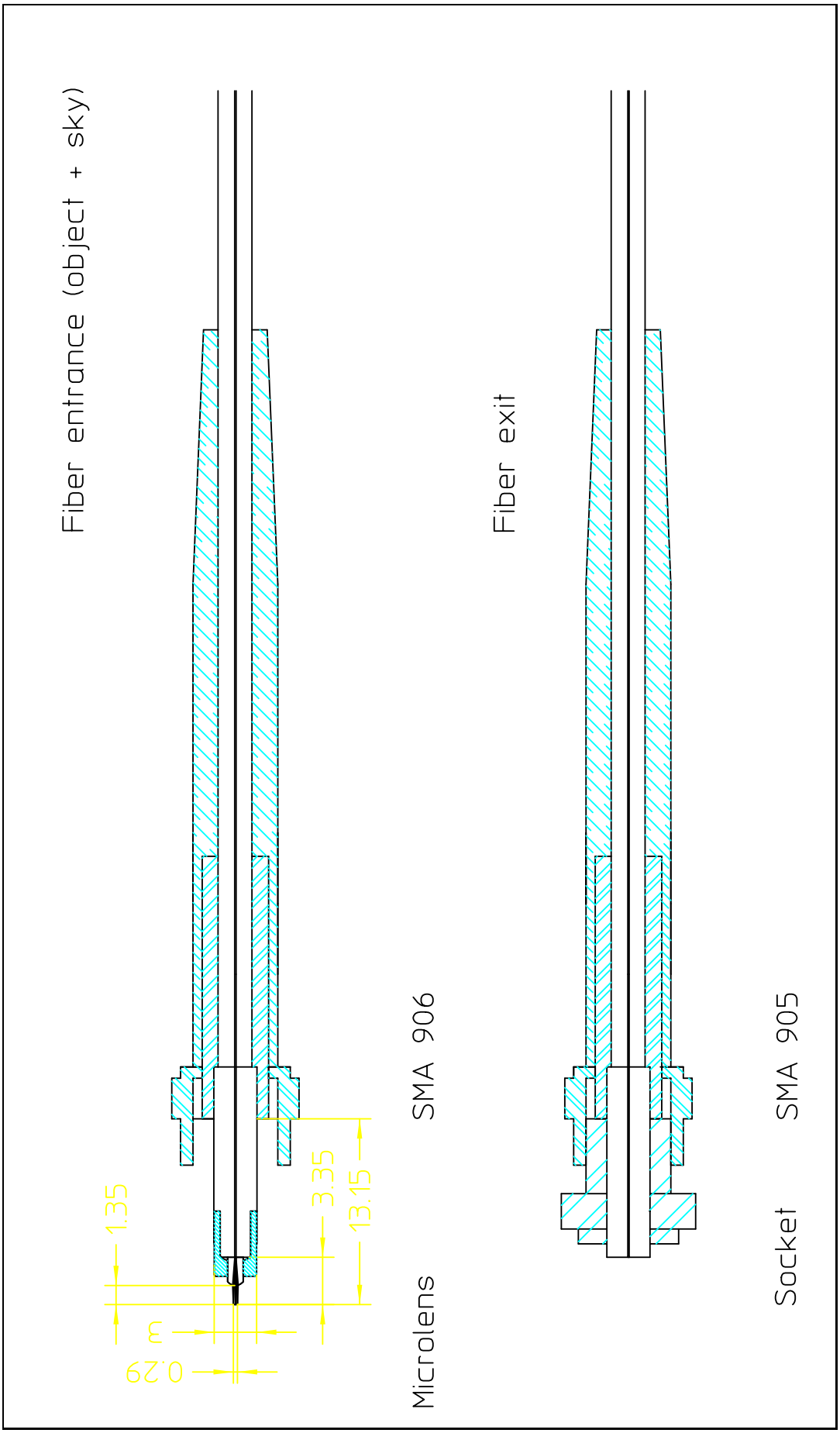

B.3 Fiber-exit unit

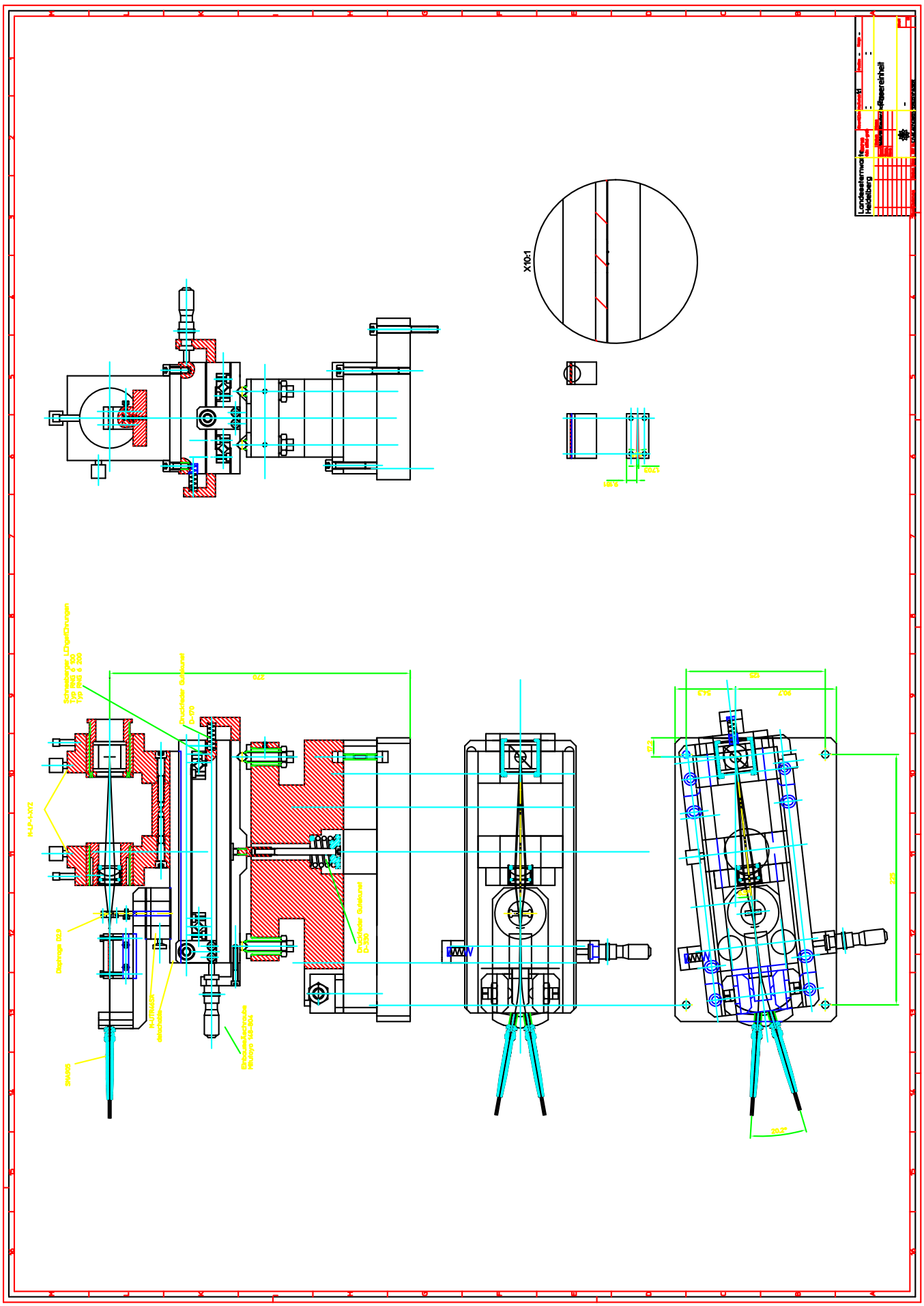

B.4 Image Slicer

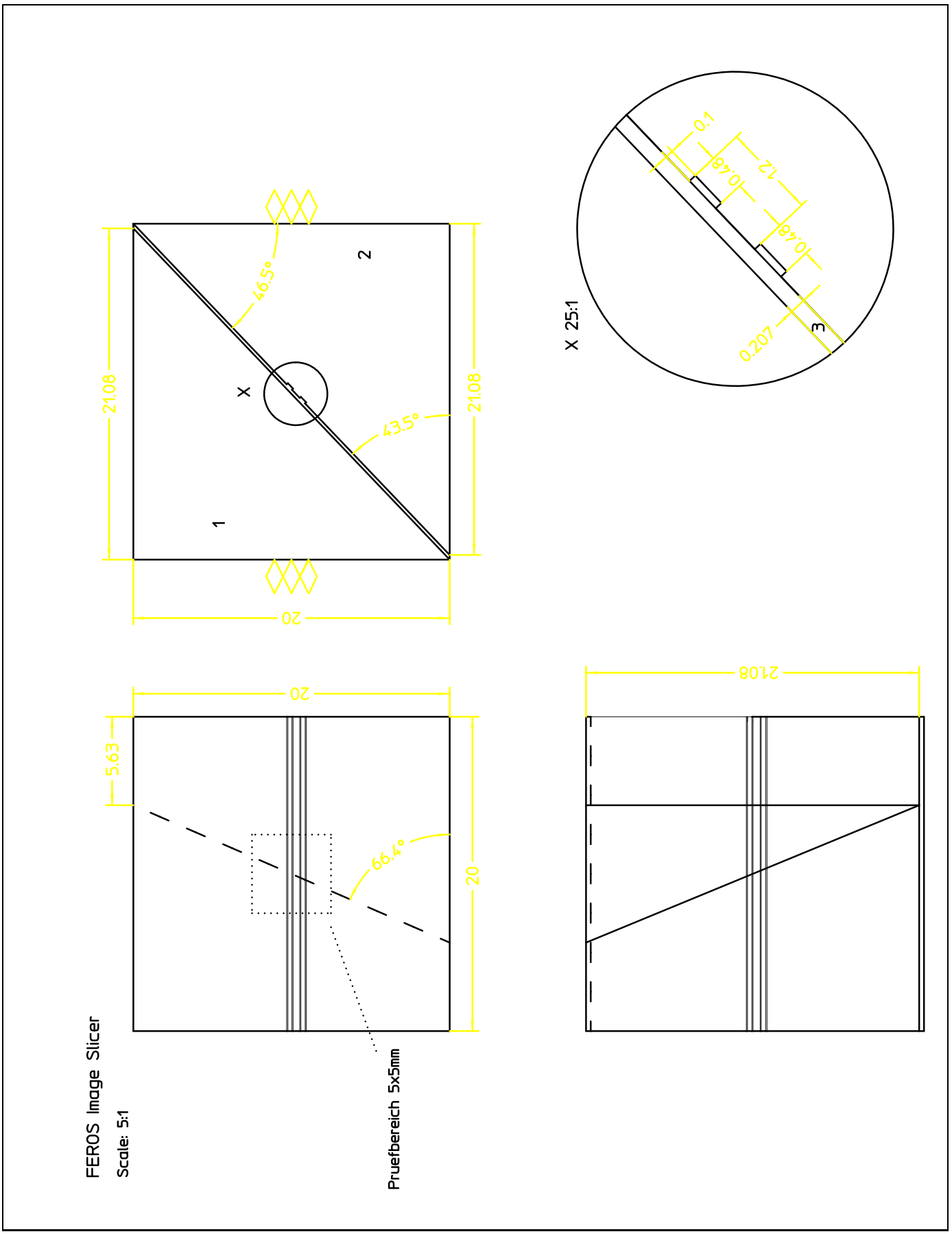

B.4.1 Slicer Prism

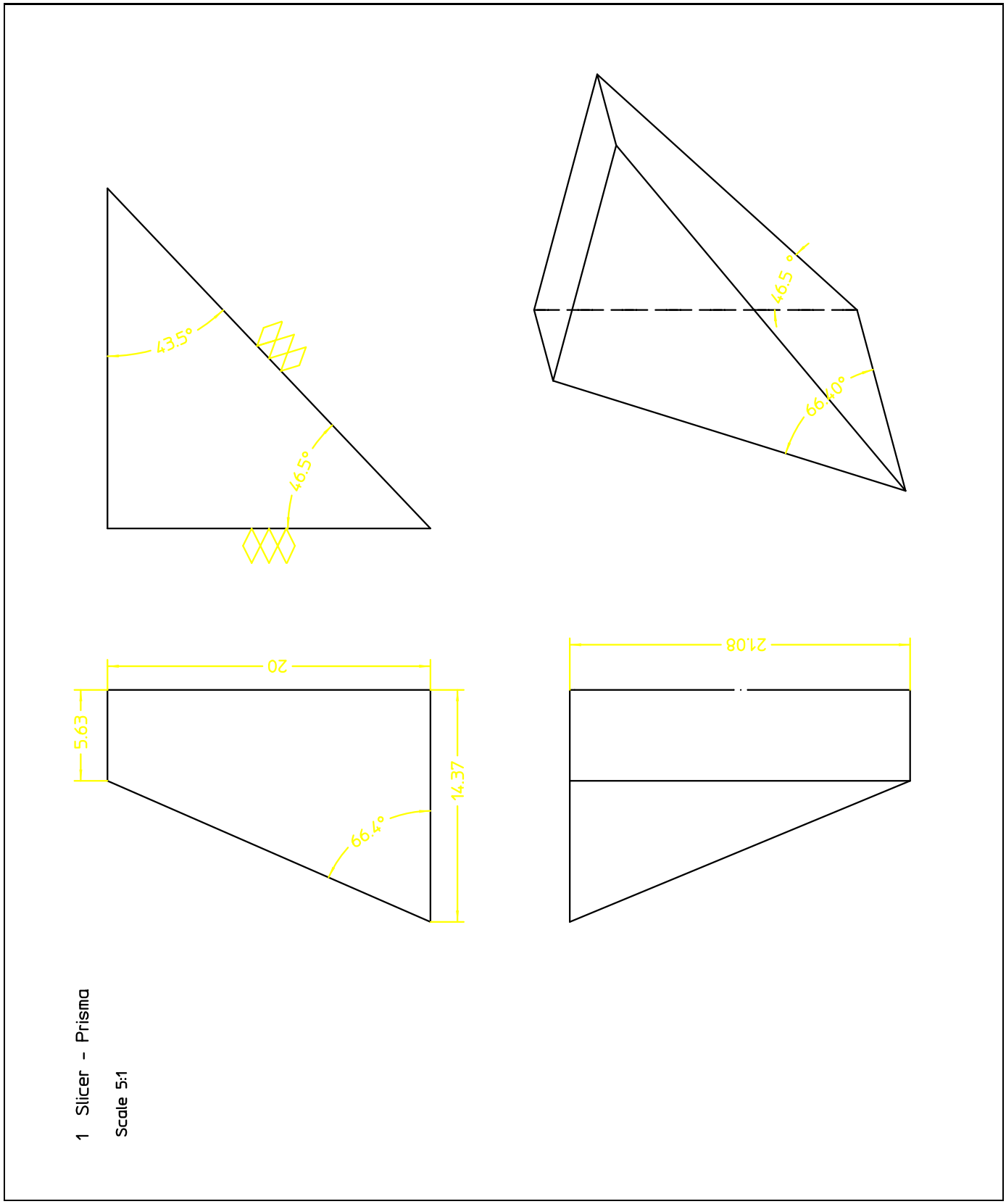

B.4.2 Entrance Prism

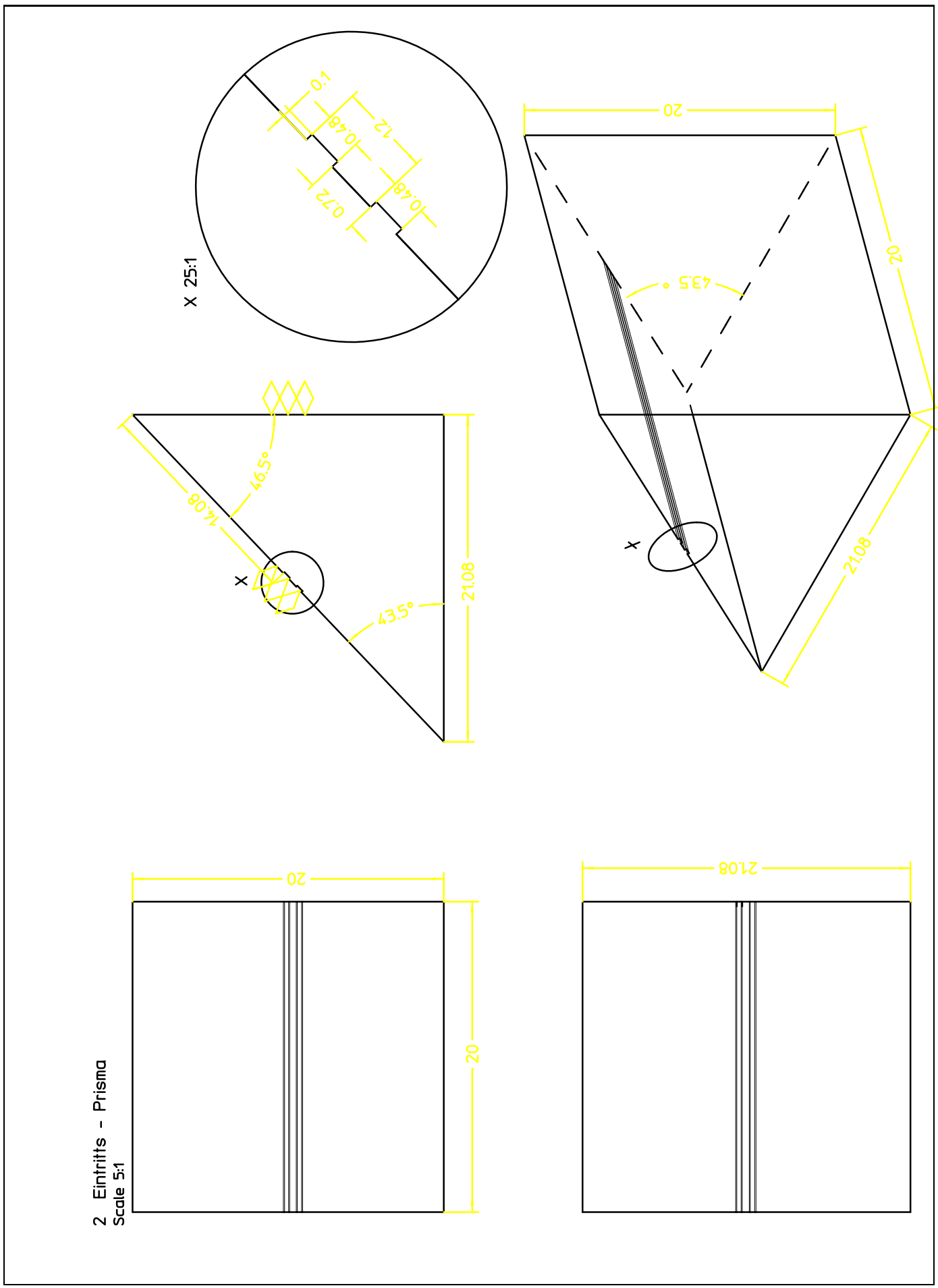

B.4.3 Slicer Plate

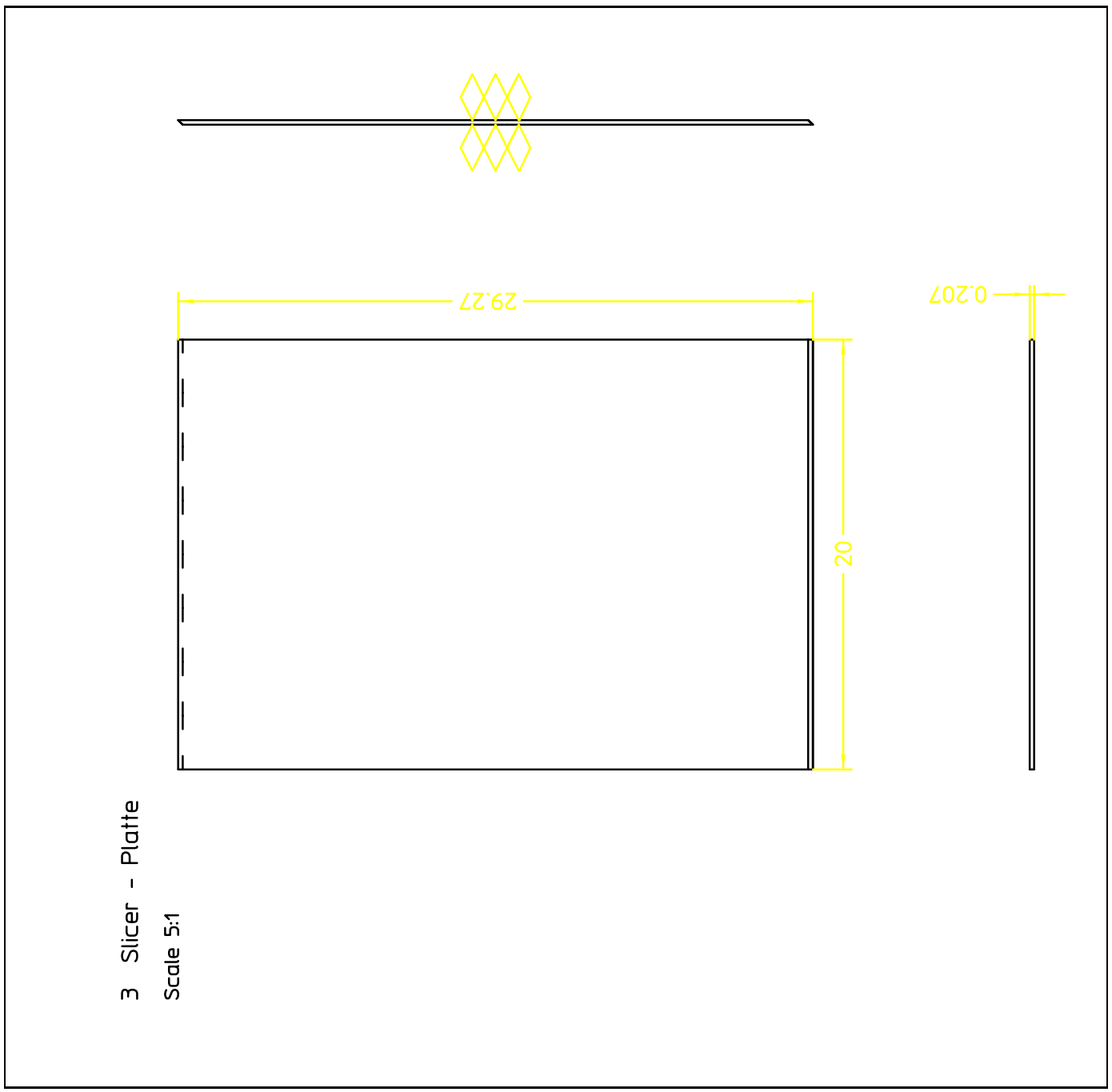

B.4.4 Image Slicer Housing

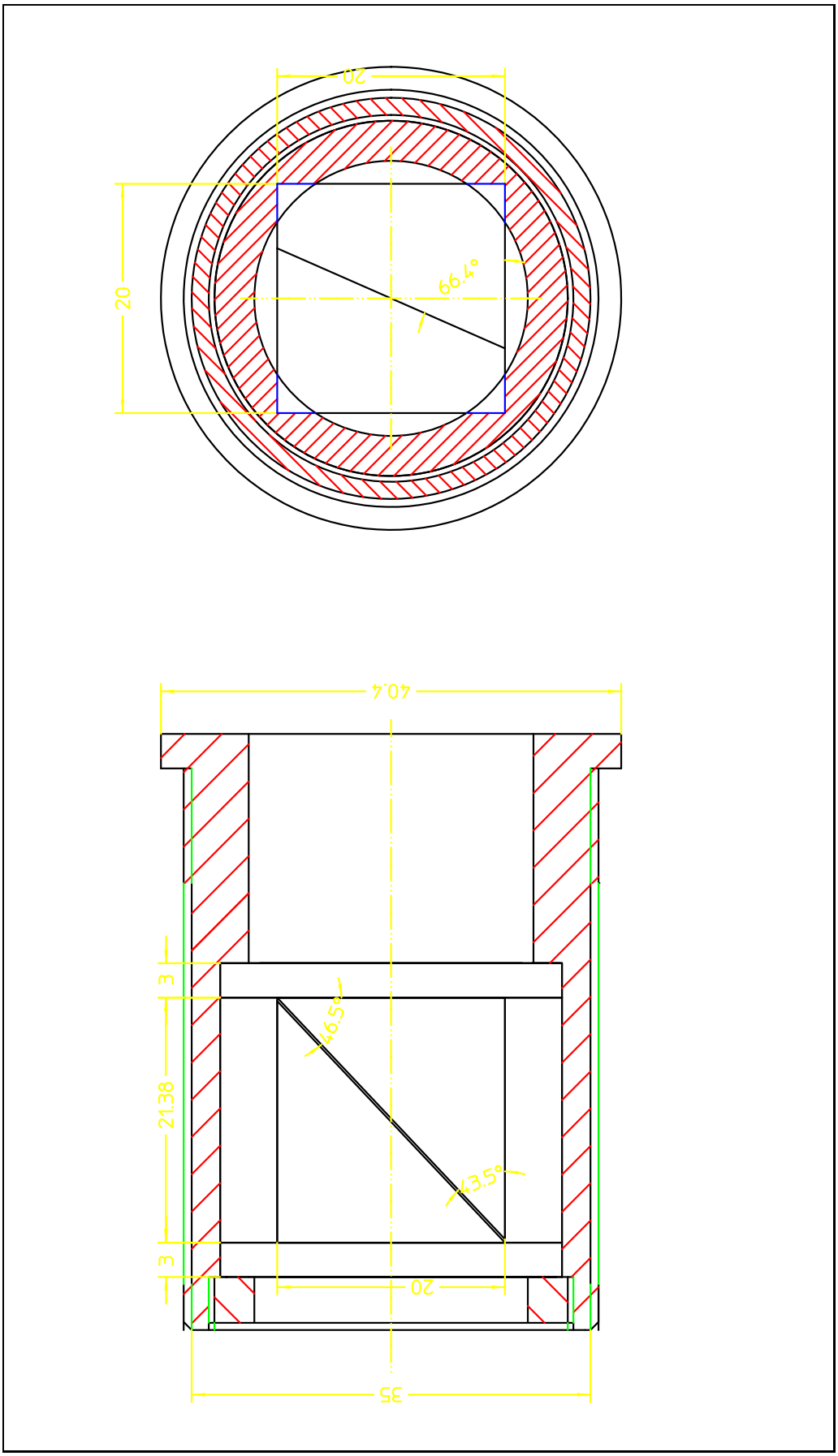

B.5 Main Collimator

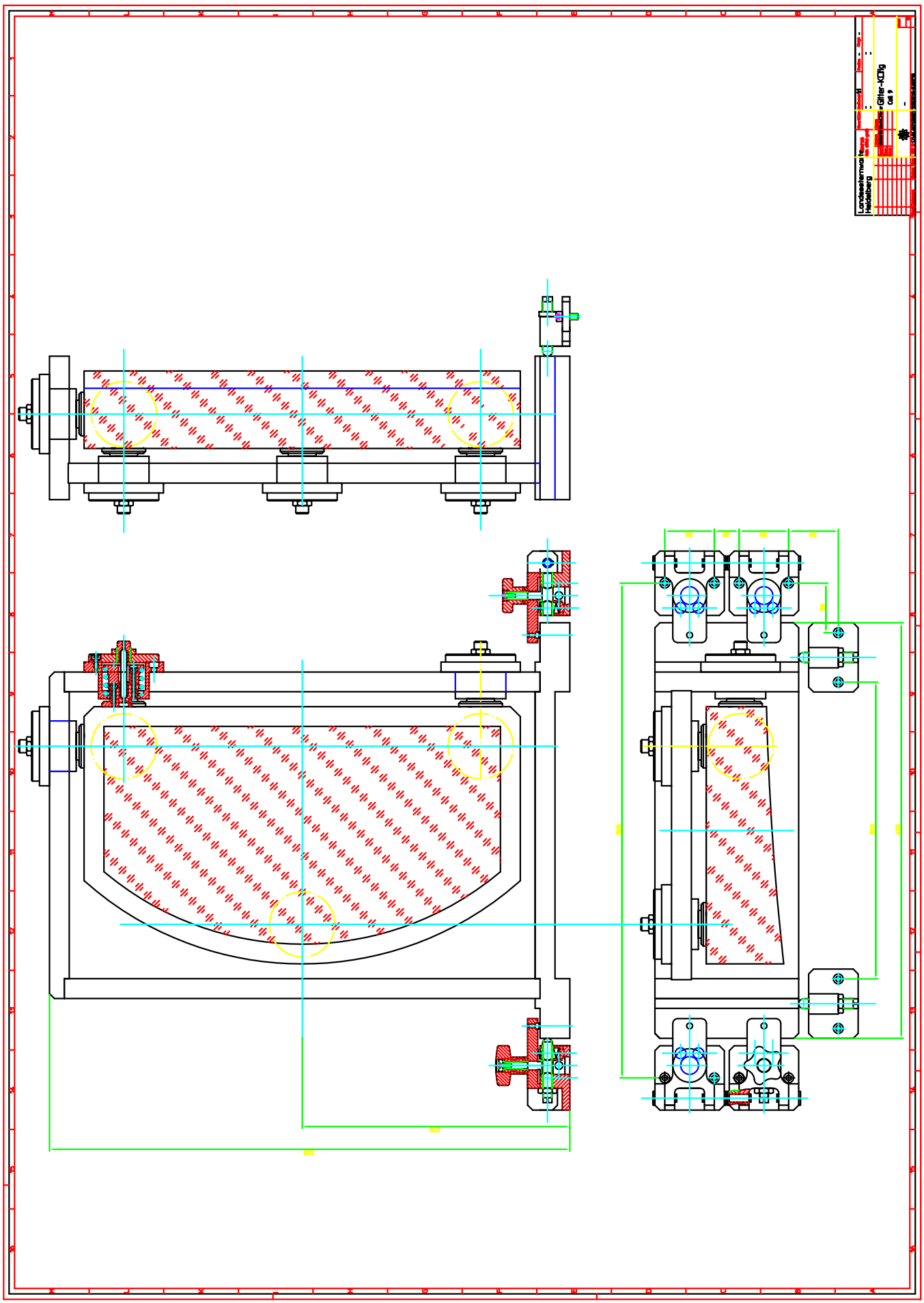

B.6 Transfer Collimator

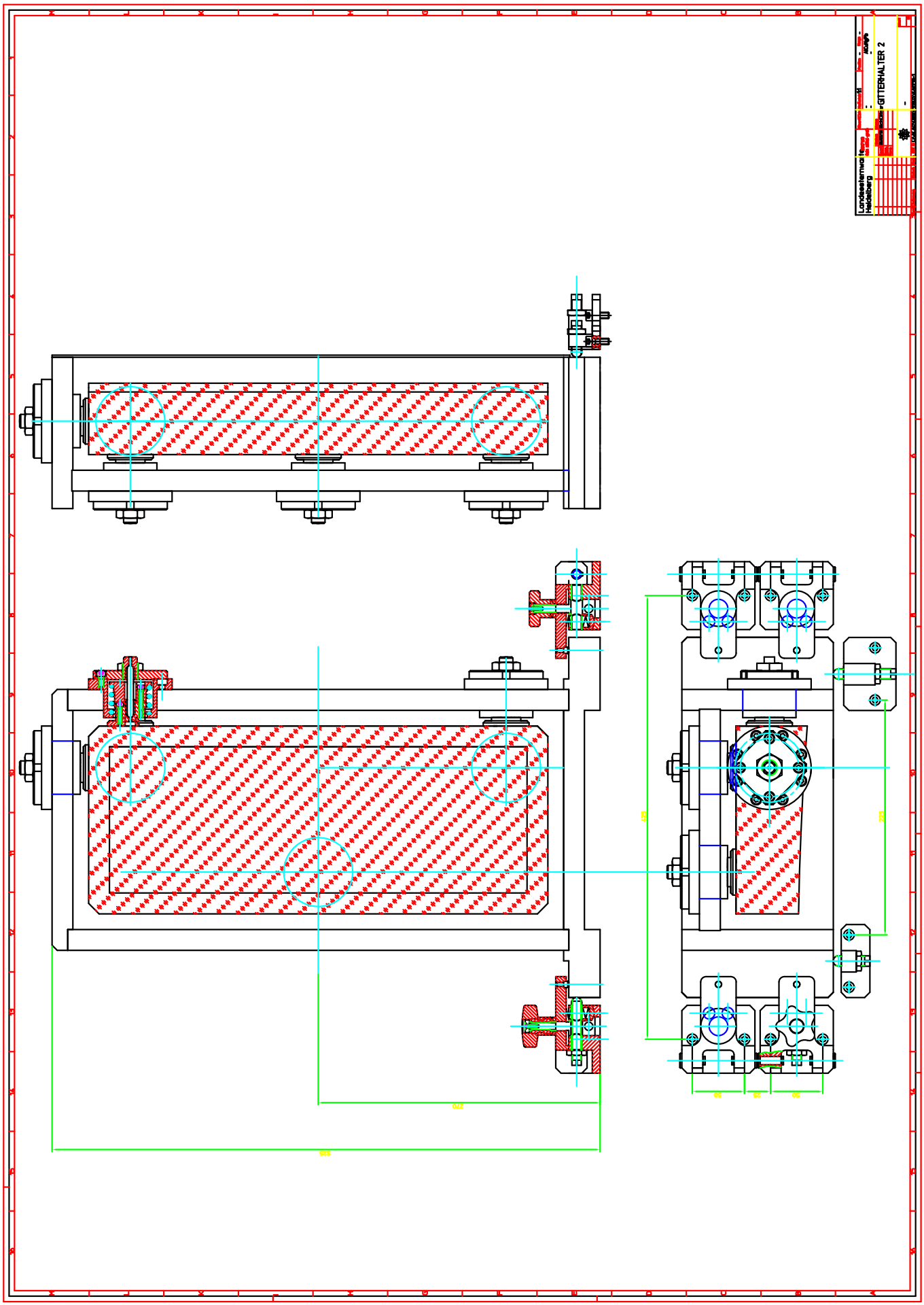

B.7 Folding Mirror

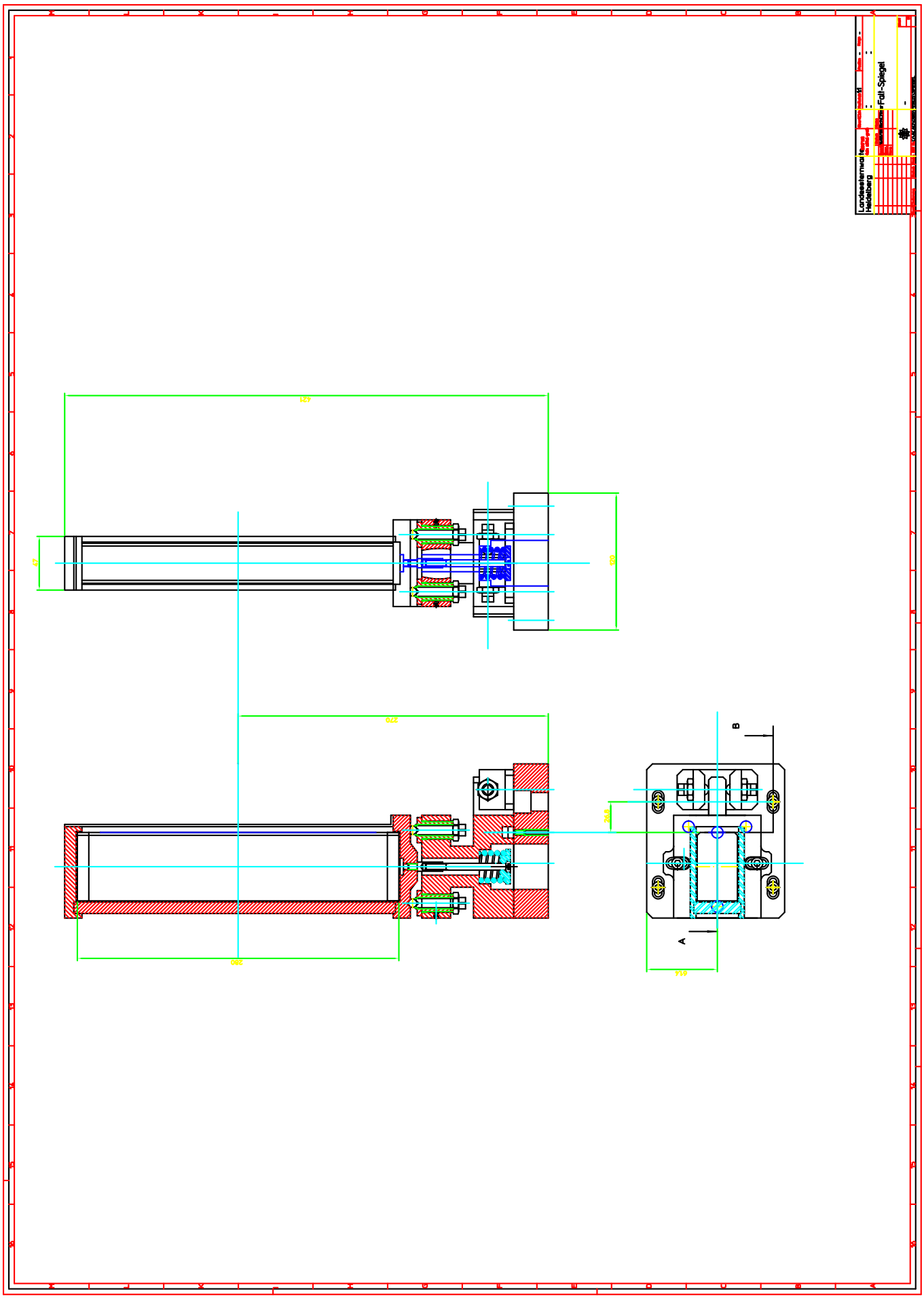

B.8 Echelle

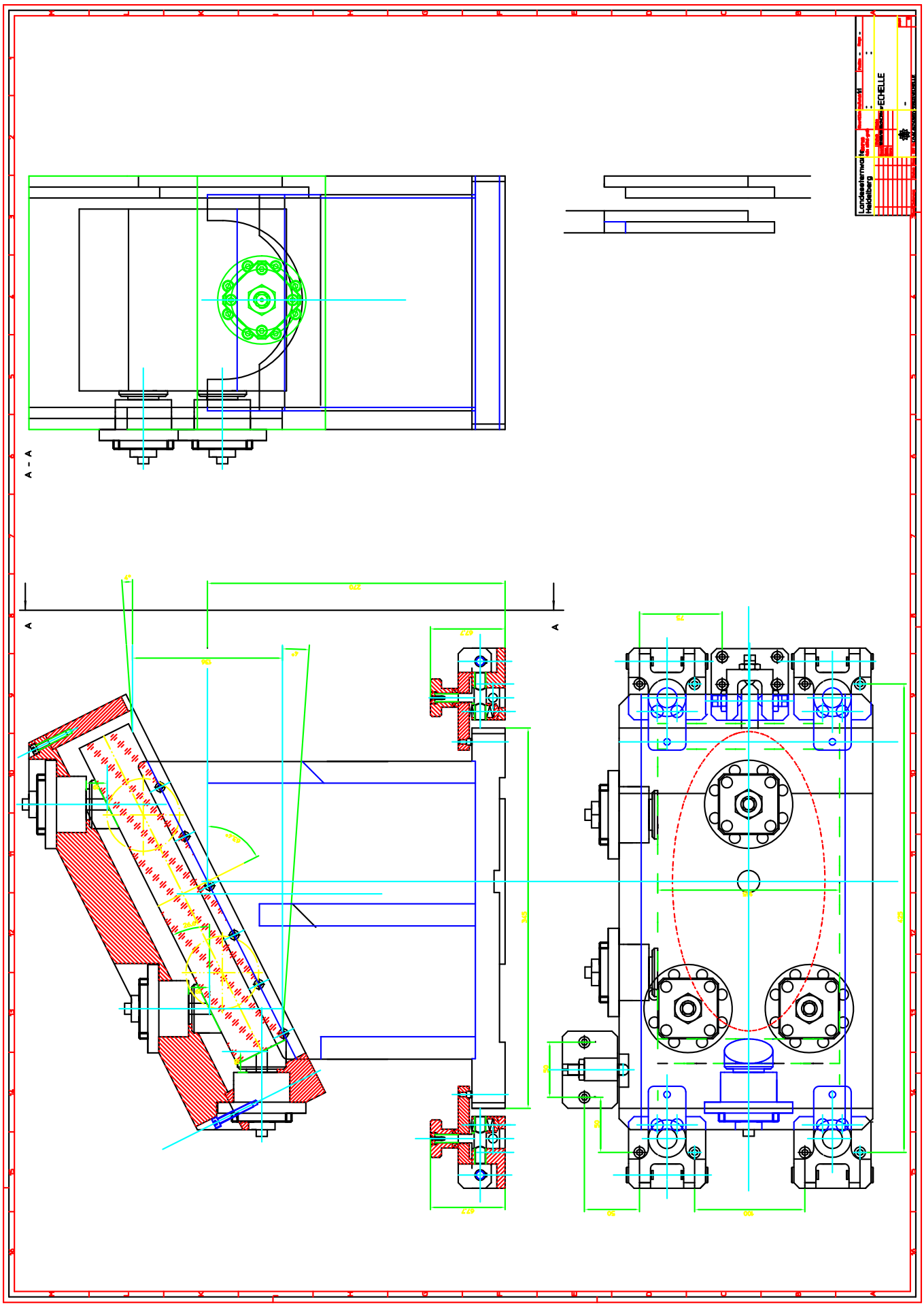

B.9 Crossdisperser Prism

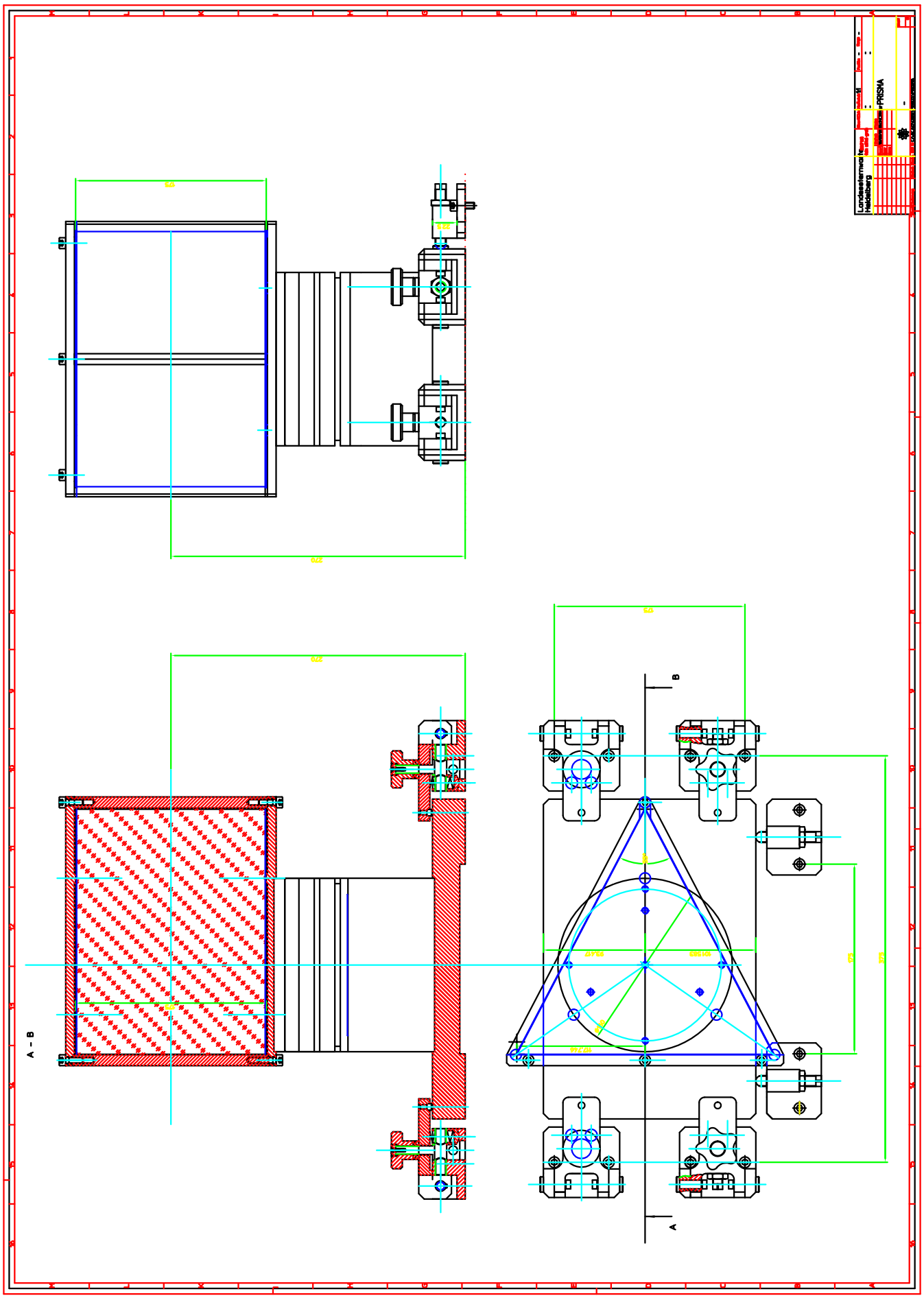

B.10 Camera – CCD Unit

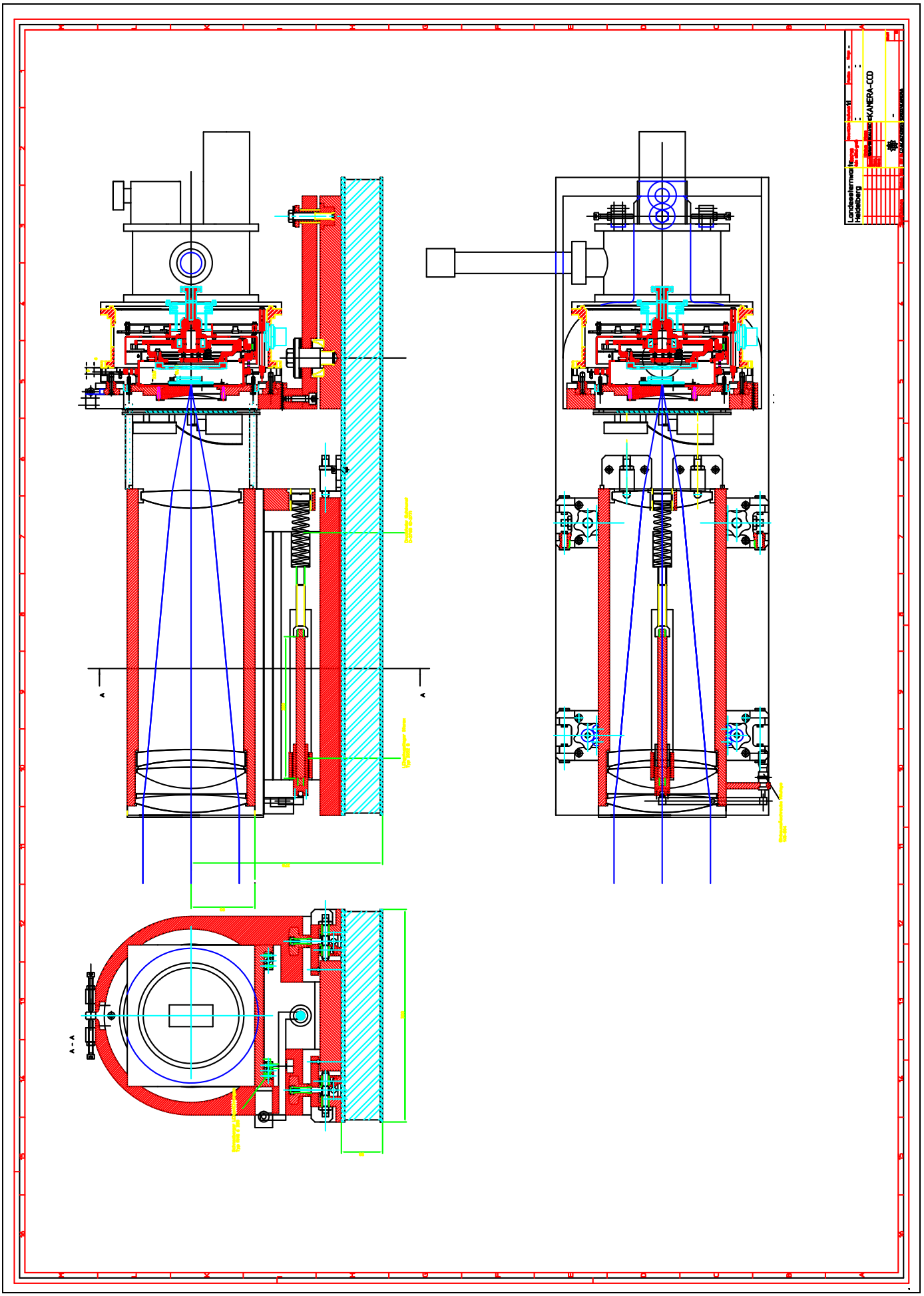

B.11 Axial Supports

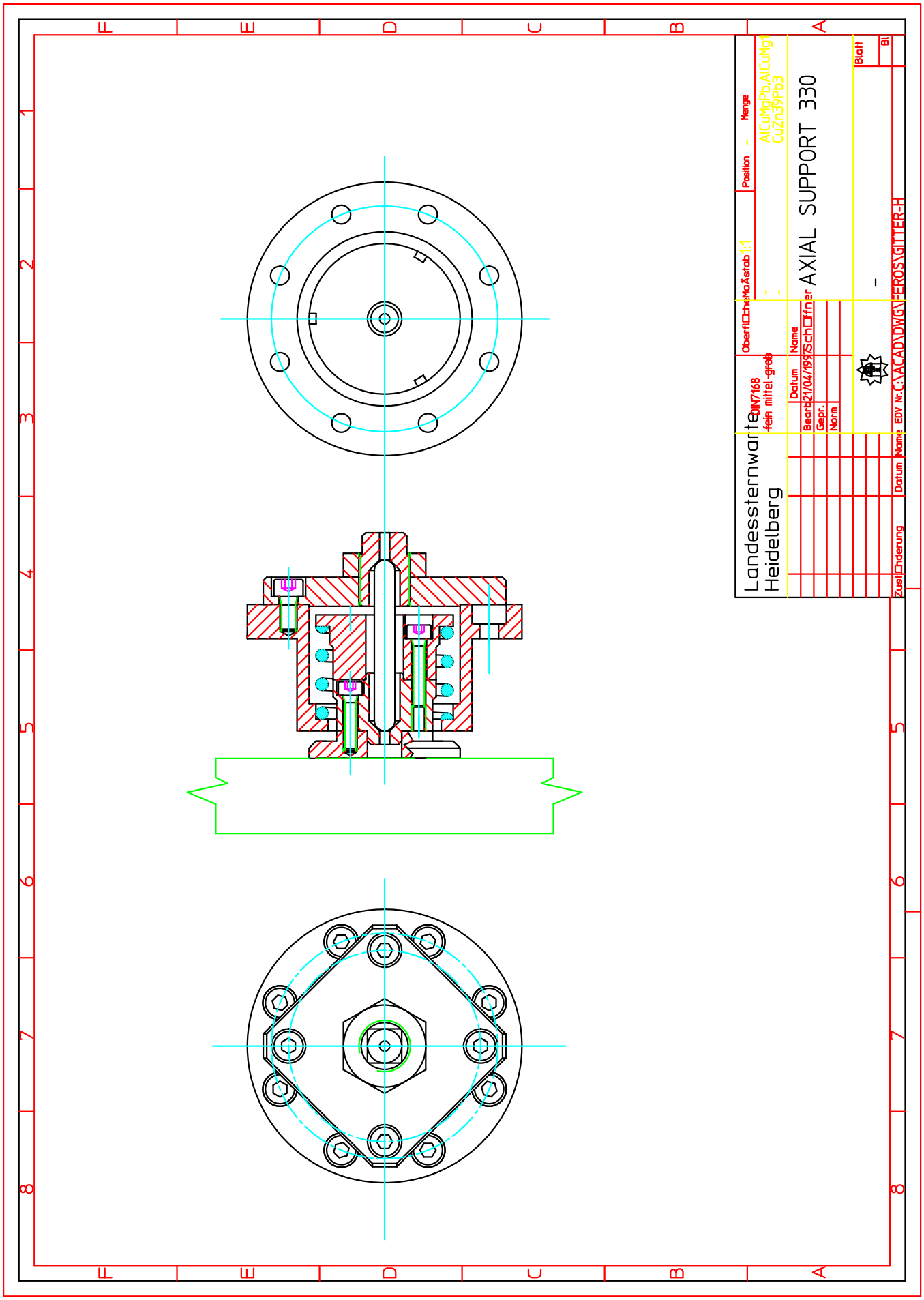

B.12 Clamps

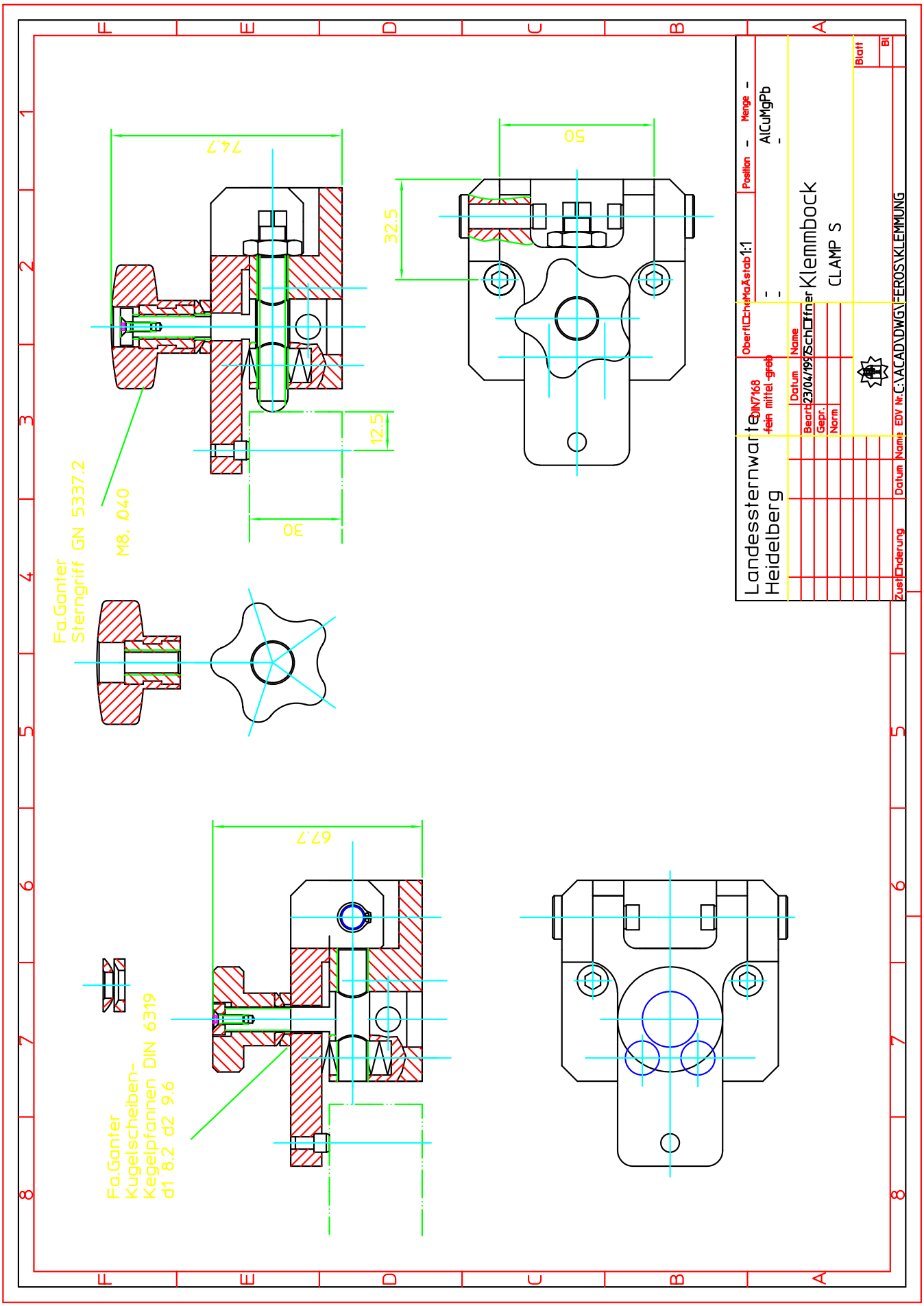
74.7
50
32.5
12.5
30
M8, 040
Fa.Ganter
Sterngriff GN 5337.2
67.7
Fa.Ganter
Kugelscheiben-
Kegelpfannen DIN 6319
d1 8.2 d2 9.6
Landessternwarte
Heidelberg
DIN7168
fein mittel grob
Datum
Name
Bearb. 23/04/199
Gepr.
Norm
Oberfl.Chd.
Ma.Astab 1:1
Position
Menge
AlCuMgPb
Klemmbock
CLAMP S
Blatt
Zust.Chderung
Datum
Name
EDV Nr.
C:\ACAD\DWG\EROS\KLEMMUNG

B.13 Stops

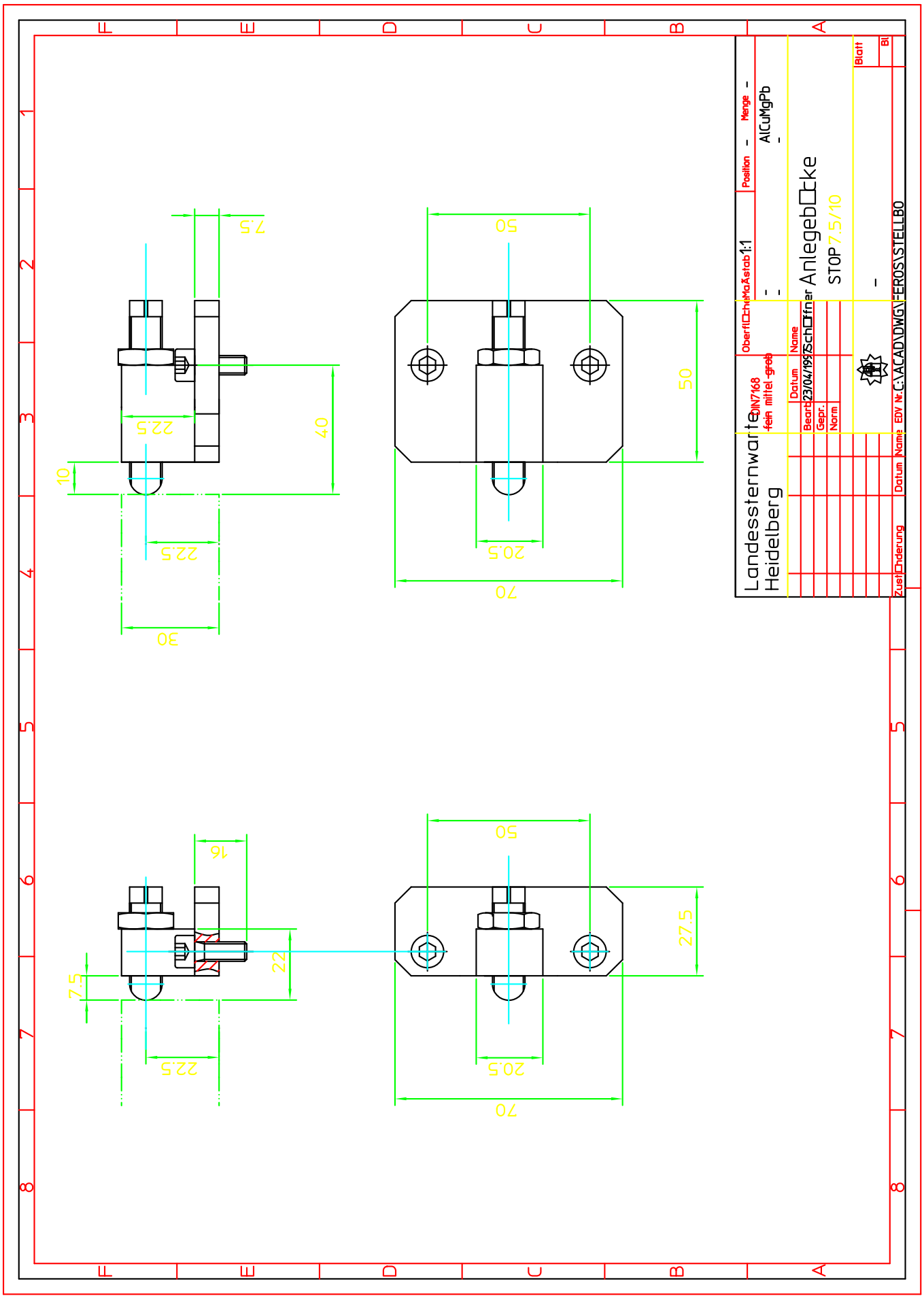
Landessternwarte
Heidelberg
Anlegebücke
STOP 7.5/10
AlCuMgPb
Position
Menge
Datum
Name
Gepr.
Norm
Blatt
Zuständerung
Datum
Name
EDV Nr.
C:\ACAD\DWG\FEROS\STELLB0
7.5
50
22.5
40
10
20.5
70
30
16
22
27.5

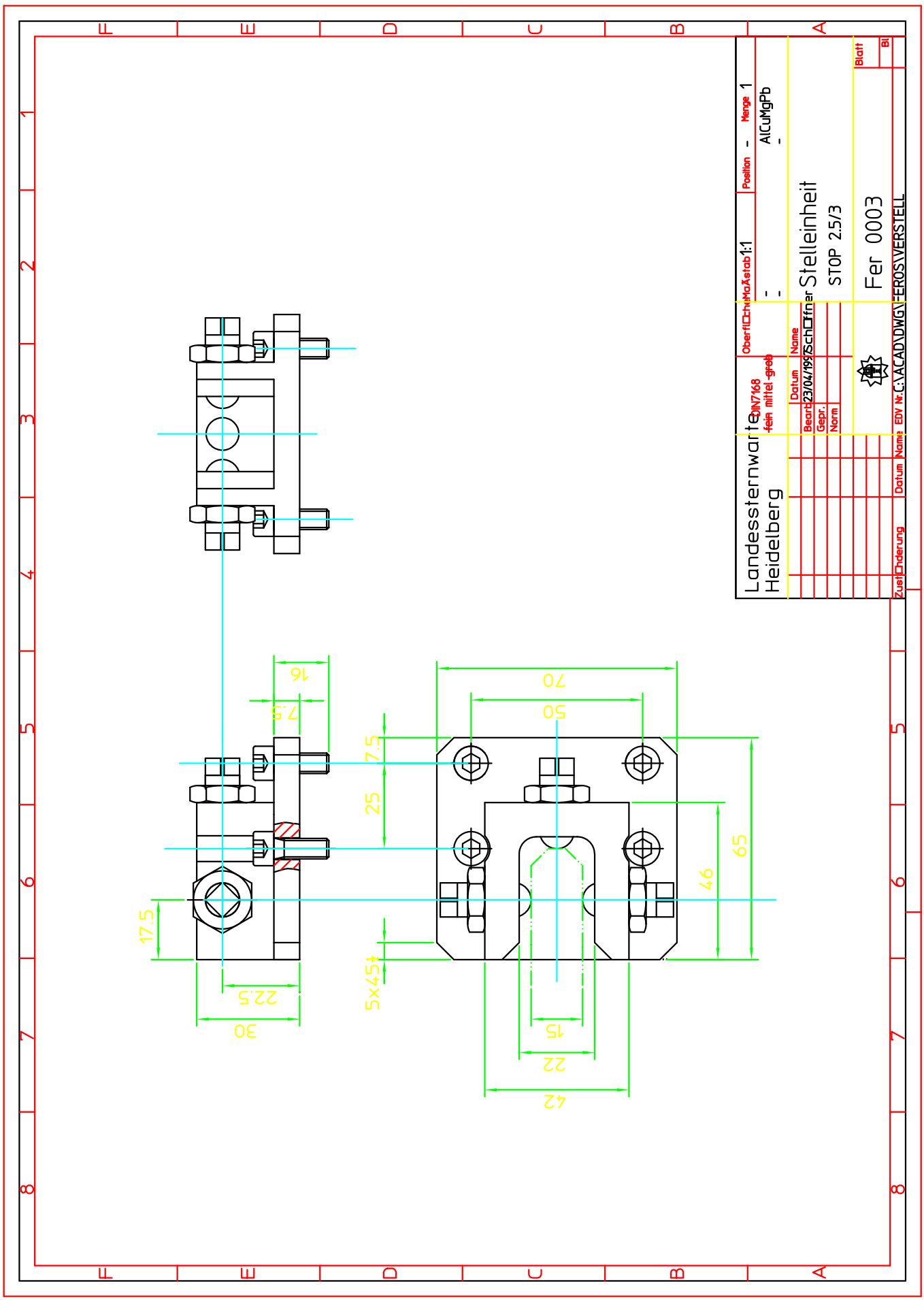
Landessternwarte
Heidelberg
Stelleinheit
STOP 2.5/3
Fer 0003
AlCuMgPb
Position
Menge
Datum
Name
Gepr.
Norm
Blatt
Zustellung
Änderung
EDV Nr.
C:\ACAD\DWG\FEROS\VERSTELL
16
7.5
7.5
25
17.5
22.5
30
70
50
65
46
5x45
15
22
42

B.14 Removable Enclosure

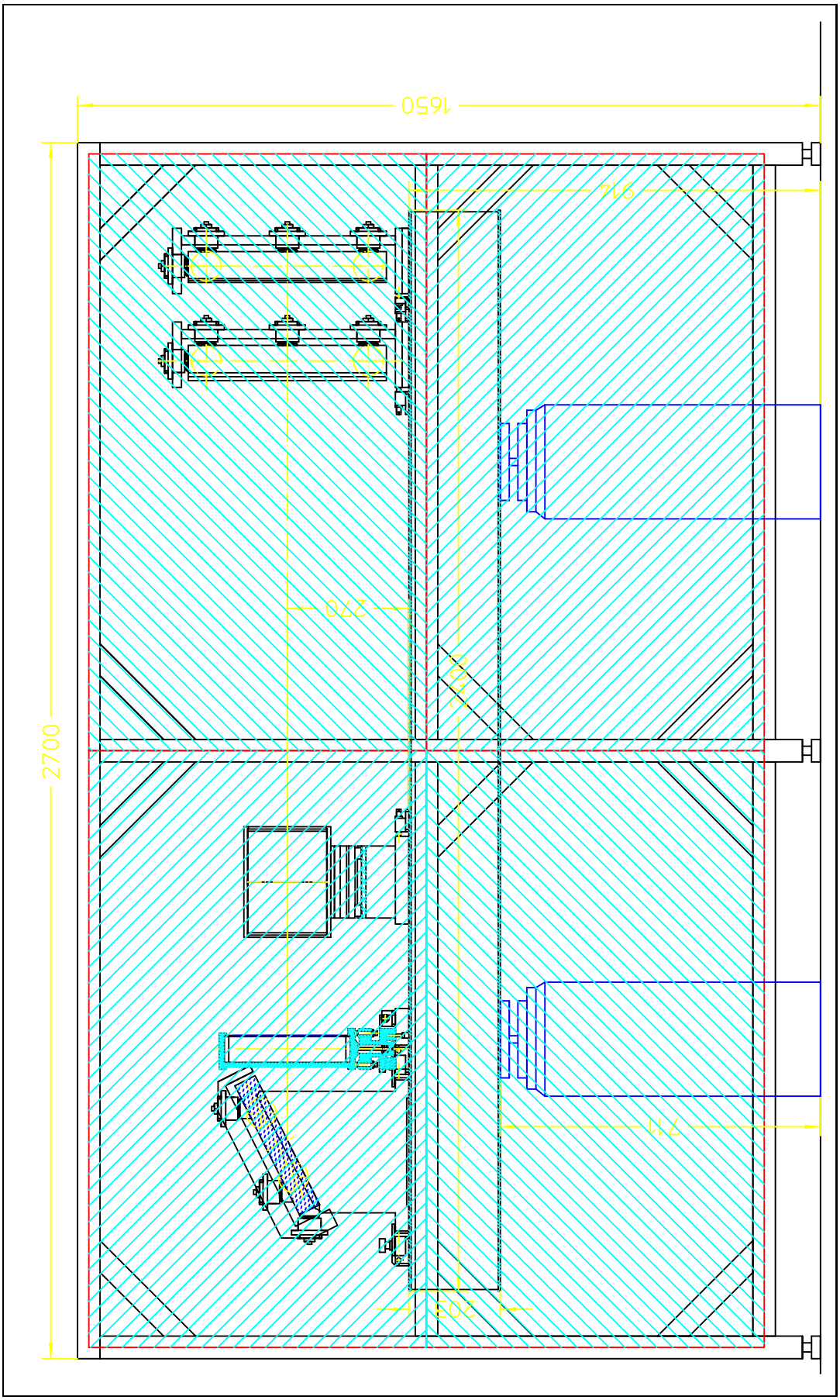

B.15 Calibration Unit

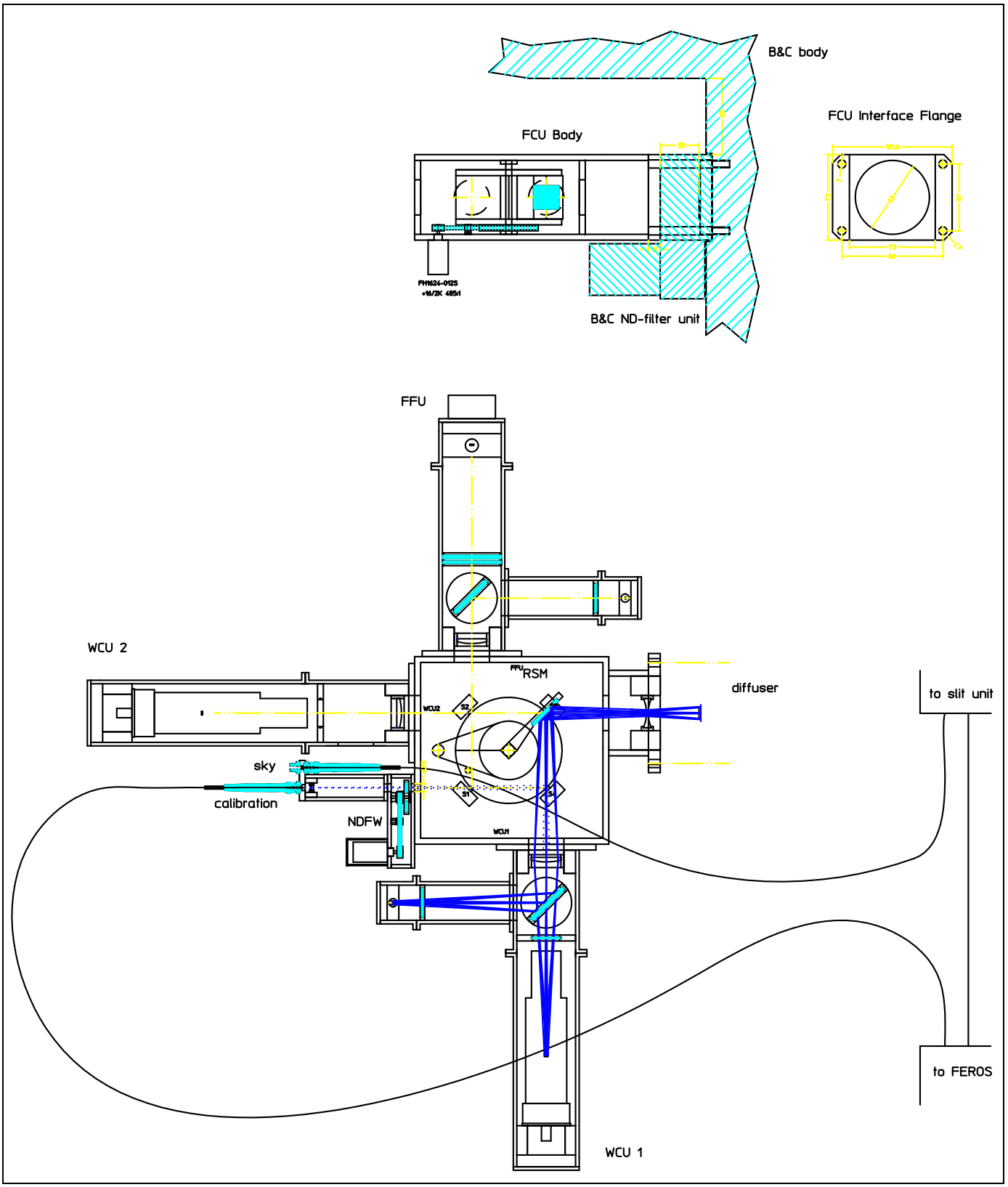

B.15.1 Boller&Chivens interface

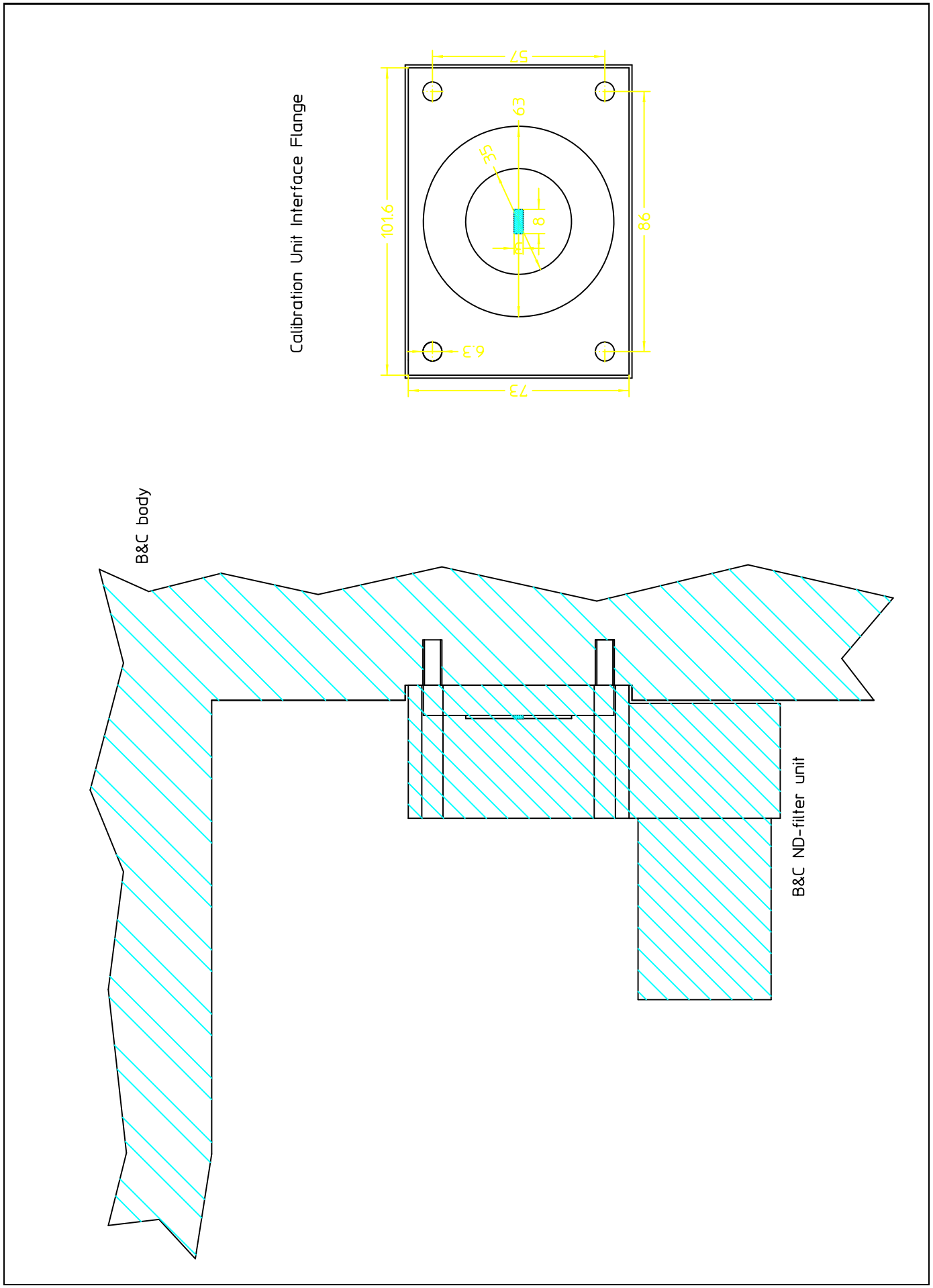

B.15.2 Wavelength-Calibration Unit 1 (WCU1)

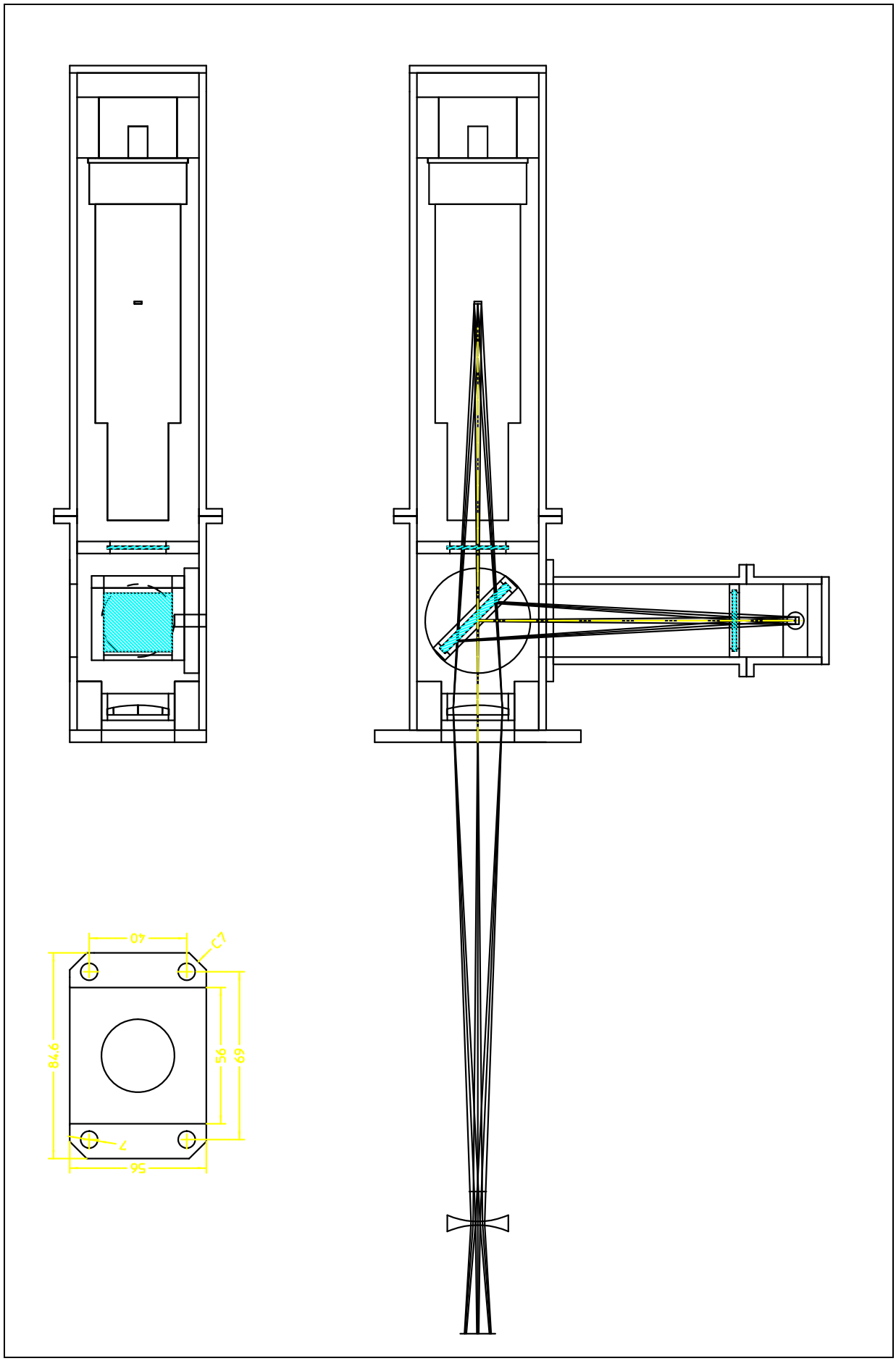

B.15.3 Wavelength-Calibration Unit 2 (WCU2)

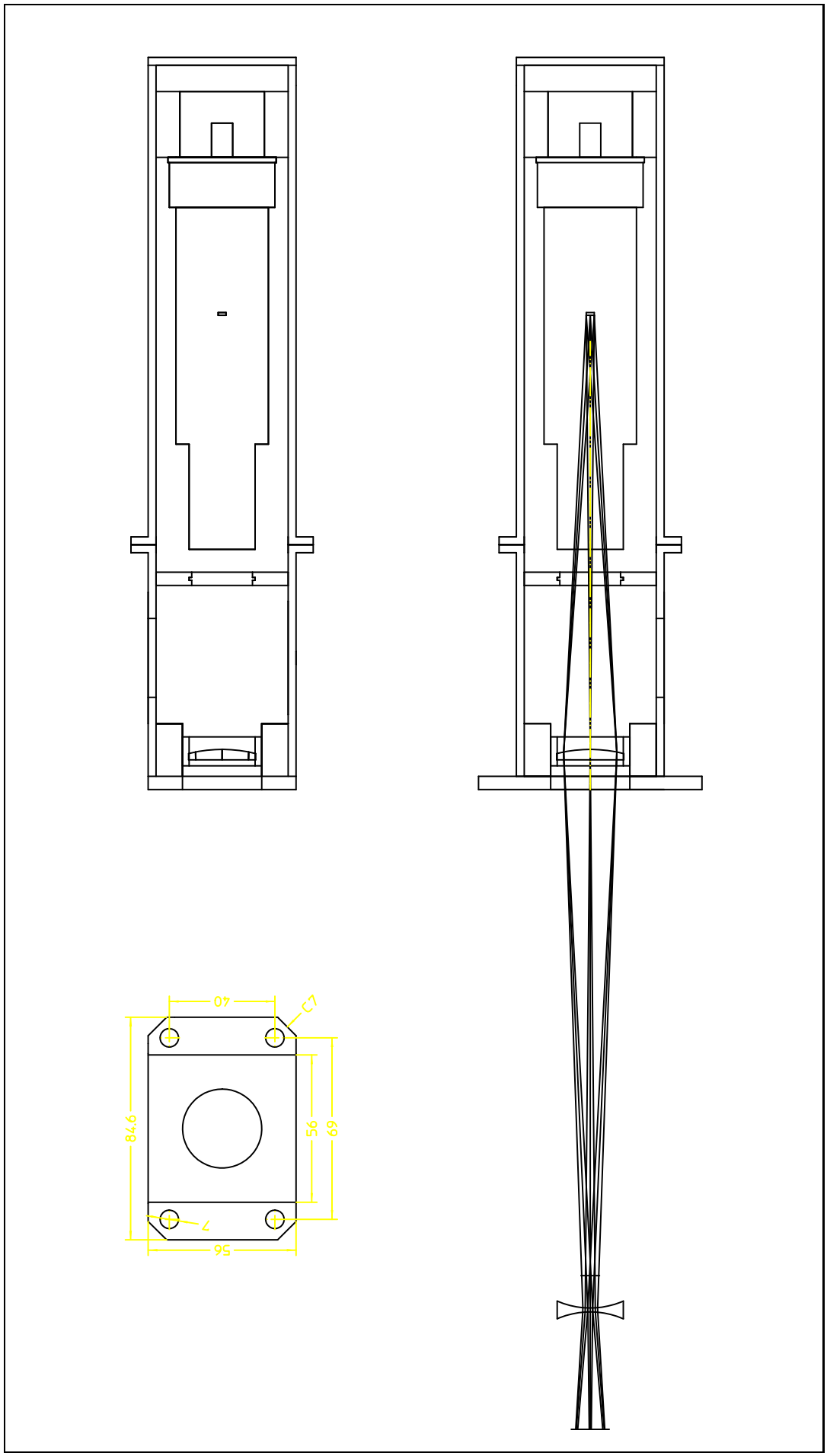
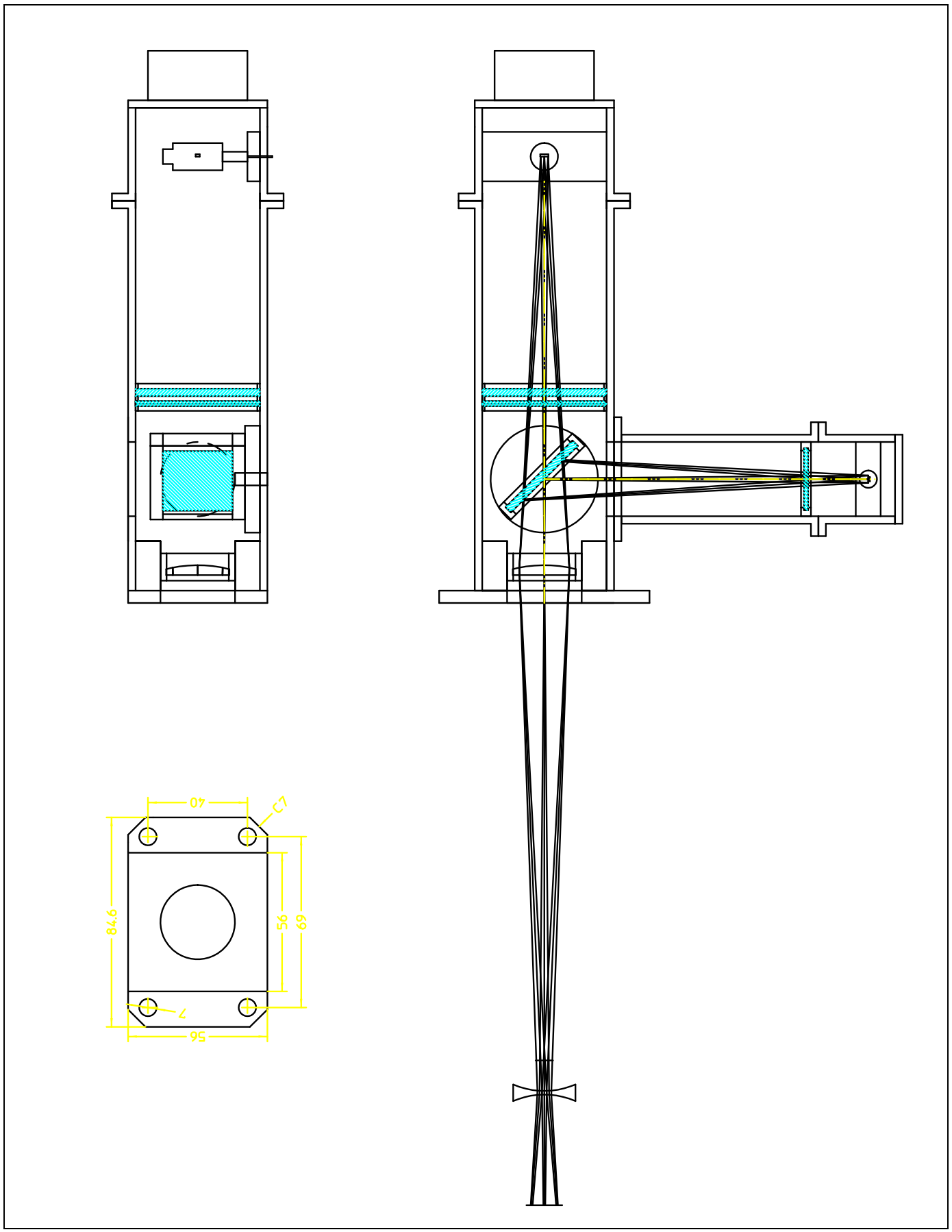
B.15.4 Flatfield Unit (FFU)